The natural armor of fish: an exploration of a biological composite

Sandra C Murcia

A dissertation

submitted in partial fulfillment of the

requirements for the degree of

Doctor of Philosophy

University of Washington

2017

Reading Committee:

Dwayne Arola, Chair
Brian Flinn
Junlan Wang

Program Authorized to Offer Degree:

Materials Science and Engineering

University of Washington

Abstract

The natural armor of fish: an exploration of a biological composite

Sandra C Murcia

Chair of the Supervisory Committee:
Dr. Dwayne Arola
Materials Science and Engineering

In the search for advanced structural materials, scientists are finding inspiration from materials in nature and biological composites. The need for lighter protective materials has directed attention to armored skins, which possess a combination of flexibility, puncture resistance and capacity for energy dissipation. This rare combination of properties is found in the armored skin of modern fish, and achieved by overlapping scales with exceptional specific strength and toughness. Research on these materials has focused on their mechanical properties, with limited regard for the microstructure and potential spatial variations over the fish body. If fish scales will serve to inspire future generations of flexible wearable armor, a better understanding of the relationships between structure and properties is essential. Therefore, the main objectives of this research were to develop new understanding on the constituent layers and lamination patterns of elasmoid scales from teleost fish, and understand their importance to the mechanical properties relevant to

armor performance. The investigation consists of five aims that address properties of the scales as a structural material, the spatial variations over the body of fish, the microstructure and properties of the individual layers, and the design and performance of the interface between these layers.

This investigation enrolled a combination of experimental, analytical and numerical efforts to achieve the aims. An exploration of scales from *Cyprinus carpio* showed that the fracture resistance of elasmoid fish scales is largely dependent on the anatomical position and the corresponding microstructure. Elasmoid scales were found to consist of three principle layers, including the external highly mineralized limiting layer (LL), as well as the external (EE) and internal (IE) elasmodine, which consist of a number of lamina (or plies) of unidirectional type I collagen fibrils. While the fracture resistance increased with scale thickness, it was highly correlated with the number of plies in the elasmodine and ratio of mineralized plies in the EE. Furthermore, the hierarchical structure of the scales and the molecular level bonds were found to be of importance. Removal of the intra molecular water enabled inter-peptide bonding of the collagen fibrils, which increased the strength and elastic modulus. Furthermore, mineral crystals at the intra-fibrilar spaces impeded the formation of new inter-peptide bonds and reduced the degree of toughening achieved.

Through an evaluation of the laminate structural characteristics, it was found that the ply stacking sequence and the distribution of mineralized plies play a key role on the mechanical response of fish scales. In light of that importance, this study was the first to fully characterize the lamination patterns of fish scales from different species, to distinguish differences in the LL thickness and the EE ratio between species and across anatomical locations, and connect those qualities to their unique needs for locomotion and protection. Results from this phase of the

investigation detailed the differences in microstructure between selected fish species, the need to characterize the microstructure of the scales in characterizing the structural behavior and how spatial variations in structural behavior are achieved through modulation of the LL and EE.

An analytical model was developed for the elastic properties of scales that describes the elastic behavior in terms of the relative contributions of the LL and the EE and IE. The mechanical properties of scales from the *Megalops atlanticus* (i.e. tarpon) were characterized in tension and compared with predictions from the model. The average error between the predictions and experimental properties was 7%. It was found that the mineralization gradient and aspect ratio of the apatite crystals in the LL played the most important roles on the elastic modulus of the scales. Furthermore, misalignment of the EE plies was shown to reduce the elastic modulus significantly and is one approach that appears to be employed by fish to modulate the scale flexibility for a specific mineral content that is required for protection.

The detailed exploration of the limiting layer revealed a suture-like transition area between the LL and the EE in both carp and tarpon scales. This region was found to exhibit a geometry akin to the distribution of circuli that are formed by mineral protrusions on the surface of the scale.

The effect of the LL profile and suture line geometry on the structural behavior of the scales and bioinspired analogues was studied using complementary experimental and numerical efforts. Results showed that the bending stiffness and work to fracture of the scales in flexure decrease with increasing amplitude and decreasing wavelength of the LL profile. Furthermore, the gradient in elastic modulus of the suture region was instrumental in the scale flexibility. The structural behavior of the scales can be effectively tuned by the suture line shape, its relative position in the LL and the LL profile. The results establish the potential for tailoring the mechanical response of flexible composite laminates by carefully adjusting the layer

architectures and their interfaces. The suture line geometry appears to play a key role on the scale protecto-flexibility, and can help extend the possibilities for bioinspiration derived from scales well beyond applications for body protection.

TABLE OF CONTENTS

LIST OF FIGURES

LIST OF TABLES

ACKNOWLEDGEMENTS

First I want to thank to my previous advisor Dr. Alexander Ossa at EAFIT University, his guidance played a vital role into my desire to begin the search for new knowledge and his valuable feedback taught me how to be a better researcher. Having him as mentor in the academic world allowed me to start my PhD studies under the advisory of Dr. Dwayne Arola at the University of Maryland, Baltimore County to whom I extend my most sincere gratitude. His leadership, never ending thirst for excellence and hard work promoted an improvement of my initial set of skills as an engineer and helped me to develop new ones that will come handy in my future. I also want to thank the members of my graduation committee, Dr. Brian Flinn, Dr. Mark Tuttle and Dr. Junlan Wang. Hereby I also want to extend recognition to the MSE department, especially to Dr. Jihui Yang and Dr. Fumio Ohuchi who helped me finding the needed funding in order to finish my degree. I also extend special acknowledgement to Ellen Lavoie at the Molecular Analysis Facility at UW, her guidance was of significant importance for the microstructural characterization of the scales. Furthermore, I want to thank Dr. Marco Salviato at the Aeronautics and astronautics department at UW for the valuable discussions and guidance on the numerical simulations enclosed in Chapter 7.

I also cherish the support given by all the members of Dr. Arola's lab, in particular the advice and guidance of Dr. Hessam Majd and Dr Mobin Yahyazadehfar during my time at UMBC. Finally, I want to thank my family and friends for all the encouragement that pushed me to finish this degree.

DEDICATION

To those close to my heart that made this achievement possible.

Chapter 1. Introduction

Mankind has historical threads that connect the present-day struggles to those of our ancestors, and unfortunately, armed conflict is one of them. Regardless of whether the conflict is between nations or a civil war, human lives are lost. An increasingly common part of war is the use of landmines, and the majority are undocumented. It is estimated that there are 110 million active landmines in over 70 countries across the world [1]. One person is killed or maimed every 20 minutes by a landmine, and as a consequence there is an expanding global effort to detect and deactivate landmines. Soldiers working on these missions currently wear heavy body armors (10-20 kg) for protection [2]. The extra weight makes their task difficult since these antipersonnel mines can be triggered by a difference of 6 kg. In addition, the current gear restricts their range of motion, which reduces the soldier's effectiveness and safety. Even worse, no protective gear is available for the civilians who must farm these areas for survival. For these reasons, the search for new materials for body armors is a global research topic of significant importance.

While no longer new, the field of bio inspiration is contributing to the development of novel structural materials with exceptional properties. This approach can be applied to the design of improved armor materials. Scales form a natural layer of armor for fish and reptilians. As a consequence, there was an adaptation of scales in the design of military armor as they proved effective in providing protection from physical attacks involving weapons developed to puncture and cut. The armor covering of scales conforms to the body of the fish or animal, deflecting attacks without sacrificing mobility; the same design is sought in body armor designed for personal protection [3]. But from an evolutionary point of view, scales provide a unique approach to protection. Instead of surrounding an animal in rigid segments, scales cover an organism in a

network of small, flexible, armored plates. Scales can overlap, forming an imbricated network, which fully covers the animals without the weak points of exoskeleton joints [4].

The use of scales in protective armor dates back at least to the ancient Persians [5]. Scale armor remained prominent throughout the reign of the Roman Empire, where two types of fish scale mimicking lorica's were developed. The first one, Lorica Squamata, was a type of scaled armor used in Rome as equipment for soldiers **Figure 1.1.A**. The second type of lorica, Lorica Plumata was a hybrid mail covered in very small scales. It was used by officers as well as tribunes and above, but more typically generals, due to the high cost of production and maintenance (**Figure 1.1.B**). In both cases, the "squamae", or individual scales, were either brass iron, or other alternating metals on the same shirt, depending of the availability of materials. Armor made of scales and plates remained popular long after the decline of the Roman Empire, finally falling out of fashion during the Middle Ages [3].

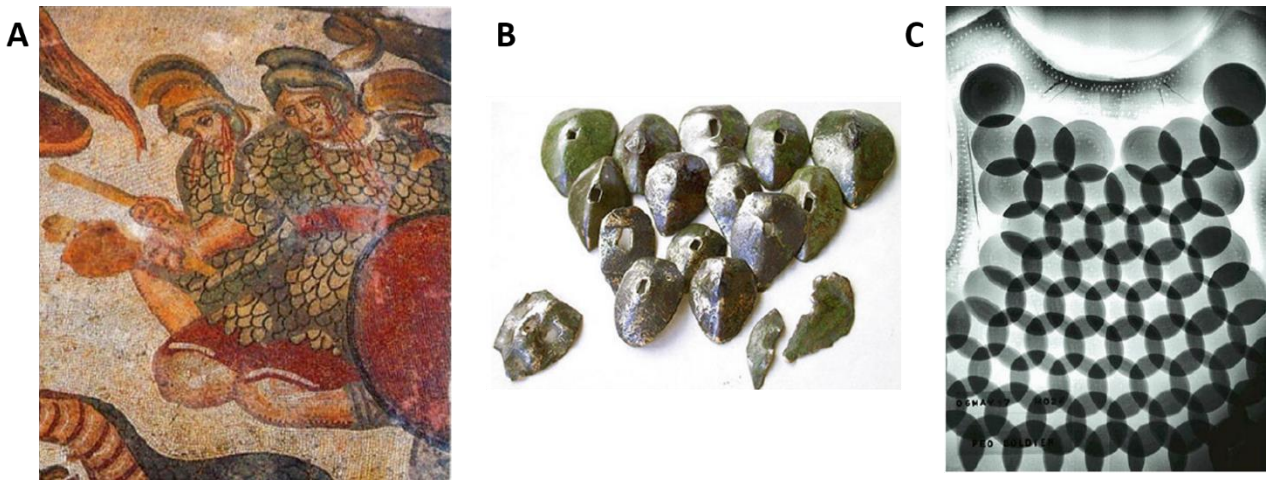

Figure 1.1. Examples of scaled armors and changes over time. A) Soldiers in lorica squamata. Fragment of the mosaic from Villa del Casale, Piazza Armerina – Enna, Italy, datable at about IV century bCA. B) Fragments of lorica Plumata. C) X-ray of Dragon Skin armor (PEO Soldier (U.S. Army 2010) [3].

Although scaled armor declined in popularity, the use of scales to provide flexible protection persists. Inflexible and heavy body armors limit the speed and agility of soldiers on the battlefield. Therefore, efforts dedicated to developing better armor materials are not only focused on providing protection against land mines. For example the Dragon Skin shown in **Figure 1.1.C** is a modern ballistic vest produced by the Pinnacle Armor Corporation (USA). However, the US Army rejected Pinnacle Armor's Dragon Skin system in 2008 [3].

In recent years the search for bioinspiration has extended to the "armored skins" of crocodiles [6], turtles [7], and fish [8,9]. While the "armor" of these animals may appear disparate from the pattern of assembly [10], they share the quality of most composite materials, i.e. they are constructed of a combination of constituents and possess mechanical properties superior to those of the individual components. For instance, fish scales are presently inspiring the next generation of body armors[11,12], and consist of a compliant matrix of collagen fibers reinforced by crystals of apatite.

The scales of fish are distributed along the body, overlapping such that the posterior region of a single scale covers a portion of both adjacent lateral and posterior scales. This staggered arrangement endows fish with a combination of protection from physical attack and essential flexibility for locomotion [13]. Scales in modern fish are classified in four groups including cosmoid, placoid, ganoid and elasmoid [13,14]. Placoid scales of sharks have been studied for hydrodynamic purposes [15]. Ganoid scales, known as bony scales, exhibit a microstructure similar to that of bone [14,16–18] and are found in the alligator gar. The microstructure of ganoid scales can be divided into two principal layers. The outer ganoine layer consists of apatite crystals (similar to tooth enamel) and the inner bone basal layer is largely constructed of mineralized type

I collagen fibers [17]. The mechanical properties of ganoid scales have been characterized from different teleost including the alligator gar (*Atractosteus spatula*) [16,17,19], and *Polypterus Senegalus* [18,20,21]. Yang et al [22] characterized the tensile and compressive properties of the alligator gar scales, and found that the scales exhibit inelastic behavior when hydrated. The investigators also evaluated the fracture toughness of scales from the alligator gar in situ within an electron microscope. The fracture toughness ranged from 2.5 to 6 $MPa \cdot m^{1/2}$, which is comparable to that of other mineralized tissues such as bone and dentin.

While the segmented assembly of ganoid scales bestows flexibility, single scales are far less compliant. In contrast, elasmoid scales are flexible and relatively thin, which endow ease of movement to the fish. Elasmoid scales consist of type I collagen fibers and apatite. Both are widely encountered in natural mineralized systems [8,23,24]. These scales can be divided into two primary layers that correspond to the relative mineral content (**Figure 1.1**). The outermost layer, known as the Limiting Layer (LL), is a highly mineralized matrix and consists of calcium-deficient apatite crystals with dispersed thin collagen fibers [8,23,25]. The internal layer or elasmodine consists of discrete plies of unidirectional type I collagen fibers and can be further divided into the external (EE) and internal (IE) layers according to the mineral content (**Figure 1.1A**). The fibers are arranged in the form of a plywood structure, with rotation between plies ranging between 60–90° depending of the fish [26]. The diameter of the collagen fibers is near 1 μm, and they are constructed of an assembly of fibrils roughly 100 nm in diameter [23,27].

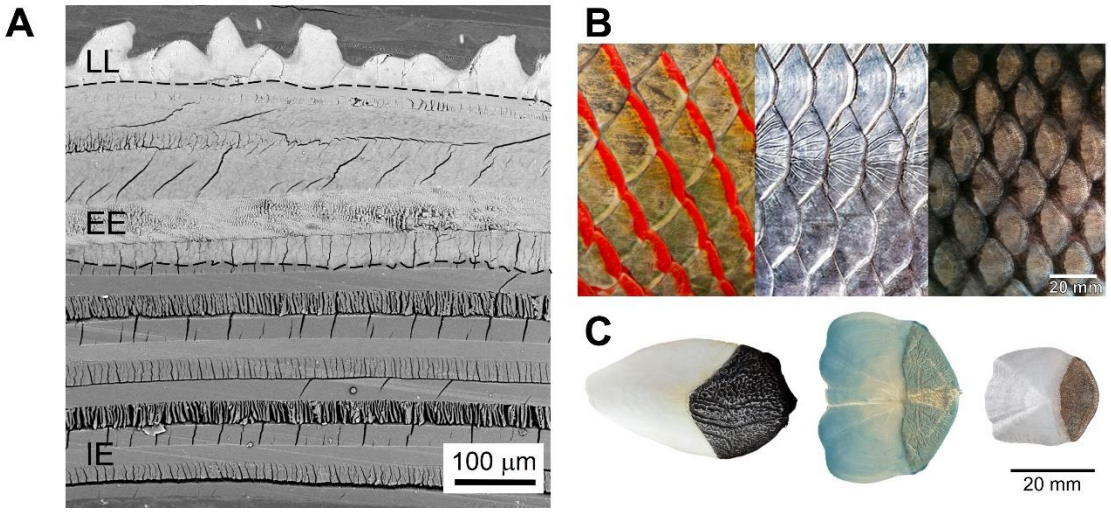

Figure 1.2. A comparison of the scales for the three Teleost. A) A cross sectional SEM image from the scale of the tarpon denoting the three distinct regions including the limiting layer (LL), external elasmodine (EE) and internal elasmodine (IE). B) Scale patterns for the *A. gigas* (arapaima), tarpon and carp (left to right). C) A comparison of single scales from the arapaima, tarpon and carp (left to right).

A number of studies have been conducted on elasmoid scales including those of the carp (*Cyprinus carpio*) [23], striped bass (*Morone saxatilis*) [24,28,29], *Pagrus major* [30], tarpon (*Megalops atlanticus*)[31] and *Arapaima gigas* [8,32–36]. As a result of the rather large organic content, the mechanical behavior of fish scales has been found to be sensitive to hydration. Ikoma et al [30] evaluated the tensile properties of dehydrated scales of *P. major* and reported an elastic modulus and tensile strength of 2.2±0.3 GPa and 93±1.8 MPa, respectively. Scales of *A. gigas* exhibit an elastic modulus of 0.8 ± 0.1 GPa and tensile strength of 22.3 ± 3.9 MPa in the hydrated condition, which increases to 1.4 ± 0.2 GPa and 53.9 ± 8.4 MPa, respectively with dehydration [8]. Garrano et al [23] found that the relative importance of hydration to the mechanical behavior is a function of anatomical position, and greatest for scales near the tail. Equally important, evaluations of scales in uniaxial tension showed evidence of mechanical anisotropy [24,31,37].

Due to the strong gradient in mineralization across the thickness, there is a substantial reduction in the hardness and elastic modulus distributions from the exterior to the interior layers [8]. This

gradient in properties plays an important role on the puncture resistance [24]. The LL acts as an initial barrier that dissipates energy by brittle fracture. Fracture propagates to the interface with the EE, resulting in delamination between adjacent plies and fibrils. This process of interfacial failure at multiple levels is key to the fracture resistance of scales and bestows them with incredible notch insensitivity [28]. Once the LL and EE have undergone gross failure, further penetration is resisted by the IE via stretching, rotation and delamination of the collagen plies [38,39]. Due to its composition and the host of contributing mechanisms, the IE undergoes substantial deformation and contributes to the large strain to failure (≥15%) of the scales [23,24,30,37,40].

For the majority of investigators interested in fish scales and the potential for bioinspired materials development, the primary focus of their efforts has been on the mechanical behavior. In comparison, the microstructure of these natural composites and the importance of differences between fish species have been largely overlooked. For fish scales to inspire future generations of flexible "wearable" armors, a better understanding of their design and its contribution to their performance is essential. Therefore, the overall objective of the proposed research is to develop new understanding on the integral components of the LL and EE and the lamination sequence of scales, as well as their importance to the mechanical properties of these materials. This knowledge is essential for achieving bioinspired design of wearable armors for personal protection. An ideal armor would be one whose performance is also independent of environmental factors including temperature and moisture. Furthermore, with the increasing interest in fish scales as a structural material, it is important to understand the unique design of scales from different species of fish, and elucidate the purpose of those differences with respect to scale function and resistance to threat. Lastly, one of the most important aspects of fish scale design as a structural material is the interface between the LL and EE, which couples a highly mineralized stiff material to one that is

very compliant. This interface does not undergo apparent degradation under the flexure of scales. Nevertheless, the structure and function of the interface has been overlooked. Therefore, the following investigation has been designed to address these issues and consists of the following five specific aims:

Aim 1: Evaluate the importance of temperature changes on the fracture resistance of fish scales

Aim 2: Evaluate the changes in mechanical behavior of teleost scales with exposure to polar solvents

Aim 3: Evaluate and compare the scales from three different teleost fish to develop a quantitative description of the microstructure

Aim 4: Characterize the limiting layer of different fish to develop knowledge on this important mineral system

Aim 5: Evaluate the interface of the limiting layer and external elasmodine and determine the effects of the geometry on strength and toughness

The dissertation is organized into six chapters and presents results of the investigation in the manner they were presented and published in the archival literature. Chapter 1 provides a brief introduction and describes the results of previous research on the mechanical properties of fish scales. Chapter 2 presents the results on an evaluation of the tear resistance of scales and its dependence on temperature and anatomical location. Then, Chapter 3 compares the mechanical response of the fish scales in a hydrated condition with the response after chemical dehydration. Chapter 4 evaluate the microstructure of scales from different teleost fish and performs a quantitative comparison for the first time. Chapter 5 explores the most outer layer of the scales, its

chemistry, morphology and mechanical properties. Followed by Chapter 6, where a semi-empirical model for the prediction of the elastic modulus and strength of scales is developed. Then, Chapter 7 examines the role of suture like features as an interface between natural materials with highly dissimilar elastic moduli. Chapter 8 summarizes the important findings and provides recommendations for future research direction.

Chapter 2. Temperature effects on the fracture resistance of scales from *Cyprinus carpio*

2.1 SYNOPSIS

In this investigation the fracture resistance of scales from *Cyprinus carpio* was evaluated as a function of environmental temperature. Tear specimens were prepared from scales obtained from three characteristic regions (i.e. head, mid-length and tail) of multiple fish. The fracture resistance was characterized in Mode III loading and over temperatures ranging from -150°C to 21°C. Results showed that there was a significant reduction in tear resistance with decreasing temperature and the lowest resistance to fracture was obtained at -150°C. There was a significant difference in the relative tear toughness between scales from the three locations at ambient conditions (21°C), but not below freezing. Scales obtained near the head exhibited the largest resistance to fracture (energy » 150±25 kJ/m2) overall. The fracture resistance was found to be primarily dependent on the thickness of the external mineralized layer and the number of external elasmodine plies, indicating that both the anatomical position and the corresponding microstructure are important to the mechanical behavior of elasmoid fish scales. These variables may be exploited in the design of bioinspired armors and should be considered in future studies concerning the mechanical behavior of these interesting natural materials.

Keywords – Elasmoid scales, tear test, fracture resistance, microstructure, anatomical position, temperature dependence.

2.2 INTRODUCTION

In 1999, Currey stated that some fish scales are so tough that they are difficult to tear, even after immersion in liquid nitrogen [41]. That comment suggests that the fracture resistance of these natural armors is independent of temperature. Yet, studies related to the fracture toughness of elasmoid scales are not available, which is attributed to the difficulties resulting from the high compliance of the system and as a consequence of hydration dependence. The importance of temperature on the fracture resistance of fish scales remains unexplored. Therefore, the primary objective of this investigation was to evaluate the fracture resistance of elasmoid fish scales and the importance of temperature for the first time.

Fish scales are expected to possess a high specific fracture toughness, which is highly desirable but difficult to characterize in compliant materials. Elasmoid scales are quite thin ($t<1$ mm) and undergo appreciable inelastic strain to failure in the hydrated state [17,23]. The fracture resistance of scales has been explored in Mode I, but the attempt was not successful. Massive delamination and defibrillation occurred without propagation of the crack [28], indicating that Mode I may not be the best mode for estimating the fracture resistance of the system. The traditional methods for characterizing fracture toughness based on Linear Elastic Fracture Mechanics (LEFM) does not apply and an Elastic Plastic Fracture Mechanics (EPFM) approach is necessary. However, instrumentation to adequately measure the strain in the vicinity of the notch while maintaining the scale submerged in a liquid environment to avoid dehydration makes the fracture toughness measurement a rather complicated task.

The fracture resistance of tissues under Mode III loading is rather seldom studied in comparison to Mode I. It does represent a very relevant mode of performance, especially in the assessment of

very compliant systems. In Mode III the direction of principal stress is out of plane of all the plies and requires substantial reorientation of the collagen fibrils to align with the direction of maximum tensile stress, which is the dominant response after puncture of fish scales during predator attack. Rivlin and Thomas[42] characterized the fracture toughness of elastomers in Mode III loading by extending Griffith's theory and relating the tear energy to the critical value for crack growth. Griffith´s theory postulated that for crack growth the energy necessary for creating new fracture surfaces is supplied by the released strain energy in the elastic body [43]. When the surface energy of the material and the crack size are known, the energy criterion can be used to predict the minimum load for fracture.

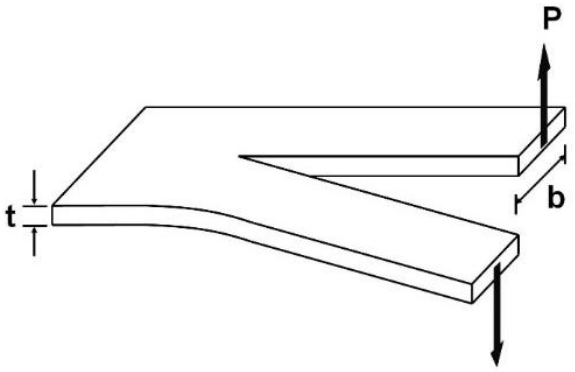

Figure 2.1. Schematic diagram of the trouser specimen used for tear testing and definition of variables

Although analytical solutions for the tearing energy require knowledge of the detailed stress distribution, a simplified approach has been developed for the trouser specimen subjected to Mode III tear (**Figure 2.1**). Testing of the specimen is achieved by pulling the two legs of the sample by equal and opposite forces out-of-plane in opposite directions. The tear energy in this configuration can be estimated according to:

$$T = \frac{2\lambda P}{t} - 2bw \tag{2.1}$$

where P is the tearing force, λ is the extension ratio of the legs, t is the specimen thickness, b is width of the legs and w is the strain energy density in the legs. If the deformation in the specimen legs is negligible in comparison to the displacement corresponding to tearing (λ =1 and w=0), then the tear energy is simply described by:

$$T = \frac{2P}{t} \tag{2.2}$$

Experimental measurements in rubber showed that when crack propagation is expressed in terms of the tear energy, the relation is independent of specimen type and geometry [44–48]. According to the relatively large compliance of hydrated fish scales, the assumptions associated with characterizing the tear behavior of elastomers apply to elasmoid fish scales as well. Therefore, this approach is adopted for characterizing the fracture resistance of carp scales.

2.3 MATERIALS AND METHODS

Five individual carp fish were obtained from a commercial vendor. These fish were marketed as East Asian carp, and no additional information was available for record. Scales were extracted from three regions of the body of each fish after Garrano et al [23], namely adjacent to the head, from within the mid-length (beneath the dorsal fin) and near the tail (**Figure 2.2.A**). The scales were obtained nearly equidistant between the ventral and dorsal aspects of the body. All of the scales were less than 1 mm thick and possessed an effective diameter that depended on the anatomical position. Scales from the head region had an effective diameter (d) equal to or greater than 25 mm. Those obtained from the middle and tail regions ranged between $22 \leq d < 25$ mm and $19 \leq d < 22$ mm, respectively. After extraction the scales were stored in Hanks Balanced Salt Solution (HBSS) at room temperature and evaluated within two weeks of harvest.

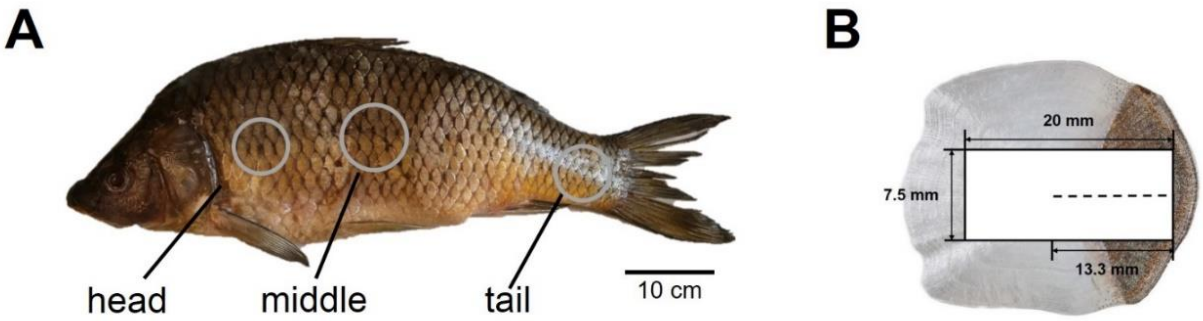

Figure 2.2. Details regarding preparation and characterization of the tear specimens. A) Scale extraction according to anatomical position, B) extracted scale showing the rectangular specimen dimensions used for development of the tear specimens.

Trouser shaped tear specimens were sectioned from the scales using a specially designed punch and stamping process. Owing to the reported anisotropy of elasmoid scales [24,31,37], specimens were stamped with orientations of 0°, 45° and 90° with respect to the longitudinal axis of the fish (**Figure 2.2.B**). Each sample was stamped from the center of the scale, such that crack extension occurred within the region of uniform thickness (**Figure 2.2.B**). After sectioning, the specimens were returned to the HBSS bath at room temperature. A central notch was cut from one edge to a length that extended through approximately 70% of the total specimen length. Eight samples were prepared from each anatomical position and for each of the three orientations. The specimen measurements were adapted to the scale diameter, maintaining that the aspect ratio of the trouser specimen for tear testing conformed to ASTM standard D1938 [49].

Tear testing of the specimens was performed under displacement control loading using a universal testing machine (Instron ElectroPuls E1000). The experiments were conducted with load cell having full-scale range of 250 N and load precision of 0.01%. To assure minimum elongation of the legs with respect to the rest of the specimen, 80-90% of the legs were clamped within the compression grips during the experiments. Tests were conducted using a stroke rate of 100

mm/min to avoid delamination or deviation of the crack from the center of the samples. If a tear deviated from the center of the sample that result was discarded due to deviation from the Mode III condition [50].

The tear energy of the scales in each of the three regions was evaluated as a function temperature. To maintain the specimen hydration and achieve a desired temperature, the specimens were submerged in specific liquid environments while testing. Separate experiments were performed at 21°C (room temperature), 0° C, -30°C and -150°C using submersion medias of HBSS, ice water, dry ice within ethyl-acetate, and liquid nitrogen, respectively. Specimens of extruded polypropylene (PP) were also evaluated in the aforementioned conditions and used as a control material; the glass transition temperature for polypropylene is -10°C [50]. These tests were performed at a stroke rate of 250 mm/min as recommended by ASTM D1938 for polymers [49]. To dismiss any possible interactions between the polymers or fish scales and ethyl-acetate, pilot tests were performed at room temperature after increasing periods of submersion. It was identified that immersion in ethyl-acetate had no significant effect ($p>0.05$) on the tear responses up to approximately one hour of exposure. That was substantially longer than the time required for completing the tear tests (less than 1 minute).

The energy required to tear the fish scales was estimated from the force-displacement curves of each specimen. The maximum force was identified from the tear history and used with Eq. (2.2) to estimate the required tear energy. The work required for fracture of the fish scales was also quantified by integrating the area under the force-displacement curves as a function of the tear displacement. With the fish evaluated, eight specimens were tested for each unique parametric condition, with one specimen obtained from each scale. Apparent differences in tear energy and

tear work attributed to the independent variables were evaluated for statistical significance using a Two-Way Analysis of Variance (ANOVA) and Tukeys HSD test at α= 0.05.

An examination of the fish scale microstructure was performed using an Olympus BX51 optical reflection microscope. Samples were taken from each of the three anatomical positions, and sectioned for inspection along the transverse plane, near the central region. The sectioned scales were embedded in resin and polished with sand paper from mesh numbers 800 to 4000. Final polishing was performed with a diamond liquid suspension of 3 microns, followed by a liquid suspension of 0.04 micron Al_2O_3. In addition, the thickness and number of plies were recorded for the scales obtained from each carp.

2.4 RESULTS

Results of the fractures resistance measurements are shown in **Figure 2.3**. A comparison of the tear energy required for fracture of specimens from the head, middle and tail regions is shown in **Figure 2.3.A**. As evident from the distribution in these results, scales from the head region exhibited a moderate degree of anisotropy. The tear energy required for fracture in the 0° orientation was significantly greater ($p \leq 0.05$) than required for the 45° and 90° orientations. However, scales obtained from within the middle and tail regions did not exhibit anisotropy. Additionally, scales extracted from the head region with 0° orientation required approximately 30% greater tear energy than that for scales from the middle and the tail regions; the differences were significant ($p \leq 0.05$).

The influence of temperature on the tear response of specimens from the head region with 0° orientation are shown in **Figure 2.3.B** and are representative of results obtained from each of the three regions evaluated. As evident from this figure there is a substantial decrease in tear energy

with reduction in temperature. Submersion of the specimens in ice water resulted in approximately 50% reduction in tear energy with respect to that at room temperature. Both the dry ice and liquid nitrogen environments caused further degradation.

An overall comparison of the tear resistance for the scales and polypropylene control in terms of the required energy and work is shown in **Figure 2.3.C** and **Figure 2.3.D**, respectively. The density of the carp scales ranges from roughly 1.10± 0.02 g/cm^3 (head) to 0.88±0.03 g/cm^3 (tail), which is very consistent with that of polypropylene (0.95 g/cm^3). Hence, the performance ranking in **Figure 2.3.C** and **Figure 2.3.D** is the same whether considering the direct measurements or after normalization. At room temperature carp scales required almost three times more energy to fracture than the control (**Figure 2.3.C**). While both material systems underwent a significant decrease in tear resistance with reduction of temperature, the fish scales required greater energy to fracture at all temperatures, except after exposure to liquid nitrogen. When evaluated in terms of the work to fracture (**Figure 2.3.D**), there is no significant difference ($p>0.05$) between the performance of the polypropylene and scales with 0° tear orientation. Although the reduction in temperature was less detrimental to the tear resistance of specimens with 90° orientation, there were no significant differences in the tear energy or work of the two orientations, except at room temperature. Spatial variations in the tear resistance could be attributed to differences in the microstructure between the three regions. The microstructure of scales from the head, middle and tail regions of representative fish is shown in **Figure 2.4.A**, thru **Figure 2.4.C**, respectively. As evident from these images, the thickness of scales and the number of plies in the EE from the three regions are not equal, scales from the head being the thickest.

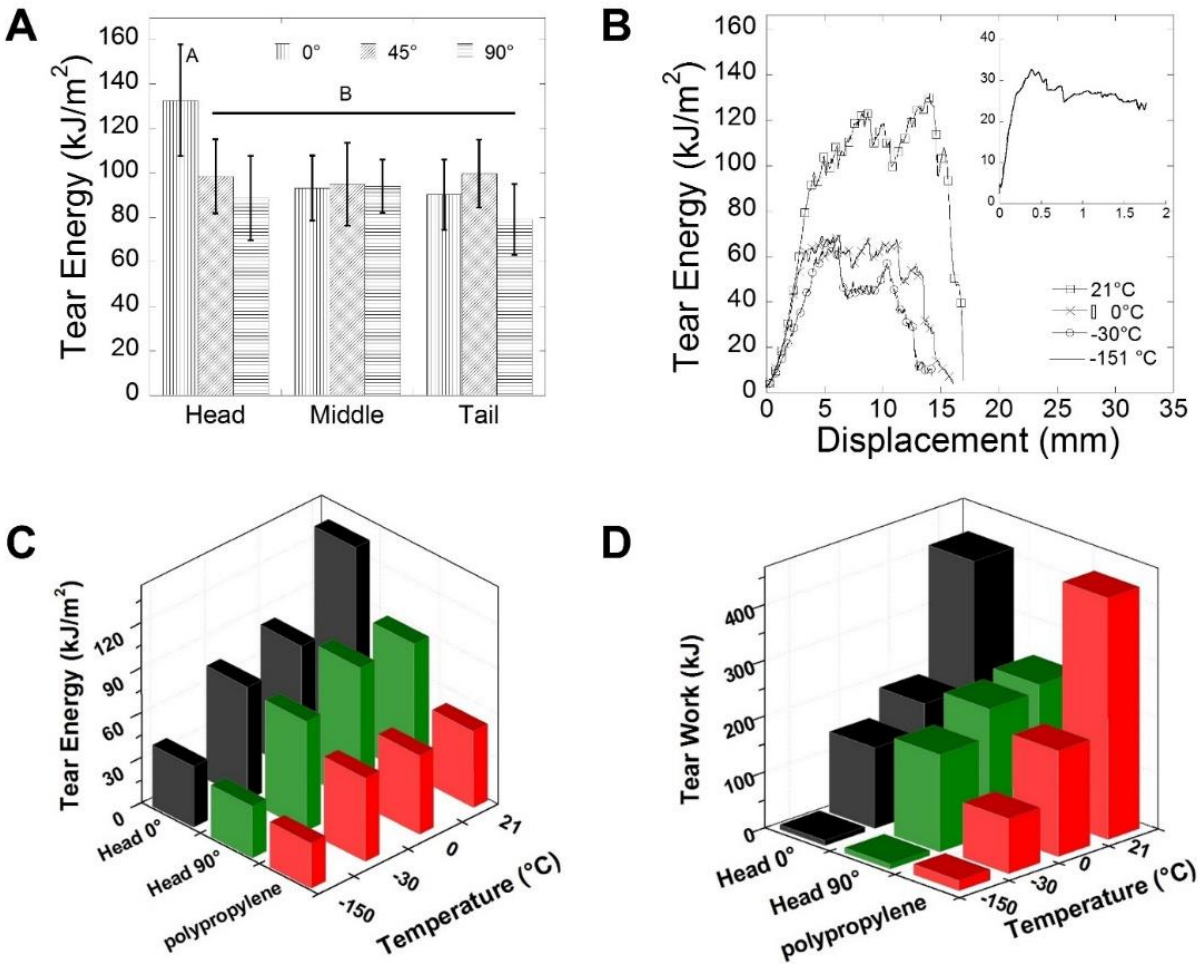

Figure 2.3. Fracture resistance of the carp scales and influence of temperature: A) A comparison of tear energy responses as a function of orientation for scales obtained from the head, middle and tail regions. Results in this figure were obtained at room temperature. Note that the tear energy of specimens with 0° orientation from the head is significantly greater than that over the remainder of the body and other orientations ($p \leq 0.01$); B) Representative tear energy vs displacement responses for the individual testing temperatures; C) Comparison of tear energy results for the carp scales (head region, 0° and 90°orientation) with that of polypropylene; D) Comparison of the tear work results for the carp scales (head region, 0° and 90°orientation) and polypropylene.

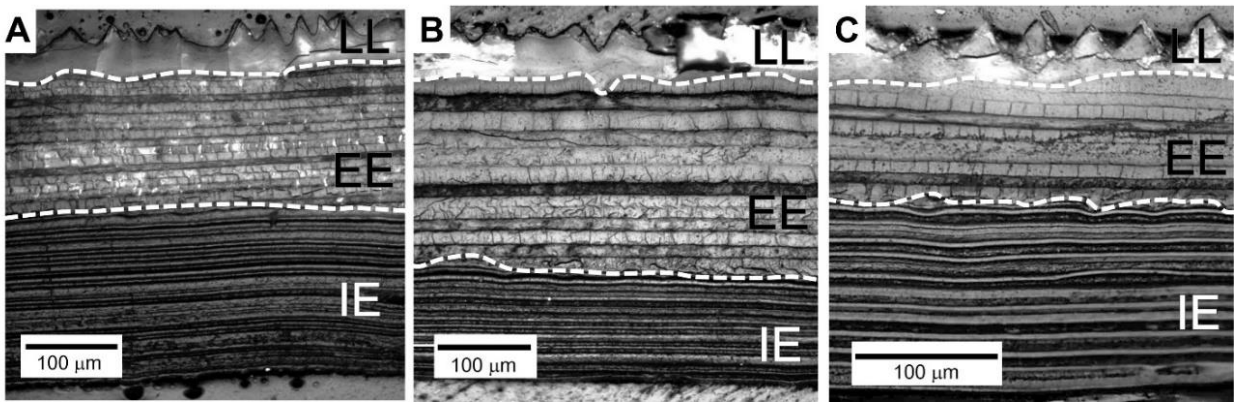

Figure 2.4. Cross-section views of the microstructure within the three regions of evaluation. Representative scales are shown for the; A) head, B) middle, and C) tail. The limiting layer (LL) is annotated at the top of each micrograph, in addition to the external elasmodine (EE) and internal elasmodine (IE) regions.

Previous studies on fish scales incorporated scales from a single fish. As natural materials are not subjected to the same standards as engineered materials, the microstructure of scales from different fish may not be equivalent. Measurements for the total scale thickness and number of plies for the scales of each of the fish used for the fracture resistance measurements are shown in **Figure 2.5.A** and **Figure 2.5.B**, respectively. There is a significant decrease ($p \leq 0.05$) in scale thickness from head to tail in each of the evaluated carp (**Figure 2.5.A**). However, there was no significant difference in the thickness of head scales between the fish evaluated. Hence, they are most appropriate for examining the importance of temperature if scales are obtained from multiple fish. According to the ply count, there is a significant decrease ($p \leq 0.05$) in the total number of plies from the head to the tail (**Figure 2.5.B**). Interestingly, there are also significant differences in scale thickness and number of plies between the individual fish.

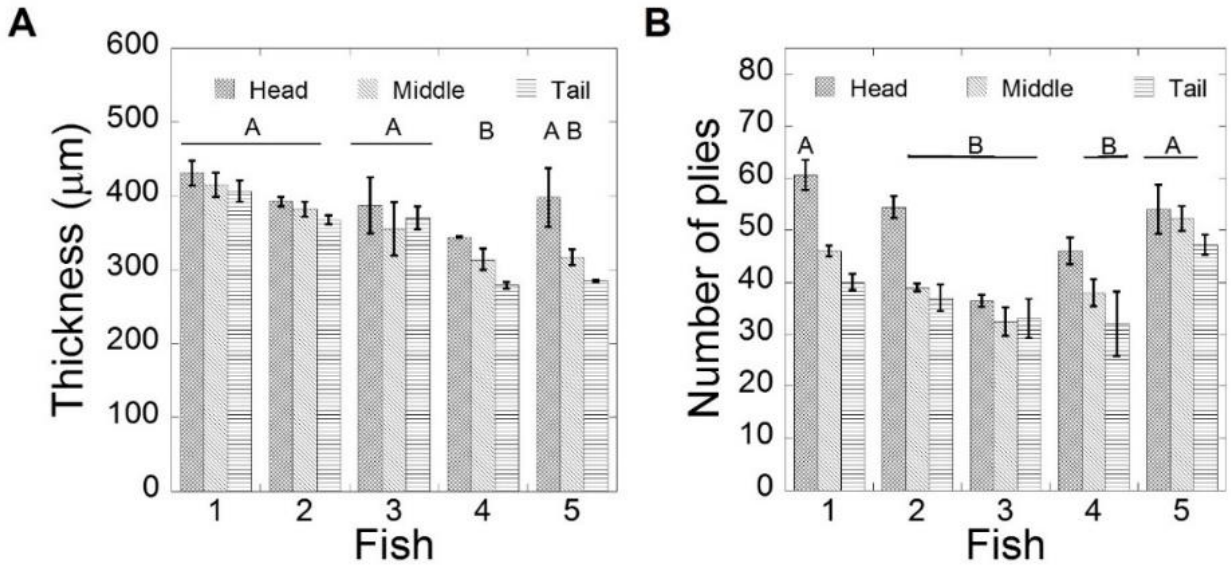

Figure 2.5. An analysis of microstructural characteristics of scales obtained from five different fish and within the three regions of evaluation. A) Scale thickness, B) total number of plies. Groups with different letters are significantly different ($p \leq 0.05$).

2.5 DISCUSSION

Fish scales have been purported to be so tough that they are difficult to tear, even after immersion in liquid nitrogen [41]. Nevertheless, results in **Figure 2.3.B** indicate that as the temperature decreased, the fish scales underwent a significant reduction in the critical tear force. Yang et al [37] reported on the mechanisms associated with deformation of fish scales in Mode I fracture at room temperature. Dissipation of fracture energy occurred through rotation and stretching of the collagen fibrils as well as via rotation and delamination of the individual plies. Those plies oriented transverse to the loading direction also undergo distributed delamination, which enables elongation at lower temperatures. Thus, the laminated scale structure appears to result in an apparent lower sensitivity to the decrease in temperature when evaluated by the work to fracture.

In contrast to the control, the scales with 0° orientation underwent a decrease in energy to fracture with reduction in temperature (**Figure 2.3.C**), which arises from the changes in critical tear force (**Figure 2.3.B**). The reduction in tear force could result from a diminished participation of the interchain hydrogen bonds of the transverse plies of the scales at the lower temperature. Alternatively, freezing of the water residing about the collagen could decrease the ability for the fibrils to undergo changes in orientation that placed them in tension, which is more favorable for resisting crack advance [51].

In comparing scales from the three regions, those from the head exhibited significantly greater tear resistance than the other two regions (**Figure 2.3.A**). In a previous investigation, the spatial variations were interpreted by ranking the need for protection and locomotion [52]. But there is a more practical explanation, which comes from the process of scale generation and maturation. Squamation[1] of scales in carp occurs first in the head region, followed by middle and then tail regions [53]. It is valuable to recognize that squamation patterns are not the same in all teleost and there is some belief that this process is initiated by mechanical stimuli [54]. The squamation chronology of cyprinodontidae shows that there is a lapse of 17 days between the appearance of the first scales in the head to those in the tail [55,56]. Furthermore, it takes 26 days to fully cover the body of the fish, a time in which differences between head and tail scales could be significant. Indeed, both the scale thickness and number of plies was greatest in scales of the head (**Figure 2.5**).

[1] Squamation is the process of formation of scales in the epidermis of the fish. The establishment of the squamation pattern has been described in several teleost species [53] In all fish species studied so far, the scales appear very late in ontogeny, i.e., after metamorphosis, when the juveniles are already miniatures of the adults.

The differences in tear energy (**Figure 2.3.A**) were not related to scale thickness as the tear energy accounts for this parameter. Regional differences in scale properties could also be a result of site-specific changes that arise during ontogeny, which influences the collagen distribution and its maturation [53]. Mineralization of fish scales begins once the scale is completely formed and proceeds downward from the limiting layer throughout the life of the fish [26,53,54]. This process results in development of the EE layer, which exhibits thicker plies due to their greater degree of mineralization. The more mineralized portion (EE) of the scales was found to exhibit the greatest variation in number of plies with anatomical position. The importance of the number of EE plies on the tear energy distribution of scales in the hydrated condition is shown in **Figure 2.6.A**. As evident in this figure, the energy to fracture increased with increasing number plies in the EE. The relationship between the IE ratio (ratio of IE thickness to total scale thickness) and the work to fracture is shown in **Figure 2.6.B**. Overall, there is an increase in the work to fracture with increase in the IE ratio.

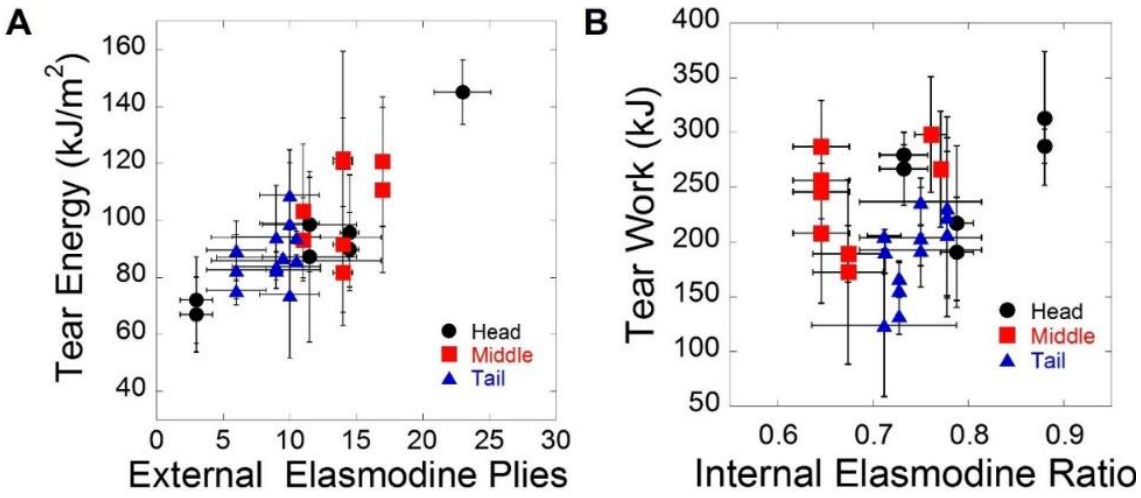

Figure 2.6. Relationship between the tear energy and the number of elasmodine plies. A) Influence of the number of external elasmodine plies on the energy to fracture. B) Influence of the internal elasmodine ratio on the work to fracture. The internal elasmodine ratio is the ratio of the number of plies in the internal elasmodine to the total number of plies in the scale.

The relationships evident in **Figure 2.6** are akin to those contributing to the performance of many engineered composites. Indeed, the number of mineralized layers of the elasmodine is critical to the fracture resistance of the scales. As shown in previous investigations of puncture resistance, the hard mineralized external layer is the first barrier against penetration [24]. The mineralized layer increases the resistance to local compressive forces, thereby bestowing greater puncture resistance than that of engineering polymers [57]. In addition, the ratio of EE and IE in the scale plays an important role as well. The function of the external plies of the EE is to protect the less mineralized layer from direct contact with the penetrating instrument, and to mitigate the stresses transmitted onto the underlying collagen layer by redistributing them over a large area. The primary function of the underlying collagen layers of the IE is in the localization of damage and in preventing its propagation throughout the scale. Considering the tear resistance (**Figure 2.6.B**), the IE appears to be essential to the work to fracture and operates to localize damage in the vicinity of the stress intensity.

One of the most important findings was the identification of differences in scale thickness and number of plies within the same species (**Figure 2.5**), and the importance of observed differences in microstructure on the mechanical behavior (**Figure 2.6**). The spatial variations in microstructure are important to the mechanical behavior of scales, and there appears to be some important connection with the signals controlling squamation, scale growth and its performance. Potential spatial variations in scale properties are easily overlooked, but should be considered in future studies of these interesting structural materials.

2.6 CONCLUSIONS

On the basis of results obtained, the following conclusions may be drawn:

1) The microstructure of fish scales is a function of the anatomical position. The total thickness and number of plies in the scales decreased from the head to the tail region. This distribution agrees with the squamation pattern for the *C. Carpio*.

2) At room temperature there were spatial variations in the tear resistance of scales obtained from the three characteristic regions evaluated. Those scales obtained from nearest the head required significantly greater energy to tear than those within the mid-length and tail regions. There was no significant difference between the tear energy of scales from the mid-length and tail.

3) There was a significant decrease in the resistance to fracture of the scales with reduction in temperature from ambient conditions to liquid nitrogen environment. Over this range in reduction of temperature there was a 75% decrease in the required work to fracture of the scales overall.

4) Scales obtained from the head region exhibited anisotropy, with the largest tear resistance obtained for tears oriented along the longitudinal direction. Those scales from the other two regions did not exhibit anisotropy. The unique behavior of the head scales appears to be attributed to the larger external elasmodine layer of scales from that region.

5) The tear energy of the scales was found to be strongly related to the number of mineralized plies of the external elasmodine layer. The tear resistance increased with increasing number of elasmodine plies and the total thickness of this layer.

2.7 ACKNOWLEDGEMENT

This investigation was supported in part by the University of Washington through seed funding (D Arola).

Chapter 3. Effects of polar solvents on the mechanical behavior of fish scales

3.1 SYNOPSIS

Fish scales are unique structural materials that serve as a form of natural armor. In this investigation the mechanical behavior of scales from the *Cyprinius carpio* was evaluated after exposure to a polar solvent. Uniaxial tensile and tear tests were conducted on specimens prepared from the scales of multiple fish extracted from near the head, middle and tail regions, and after exposure to ethanol for periods from 0 to 24 hours. Submersion in ethanol caused instantaneous changes in the tensile properties regardless of anatomical site, with increases in the elastic modulus, strength and modulus of toughness exceeding 100%. The largest increase in properties overall occurred in the elastic modulus of scales from the tail region and exceeded 200%. Although ethanol treatment had significant effect on the tensile properties, it had limited influence on the tear resistance. The contribution of ethanol to the mechanical behavior appears to be derived from an increase in the degree of interpeptide hydrogen-bonding of the collagen molecules. Spatial variations in the effects of ethanol exposure on the mechanical behavior arise from the differences in degree of mineralization and lower mineral content in scales of the tail region.

Keywords – *Cyprinus carpio*, fish scales, fracture resistance, mechanical behavior, polar solvents

3.2 INTRODUCTION

Elasmoid scales owe their exceptional compliance to the highly organic composition and their hierarchical structure. Scales consist largely of collagen type I fibrils arranged in unidirectional lamina. Consequently, the mechanisms of deformation are likely dependent on the covalent cross-linking of the fibrils and interpeptide hydrogen bonding, as well as the interactions between the mineralized crystals and fibrils. Due to the high organic content, changes in mechanical behavior are at least partially related to the modification of interpeptide bonding, which arises with the removal of water molecules by dehydration. New armor designs constructed from engineered materials may not have contributions from this component of intermolecular bonding to the deformation response. Thus, it is important to understand the contributions from dehydration to the mechanical behavior of scales.

A previous study on scales from the carp reported that in the hydrated condition, scales from the head exhibited a strength and toughness nearly twice that of those properties for the tail. Yet, after dehydration in air there were limited differences in the mechanical properties of scales as a function of anatomical position [23]. Changes in the mechanical behavior with dehydration of collagen-based structural materials is at least partially related to the increase in interpeptide bonding about the tropocollagen molecules with removal of the water molecules [58,59]. Dehydration of collagenous materials can be achieved by immersion in polar solvents. Water forms both intra- and inter-chain hydrogen bond bridges about the collagen molecules and peptides [60,61]. Gautieri et al [27] reported that the unique mechanical properties of collagen microfibrils originate from their hierarchical structure at the nanoscale, and the cross-linking between the tropocollagen molecules. Though hydrogen bonds are rather weak due to their lower energy in comparison to the covalent bonds, an adequate volume fraction of interpeptide bonds enabled by

removal of water can elicit substantial changes to the mechanical behavior of single fibrils [62], and dense fibril systems [63].

One limitation of the previous evaluations is that dehydration was achieved by free convection in air. That process results in removal of the free water molecules, but requires substantial time and does not remove bound water [64]. Air-drying of *A. gigas* scales resulted in a residual water content of 16% in comparison to 30% for the hydrated scale [8]. A problem that can be solved by the dehydration of the scales with polar solvents.

The effectiveness of polar solvents to form hydrogen bonds in collagen is often described in terms of the Hansen solubility parameter for hydrogen bonding (δ_h). Polar solvents with high $\delta_h$values preferentially form hydrogen bonds with collagen peptides, thereby preventing the molecules from developing interpeptide bonds. Water has one of the highest reported δ_h values for polar solvents 37.3 $(J/cm^3)^{1/2}$. In the absence of water, or when the matrix is immersed in solvents with below 19 $(J/cm^3)^{1/2}$, which is the value postulated for collagen in air [61], interpeptide hydrogen bonding occurs. Thus, exposure of the scales to ethanol with δ_h of 19 $(J/cm^3)^{1/2}$) is expected to cause an increase in the stiffness and strength of the scales due to the displacement of water molecules and development of interpeptide hydrogen bonds.

3.3 MATERIALS AND METHODS

Scales of the *Cyprinus carpio* (i.e. the common freshwater carp) were obtained by extraction from across the body of seven different fish after the methods of Garrano et al [6]. These fish were marketed as East Asian carp, and no additional information was available for record. The scales were obtained nearly equidistant between the ventral and dorsal aspects of the body and from three

regions including adjacent to the head, mid-length (beneath the dorsal fin) and near the tail (**Figure 3.1.A**). All of the scales were less than 1 mm thick and possessed a diameter that depended on the anatomical position. Scales from the head region had an effective diameter (d) ≥ 25 mm. Those obtained from the middle and tail regions ranged between 22 ≤ d ≤ 25 mm and 19 ≤ d ≤ 22 mm, respectively. After extraction, the scales were stored in Hanks Balanced Salt Solution (HBSS) at room temperature and evaluated within two weeks of harvesting the fish.

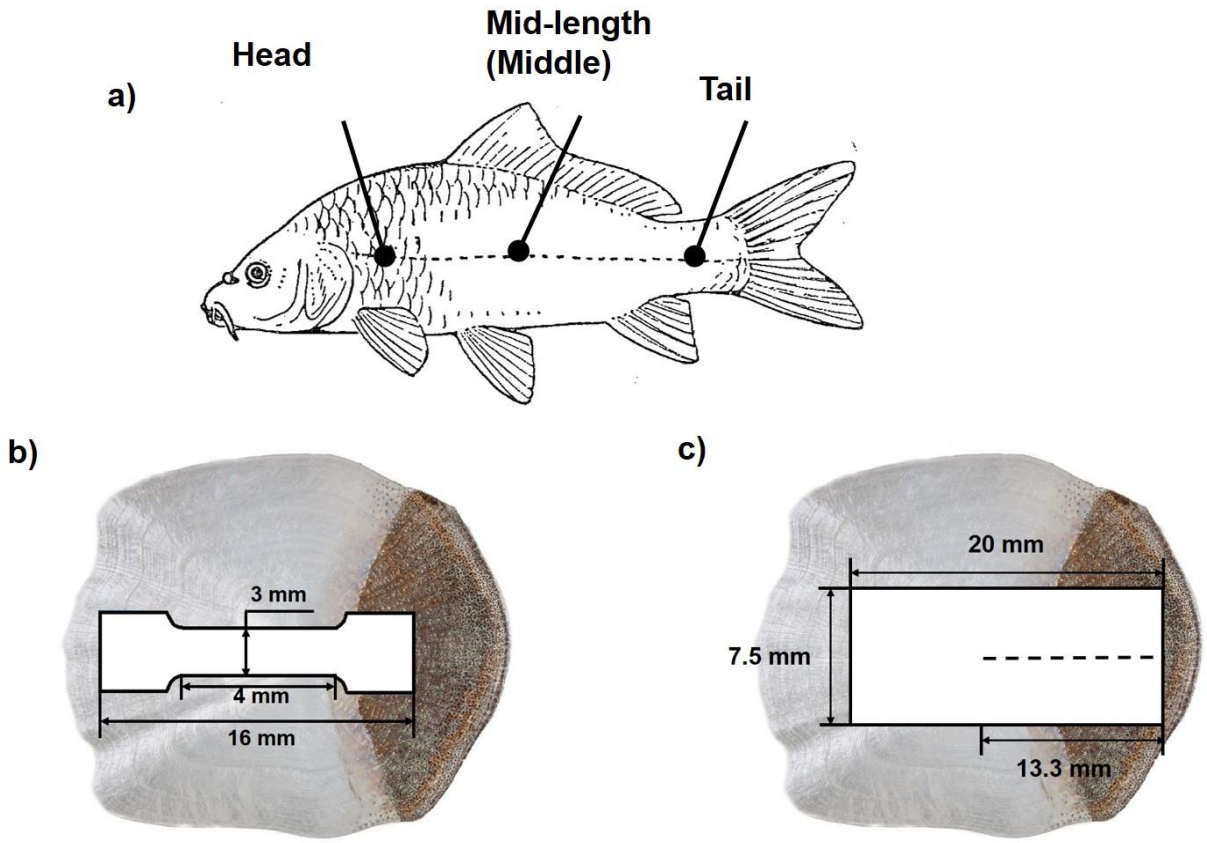

Figure 3.1. Details regarding the specimens prepared for characterizing mechanical behavior. A) Anatomical position of the extracted scales [1], B) extracted scale with location and geometry of the stamped tensile specimens, and C) geometry of the tear specimens.

Conventional dog-bone shaped tensile samples were sectioned from the scales using a punch and stamping process [21]. In recognition of the variation in thickness of the scales [22], a single sample was stamped from the center region of each scale where the thickness is most uniform. After the stamp process the gage section was measured to assess the change in thickness. Overall the thickness of the samples changed less than 50 μm in the gage section and as a general procedure the lowest value was used in the calculation of the stress. The specimens possessed a gage section length and width of 8 mm and 3 mm, respectively (**Figure 3.1.B**). All of the specimens were obtained with alignment parallel to the fish length, in recognition that the scales may exhibit anisotropy [1, 7, 11]. After sectioning, the specimens were returned to the HBSS bath at room temperature.

Tensile testing of the fish scale specimens was performed to failure while submerged in a liquid bath at room temperature. The loading was performed under displacement control using a dedicated universal testing machine complemented with a microscopic imaging system. The system has a full-scale load range of 50 N and load precision of 0.1%. A stroke rate of 0.2 mm/min was utilized, which corresponded to a strain rate of roughly $5x10^{-4}$ s^{-1} according to the specimen gage length. All specimens were tested to first ply failure/fracture following Garrano et al. [6]. Tension tests were performed after time-controlled storage of the scale in an ethanol bath at room temperature for periods of t = 0, 2, 4 8 and 24 hours. The exposure period for the t=0 hour condition consisted of approximately 5 min exposure. Additional tests were performed on hydrated scales tested in HBSS, which served as the control. Five specimens were prepared from each anatomical region (head, middle and tail) and for every hydration condition, which resulted in a total of approximately 90 specimens prepared and evaluated from each fish.

The axial strains that developed within the specimen gage section were obtained using Digital Image Correlation (DIC). Details regarding DIC and applications to hard tissues and microscopic DIC can be found in [21,23,24]. The outer surface of the scales is largely mineral (of the limiting layer), rendering it brittle in comparison to the internal elasmodine. Thus, the interior surface of the scale specimens was monitored during the tensile tests as described in [6]. The optical system consisted of a F32 5.6-11 C-mount objective lens, a 5mm extension tube and a CV-A1 CCD camera (JAI America Inc) with a coherent and uniform illumination system. Sequential images were acquired incrementally during each tensile test at a frequency of 0.1 Hz, which were synchronized with the load and displacement signal by computer control. The images were obtained with a spatial resolution of 1376×1035 pixels and 256 grey scales. The images encompassed an area of approximately 5.6x4.2 mm and were processed using sub-pixel resolution, which provided a displacement resolution of approximately 4 μm.

Mechanical properties of the scales were determined from results of the tension tests of each hydration condition using the engineering stress-strain definitions. The elastic modulus (E), strength (S) and modulus of toughness (MOT) were determined for each specimen. The elastic modulus was determined using the tangent method for strains less than 1% and the strength was defined by the maximum stress realized by the sample. The modulus of toughness was calculated by integrating the area under the stress-strain curves as a function of strain until first ply failure. Ply failure was identified by a sharp reduction in the axial load.

The influence of polar solvents on the mechanical behavior was also evaluated in terms of the resistance to fracture under Mode III shear. Trouser-shaped tear specimens were sectioned from the scales using a specially designed punch and stamp as previously described [7]. Similar to the

tensile specimens, the samples were stamped with respect to the longitudinal axis to minimize potential effects of anisotropy (**Figure 3.1.C**). Each sample was obtained from the center of the scale, such that crack extension occurred within the region of uniform thickness. After sectioning, the specimens were placed in a bath of HBSS or ethanol at room temperature.

Tear testing was performed under displacement control loading using a universal testing machine (Instron ElectroPuls E1000). The instrument's load cell has a full-scale range of 250 N and precision of 0.01%. To minimize elongation of the specimen outside the region of tear, 80-90% of the legs were clamped within the compression grips during the experiments. The testing was performed using a stroke rate of 100 mm/min until complete failure of the sample after previously established methods [7]. Tear testing was conducted with the samples immersed in a bath of HBSS or ethanol at room temperature. Results of the tensile tests in ethanol revealed that after immediate exposure, further changes with additional treatment time (up to 24 hours) were negligible. Therefore, tear testing was performed directly after submersion (corresponding to t = 0 hr.) and consisted of approximately 5 min exposure total. Consequently, eight samples were prepared from each anatomical position and for each hydration condition, resulting in an evaluation of 48 specimens taken from amongst the seven fish.

The energy required to tear the fish scales was estimated from the force-displacement curves of each specimen according to $T = 2P/t$, where P and t are the tearing force and specimen thickness, respectively [7, 25]. The maximum force was identified from the tear history. The work to fracture was also quantified by integrating the area under the force-displacement curves as a function of the tear displacement. Changes in mechanical properties as a function of position of the fish body

and period of ethanol exposure were evaluated for statistical significance using a Two-Way Analysis of Variance (ANOVA) and Tukeys HSD test at $\alpha = 0.05$.

The microstructure of scales within each region of evaluation was examined using optical microscopy (Olympus BX51, Tokyo, Japan) and scanning electron microscopy (JEOL, model JSM- 6010PLUS/LA, Peabody, MA). Samples from each of the three regions were sectioned in the transverse plane near the center of the scale. The sectioned scales were fixed in resin and polished with SiC abrasive paper from mesh numbers of 800 to 4000. Final polishing was performed with a diamond liquid suspension of 3 microns, followed by a liquid suspension of 1 micron Al_2O_3. The microstructure was observed over a range of magnification to distinguish important features. Those samples evaluated using the SEM were sputtered with platinum and observed in secondary electron imaging mode. In addition, an elemental analysis was conducted across the scale thickness using Energy Dispersive X-ray Spectroscopy (EDS) to quantify the chemical composition and the distribution of mineral content as a function of anatomical position. Nine discrete measurement locations were selected across the scale thickness, including one point in the limiting layer and the remaining points distributed across the elasmodine at roughly 0.15, 0.3, 0.4, 0.5, 0.6, 0.7, 0.8 and 0.9 of the normalized thickness.

3.4 RESULTS

Results of tensile tests performed on scales from the head region are shown in **Figure 3.2**. The responses in this figure span the range of ethanol storage times and include those obtained for the hydrated condition. As evident from the relative distribution of curves before and after treatment, exposure to ethanol caused an immediate and substantial increase in the stiffness and strength of

the scales. The changes continued with increasing duration of ethanol exposure, but they became negligible after approximately 8 hours of ethanol treatment.

The stress-strain curves obtained from the specimen of each scale were used in estimating the elastic modulus, strength and modulus of toughness. **Figure 3.3** presents cumulative results for the mechanical properties in the three regions of evaluation as a function of ethanol exposure up to 8 hours of exposure. Specifically, **Figure 3.3.A** shows the importance of ethanol treatment and period of storage on the elastic modulus. There was a significant increase ($p \leq 0.05$) in the elastic modulus after immediate exposure to ethanol in all three regions evaluated. The largest change occurred in scales of the tail region, with an average increase of up to 150%. Prolonged exposure to ethanol did not cause further significant changes in the elastic modulus ($p > 0.05$). Results for the strength and the modulus of toughness are shown in **Figure 3.3.B** and **Figure 3.3.C**, respectively. There was a significant increase ($p \leq 0.05$) in both properties with immediate exposure to the ethanol. Further increases were realized for approximately two hours of exposure. However, after two hours ($t > 2$ hours) there was no further increase in the strength or MOT ($p > 0.05$).

Although both the strength and MOT exhibited similar responses after ethanol exposure, there were differences with respect to the anatomical position. The strength of scales from the middle and the tail were not significantly different from each other ($p > 0.05$), but they were significantly lower than that of the head scales ($p < 0.05$). For the MOT (**Figure 3.3.C**), results for scales from the head, middle region and tail were significantly different from each other ($p < 0.05$). It is important to note that the increase in stiffness and strength was not accompanied by a decrease in strain to failure. Rather, there was a significant increase ($p < 0.05$) in the strain at fracture after exposure to ethanol in comparison to the fully hydrated scales (not shown).

The effect of ethanol exposure on the fracture resistance of the scales was evaluated in terms of the tear energy. The energy required for fracture is shown for selected specimens from scales of the head, middle and tail regions in **Figure 3.4.A** through **Figure 3.4.C**, respectively. The responses presented in these figures include those obtained after immediate exposure to ethanol, and for the hydrated condition (i.e. in HBSS) as well. As evident from the tear responses, the fracture process was stable in both conditions of hydration and in all three regions of evaluation. In addition, the responses for the hydrated and dehydrated conditions appear to be similar.

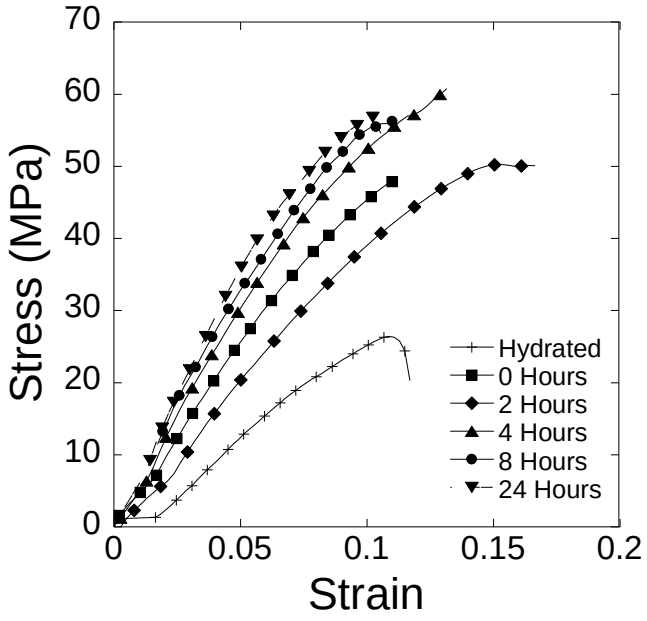

Figure 3.2. Representative stress-strain curves resulting from tensile tests performed on the scale specimens after ethanol treatment for periods of 0 to 24 hours. Results for the hydrated condition (in HBSS) are shown for comparison. The responses in this figure were obtained from scales of the head region.

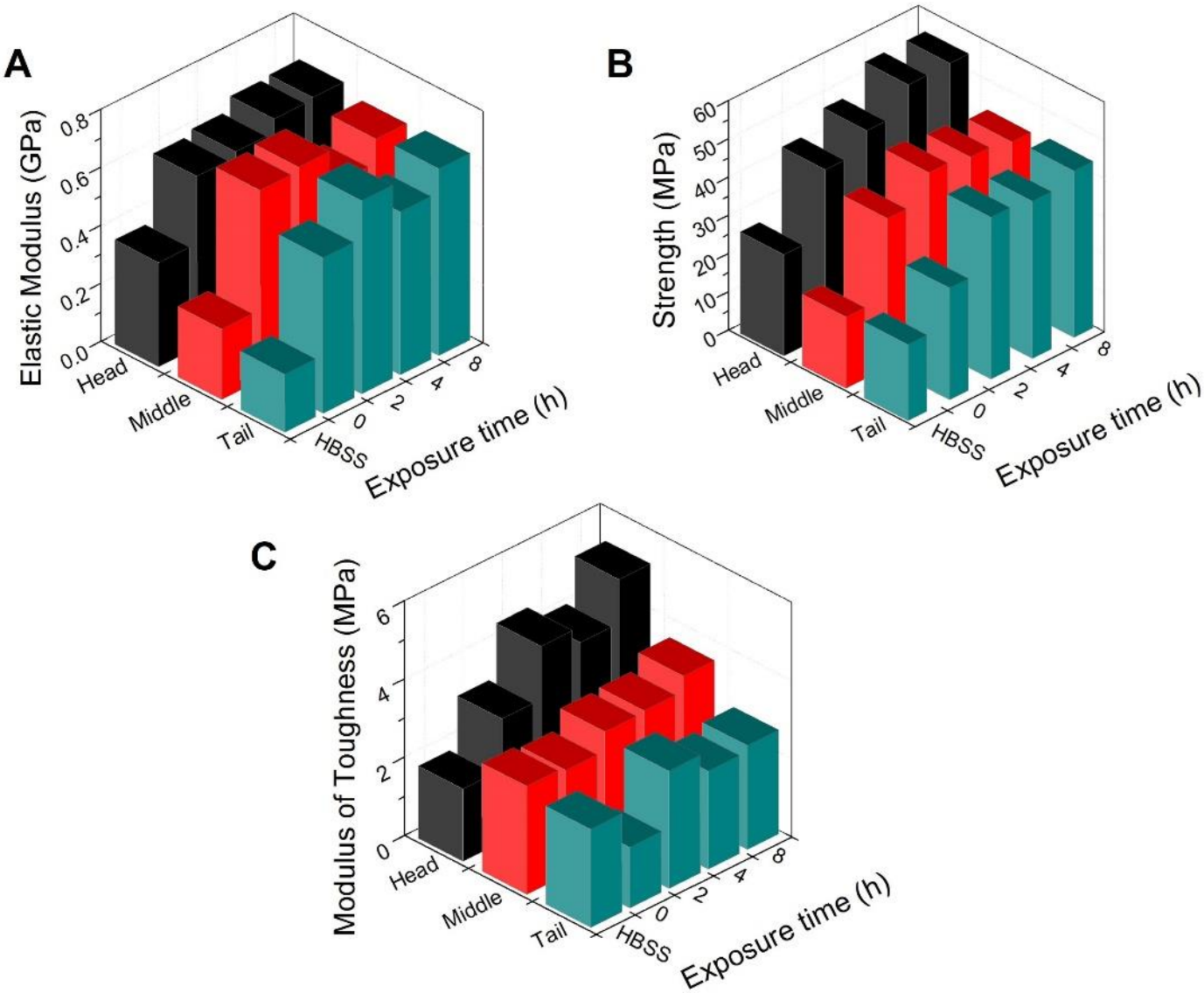

Figure 3.3. Importance of ethanol exposure time on the mechanical behavior of the scales under uniaxial tension. A) Elastic modulus, B) strength, C) modulus of toughness.

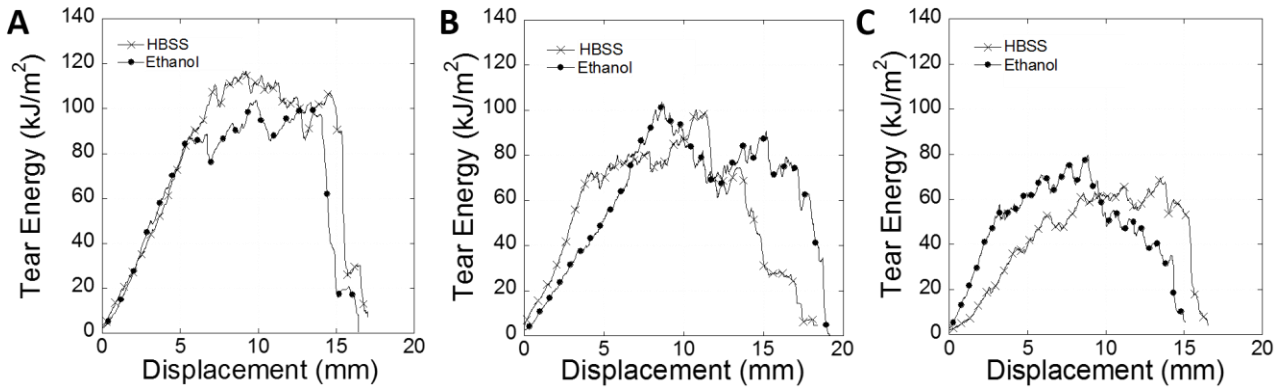

Figure 3.4. Representative load vs. load-line displacement responses from the tear tests performed on scales from the A) head, B) middle and C) tail regions. Results for the ethanol treatment correspond to immediate exposure (0 hrs.).

A summary of results for the fracture resistance is shown in **Figure 3.5**. Specifically, **Figure 3.5.A** shows the cumulative results for the tear energy as a function of hydration in the three regions of evaluation. Analogous results for the tear work are shown in **Figure 3.5.B**. Note that results obtained for the scales subjected to ethanol treatment corresponded to a storage period of t=0 hrs. (immediate response). Clearly the influence of ethanol treatment on the fracture resistance in Mode III loading was not consistent with that for tensile loading. For instance, for scales from the head there was a significant reduction ($p < 0.05$) in the tear energy and work to tear of with exposure to ethanol. In contrast, there was a significant increase ($p < 0.05$) in both the tear energy and work required to tear for scales from the middle region, whereas there was no significant difference ($p > 0.05$) in the tear resistance caused by exposure to ethanol for scales of the tail. When compared as a function of location, there is a reduction in the resistance to fracture of the scales from the head to the tail in the hydrated condition. Yet, the spatial distribution of the responses changes after exposure to ethanol. In terms of the tear energy, scales from the tail exhibited significantly lower values ($p \leq 0.05$) than the head and middle regions. But when evaluated in terms of the work, there was no significance difference ($p > 0.05$) in the tear resistance between the scales of the head

and tail regions after ethanol exposure. Scales from the middle region exhibited the greatest tear resistance overall.

Figure 3.6 shows the elemental composition of the scales in the three regions of evaluation. The composition was evaluated at nine discrete locations as described in **Figure 3.6.A**, with one point located in the limiting layer and the remainder distributed over the remaining thickness of the elasmodine as a function of normalized distance. Results of the EDS analysis showed that the four main elements detected were Phosphorus, Calcium, Oxygen and Carbon. The mineral portion of the scales consisted of calcium deficient hydroxyapatite, as reported previously [6, 13]. The relative presence and distribution of the major elements over the thickness of scales from the head region is shown in **Figure 3.6.B**. The Phosphorus and Calcium content were greatest within the limiting layer and decreased with distance from this layer within the elasmodine. A comparison of the elemental composition for scales from the three regions of evaluation is presented in **Figure 3.6.C-F**. Clearly the presence of Phosphorus (**Figure 3.6.C**) and Calcium (**Figure 3.6.D**) is limited to the region adjacent to the limiting layer, especially in scales from the middle and tail regions.

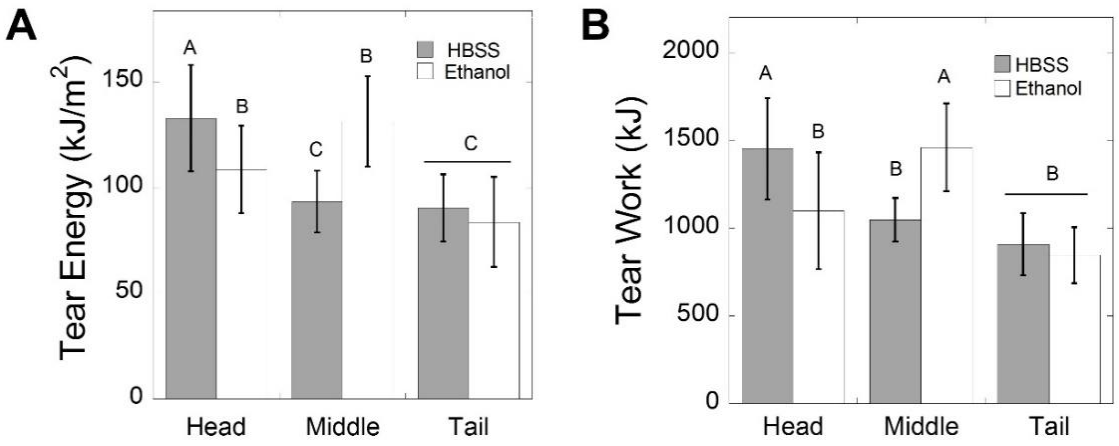

Figure 3.5. Importance of ethanol exposure on the resistance to fracture of the scales under Mode III tear loading. A) energy to failure, B) work to failure. Columns with different letters are significantly different ($p \leq 0.05$).

3.5 DISCUSSION

Previous studies concerning the structural behavior of fish scales have identified that the mechanical properties are dependent on the level of hydration and that a reduction in water content results in an increase in stiffness, strength and toughness [6, 12, 13]. Also relevant to the behavior of elasmoid scales, Garrano et al [6] noted that the properties of scales from *Cyprinus carpio* are dependent on the anatomical position. When fully hydrated, scales from the head exhibited a strength and toughness nearly twice the values of those properties for the tail, whereas after dehydration in air there were limited differences in the mechanical properties of scales obtained from over the entire length of the fish. Those findings are not consistent with the distribution of properties resulting from chemical dehydration by ethanol treatment in **Figure 3.3**. While the elastic modulus of scales from all three regions increased to the same maximum value, both the strength and MOT continued to exhibit differences with location after ethanol treatment. The effects of ethanol on the mechanical behavior and importance of spatial variations in microstructure on the observed responses require further discussion.

One of the primary contributions to the changes in properties with ethanol treatment is the development of interpeptide hydrogen bonds about the tropocollagen molecules. Water forms both intra- and inter-chain hydrogen bond bridges about the collagen molecules and peptides [26, 27]. When the water is displaced by ethanol (a weaker hydrogen-bond-forming solvent), it allows direct hydrogen-bonding between the peptide chains. That results in a greater number of interpeptide hydrogen bonds at the molecular level, which in turn promotes stiffening at the macroscopic level. This mechanistic description is supported by the experimental results. Previous studies conducted with demineralized dentin have demonstrated this behavior as well and the importance of the solvent's δ_h [26, 29, 30]. Maciel et al [29] showed that chemical dehydration

by polar solvents is a time dependent process and that the removal of water requires time. Indeed, there were instantaneous changes in the mechanical behavior of the scales, but they continued over time with diffusion of the miscible solvent (**Figure 3.2**).

It is helpful to consider the changes in mechanical behavior resulting from ethanol exposure with regards to the hydrated condition. **Figure 3.7** shows the relative change in uniaxial properties with chemical dehydration after being normalized by the responses in HBSS. In **Figure 3.7.A**, the increase in elastic modulus of scales from the tail exceeds a factor of three, which is the largest of all changes documented. The elastic modulus of scales from the remaining two regions also increased with ethanol treatment, but to a lesser extent. After roughly 8 hours in ethanol the elastic modulus reached an equivalent plateau in the three regions (**Figure 3.3.A**), which is consistent with dehydration in air [6]. The air-dried [6] and ethanol-treated carp scales exhibit similar values of elastic modulus (0.4-0.8 GPa), which may be expected due to the consistency in the Hansen solubility parameters for ethanol- and air-dried collagen.

What could cause the spatial variations in the degree of changes in elastic modulus with ethanol treatment? The difference in "stiffening" between the head, middle and tail regions is expected to arise from the spatial distribution in mineral (**Figure 3.6**) and its interference with the hydrogen bonding. For instance, Pashley et al., [26] reported an increase in stiffness of fully demineralized and hydrated dentin of over 12 times when exposed to acetone. In the hydrated condition, the stiffness of scales is primarily dependent on the number of highly mineralized plies of the external elasmodine, which decreases from head to tail [7]. The mineral has been described as partially "shielding" the collagen in the hydrated tissues, and a reduction of load accommodated by the collagen [31]. The higher mineral content of scales from the head region (**Figure 3.6**) resulted in

larger stiffness in the hydrated condition (based simply on the rule of mixtures), but also limited the extent of additional hydrogen bonding during ethanol treatment. Increasing mineralization displaces water from collagen and the mineral crystals are also sites for water to bind [27]. Here we believe that the mineral interfered with the process of interpeptide hydrogen bonding in the presence of ethanol, which decreased the degree of stiffening overall.

Figure 3.7.B shows the normalized changes in strength with ethanol treatment. There was a uniform increase in strength of approximately a factor of two with respect to the hydrated condition for all three regions. Due to the uniformity in strengthening across the body of the fish, the head scales exhibited significantly larger strength ($p \leq 0.05$) than the other two regions after completion of the chemical dehydration. The increases in strength are lower than those for the modulus, which agrees with the results for chemical dehydration of demineralized [26] and fully mineralized [31] dentin. Surprisingly, the increase in strength of the scales is nearly equal to that reported for dentin. Furthermore, chemical dehydration by ethanol was more effective at promoting an increase in strength than dehydration in air [6]. As the effectiveness of air-drying is a function of the ambient humidity, the larger increase in strength by ethanol treatment are expected and results from the larger volume fraction of hydrogen bonds achieved by the polar solvent.

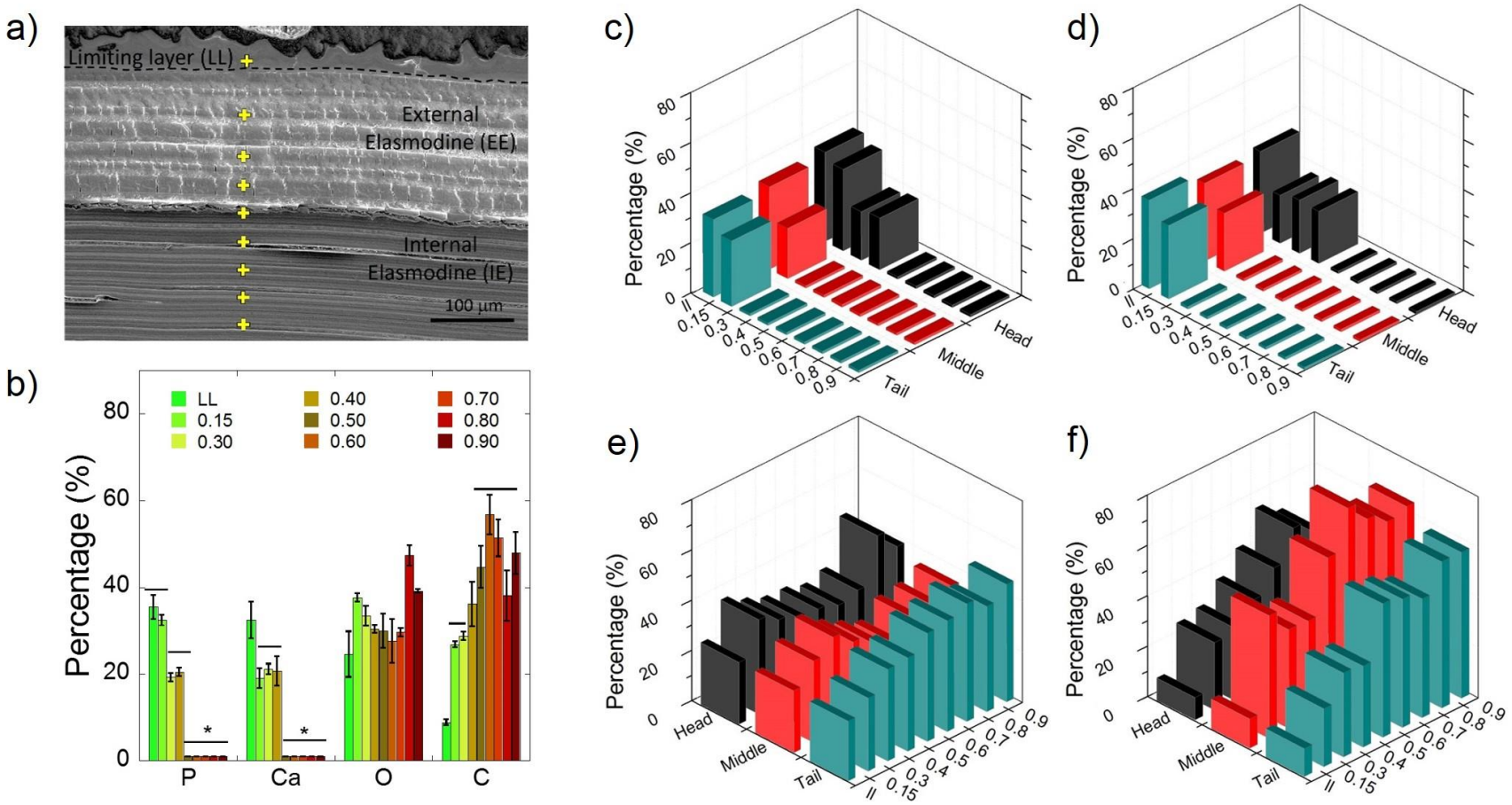

Figure 3.6. Evaluation of the elemental composition of the scales and the differences with location. A) Micrograph from a head scale distinguishing the limiting layer (LL), as well as the internal (IE) and external elasmodine (EE). The series of points across the scale thickness represent the approximate locations for EDS analysis. The measurement depth from the LL was normalized with respect to the combined thickness of the external and internal elasmodine layers. B) Distribution of elements over the thickness of the head scales. Columns with different bar are significantly different. A comparison of the elemental distributions for the three regions of evaluation (head, middle and tail) is shown in C-F. Elemental distributions for C) Phosphorus, D) Calcium, E) Oxygen, and F) Carbon are shown across the scale thickness. Note that there is no Phosphorus or Calcium in the internal elasmodine and the bars are shown for completeness across the thickness.

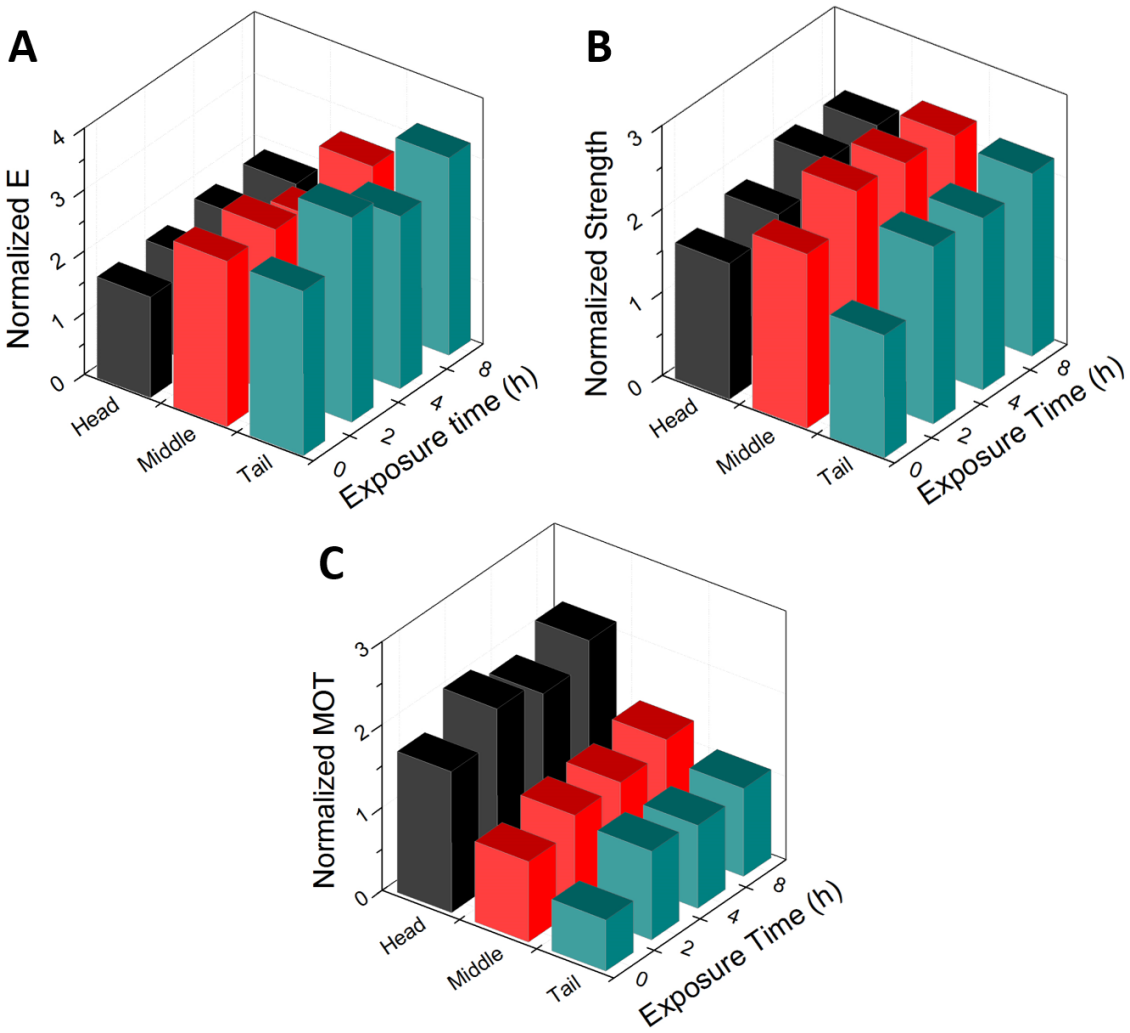

Figure 3.7. Normalized mechanical behavior of the fish scales under uniaxial tension after exposure to ethanol with respect to the hydrated state: A) elastic modulus, B) strength, C) modulus of toughness.

The distribution of normalized modulus of toughness after ethanol treatment is shown in **Figure 3.7.C**. Consistent with the changes in strength with dehydration, the largest increase in the MOT was approximately a factor of two. However, in contrast to the other properties, the maximum increase in toughness occurred to scales from the head region and not the middle or tail. We expect that this difference in behavior of the MOT is attributed to its dependence on sliding of the collagen molecules. Replacement of the water with weak hydrogen-bonding polar solvents not only promotes interpeptide bonding, but may also change the structure of the collagen [30, 31]. This

disruption in molecular structure would undoubtedly interfere with the sliding of fibrils and potentially improve the effectiveness of the mineral platelets in providing resistance to inelastic deformation.

One interesting finding is that chemical dehydration of the scales with ethanol resulted in a higher modulus of toughness than dehydration in air [6]. Scales of the head exhibited a modulus of toughness of 3.5 MPa after 24 hours in air, which is substantially lower than the maximum obtained for ethanol treatment of the head scales in **Figure 3.3.C** (5.5 MPa). Besides the influence of humidity in air-drying, there are two additional contributing factors. Both forms of dehydration (air and polar solvents) enable the development of interpeptide hydrogen bonds, which increase the resistance to sliding of the molecules. However, the ethanol also serves as a molecular lubricant and facilitates the rapid redevelopment of new hydrogen bonds with the nearest interpeptide neighbors without fracture. Free convection is not as efficient at removing the unbound water (related to ambient humidity), and does not result in removal of bound water. In contrast, polar solvents are able to remove free and even some bound water [28]. Nyman et al. [27] noted that the modulus of elasticity and strength of cortical bone were inversely correlated with the degree of bound water, whereas the toughness of bone was inversely correlated with free (mobile) water. Bone possesses a much higher mineral content than fish scales, and the differences in water content were associated with difference in age not dehydration by ethanol treatment. Hence, bone may not serve as an appropriate model for fish scale collagen. Nevertheless, it is clear that the presence of a fluid layer is essential to the toughness of collagen-based materials due to its contribution to plasticization of the fibrils [18, 29, 31].

In a recent study on the importance of temperature to the fracture resistance of carp scales under Mode III loading, the largest energy to fracture overall was exhibited by scales of the head region [7]. The resistance to fracture was found to correlate with the thickness of the external elasmodine and the number of highly mineralized plies of this region [7]. The resistance to fracture decreased with temperature and was speculated to result from the lower compliance of the scales, which prevented realignment of the fibrils to the direction of principal stress. Nalla et al [18, 31] found that chemical dehydration of dentin using polar solvents caused a significant increase in the fracture resistance of dentin under Mode I loading. The fracture toughness nearly doubled after submersion in alcohol with respect to the response in the fully hydrated condition (HBSS) and the process was also shown to be reversible with rehydration of the tissue. In those studies the rise in fracture toughness resulted from an increased potency of the extrinsic mechanism of toughening, which largely occurs as a result of the unbroken posterior bridging ligaments operating behind the crack tip. Although chemical hydration increased the stiffness and strength of the more highly mineralized scales of the head, the resistance to fracture decreased.

The fracture resistance of tissues under Mode III loading (i.e. the tear resistance) is rather seldom studied in comparison to Mode I. It does represent a very relevant mode of performance, especially in the assessment of very compliant systems. In Mode I, the direction of principal stress is coincident with one of the principal ply orientations. However, in Mode III the direction of principal stress is out of plane of all the plies and requires substantial reorientation of the collagen fibrils to align with the direction of maximum tensile stress. Yang et al [1] recently evaluated the tear resistance of skin in tension and observed that it is nearly impossible to tear notched samples. They found that the remarkable tear resistance is attributed to straightening of the fibrils and reorientation to the tensile direction, elastic stretching and interfibrillar sliding. Reorganization

and sliding of the fibrils are responsible for a redistribution of stress that causes notch blunting. Here is where we may understand the rather unexpected tear response of the head scales after ethanol treatment. If the tear resistance is dependent on fibril reorientation, it is perceivable that the combination of interpeptide bonding and larger mineral content inhibited this process. Indeed, the significant reduction in tear resistance of scales with reduction in temperature is at least partly due to the reduced mobility of fibrils and inability to undergo reorientation [7]. There was no significant difference in the tear resistance of scales from the tail in the HBSS and ethanol environments. Due to the low mineral content (**Figure 3.6.B-C**) of scales from this region, fibril reorientation should have been encumbered the least. It is plausible that intermolecular hydrogen bonding is less effective under large deformation due to the reduction in volume fraction of interpeptide bonds, and additional mechanisms of reinforcement become essential. Though speculative, that appears to be responsible for the significantly greater fracture resistance after ethanol treatment of scales from the middle region.

Results from this investigation have provided additional understanding regarding the effects from removal of water and molecular bonding to the mechanical behavior of fish scales. New findings were obtained regarding the relative importance of mineral content and molecular bonding to stiffness, strength and fracture resistance. Nevertheless, there are recognized limitations to the investigation that are important to consider. Ethanol was chosen for chemical hydration of the scales according to its application in other studies. Ethanol also has similar δ_h to that for collagen in air and provided an effective basis for examining the importance a fluid layer in chemical dehydration. Future work performed using polar solvents with $\delta_h < 19$ $(J/cm^3)^{1/2}$ could provide additional understanding. In addition, the degree of bound water removed from the collagen was not measured, which prevents the development of a complete understanding concerning the

mechanisms responsible for the changes in properties. There are techniques for measuring the bound water content in tissues [32, 32], and correlations have been established between this water and the mechanical properties of bone [27].

In bone, there are many layers of loosely and tightly bound water [34]. At the molecular scale, bound water molecules are trapped within and between the chains of the tropocollagen molecules, as well as within the apatite mineral structure (regarded as "structural water"). Water located in these individual compartments requires different levels of energy for removal. Far less is known regarding the layers of bound water in fish scale collagen. Thus, the difficulty of displacing the water in fish scales using polar solvents and the amount of remaining bound water after ethanol treatment are unknown. Future studies aimed at understanding the contributions of the bound water layers and mechanical behavior of fish scales may be fruitful, especially if the removal can be used to tune the mechanical behavior according to desired performance.

3.6 CONCLUSIONS

Elasmoid scales of the *Cyprinus carpio* were subjected to chemical dehydration by exposure to ethanol. The mechanical behavior of the scales was evaluated before and after ethanol treatment in uniaxial tension and via Mode III loading to fracture. Ethanol treatment caused an immediate increase in all components of the tensile response and additional secondary changes that reached stability after approximately two hours of exposure. Although the maximum elastic modulus, strength and toughness were exhibited by scales of the head region, the largest increase in these properties with ethanol treatment occurred to scales of the tail; the change was inversely proportional to the mineral content. There were significant and region-dependent changes in the fracture resistance of the scales with ethanol treatment, but they did not correlate with the degree

of mineralization. Results indicate that interpeptide hydrogen bonding is important to the mechanical behavior of collagen tissues and that the relative contribution to mechanical behavior is also a function of mineral content. The modulus of toughness was the only property that increased with interpeptide hydrogen bonding and an increasing degree of mineralization.

3.7 ACKNOWLEDGEMENTS

This research was supported in part by seed grants from the University of Washington, Colciencias by contract 0210-2013, the Natural Science Foundation of Anhui Educational Commission (No.KJ2014A017), and the Ministry of education scientific research foundation for Returned Overseas Students (No.2015KJS010003) and OEIAM (No.201409).

Chapter 4. The natural armors of fish: a comparison of the lamination pattern and structure of scales

4.1 SYNOPSIS

Fish scales exhibit a unique balance of flexibility, strength and toughness, which is essential to provide protection without encumbering locomotion. Although the mechanical behavior and structure of this natural armor are of recent interest, a comparison of these qualities from scales of different fish species has not been reported. In this investigation the armor of fish with different locomotion, size and protection needs were analyzed. Scales from the *Arapaima gigas*, the tarpon (*Megalops atlanticus*) and the carp (*Cyprinus carpio*) were compared in terms of the stacking sequence of individual plies and their microstructure. The scales were also compared with respect to anatomical position to distinguish site-specific functional differences. Results show that the lamination sequence of plies for the carp and tarpon exhibit a Bouligand structure with relative rotation of 75° between consecutive plies. The arapaima scales exhibit a cross-ply structure, with 90° rotation between adjacent plies. In addition, results indicate that the volume fraction of reinforcement, the number of plies and the variations in thickness with anatomical position are unique amongst the three fish. These characteristics should be considered in evaluations focused on the mechanical behavior.

Keywords – Armor, collagen, fish scales, nature, stacking sequence.

4.2 INTRODUCTION

Engineered composites of ceramics, metals and polymers are designed to achieve a combination of specific stiffness and strength that are not available from the individual constituents alone. Interestingly, the biological structural materials in nature are composites by design, and have developed over centuries of evolution. These structural materials generally follow a common pattern in combining organic (soft) and inorganic (hard) materials, which are organized according to a hierarchical architecture to achieve incredible combinations of strength and toughness [9,41,57,65,66]. Despite the consistency in the constituents amongst most of nature's composites, by virtue of variations in their microstructure they achieve a range of properties that rivals that of engineered materials.

The mechanical behavior of fish scales has been the primary focus of most investigations in this area. Studies have been reported on the puncture resistance [24,29], hardness [8], tensile strength [8,23,24,30,31,33,37,39] and resistance to fracture [10,28,67]. While some have identified that the scales exhibit mechanical anisotropy, the reported degree of anisotropy is not consistent (Table 4.1). For example, in an evaluation of scales from the *Morone saxatilis* or striped bass, Zhu et al. (2012) found that the maximum strength (~60 MPa) was perpendicular to the longitudinal axis of the fish [24]. In contrast, the maximum strength of scales from the *Arapaima gigas* (~30 MPa) [37] and *Megalops atlanticus* (~20 MPa) [31] is reportedly parallel to the longitudinal axis of the fish. Moreover, in scales from *Cyprinus carpio,* the anisotropy was found to depend on anatomical position, with scales near the head exhibiting higher resistance to fracture in the longitudinal direction than in other orientations and locations [67]. Differences could be attributed to many factors. The most likely contribution is the unique microstructure of the scales from each fish, and

their functional requirements in relation to their habitat and principal predators. But in comparison to the efforts focused on mechanical behavior, the microstructure of these natural composites and important differences between fish have not been explored in detail. Therefore, an evaluation of the laminate system of scales from teleost that covers different levels of need for protection (based on threat) and locomotion (based on speed) is highly desirable.

Table 4.1. Summary of mechanical and structural properties previously reported on elasmoid scales

Fish	**Direction of maximum strength**	**Tensile strength (MPa)**	**Ply orientation**	**Source**
Pagrus major	---------	~90	Orthogonal	Ikoma et al., 2003
Cyprinus carpio	---------	~30 (Head scales)	---------	Garrano et al,. 2012
Morone saxatilis	perpendicular	~60	Orthogonal	Zhu et al.,2012
Megalops atlanticus	parallel	~20	Boulligand (60°)	Gil-Duran et al., 2016
Arapaima gigas	parallel	~30	Boulligand (angles between adjacent lamellae vary)	Yang et al., 2014

4.3 MATERIAL AND METHODS

Scales were obtained from the bodies of three different fish including the *Cyprinus carpio* (i.e. freshwater carp), the *Megalops atlanticus* (i.e. tarpon), and the *Arapaima gigas* (i.e. Pirarucú). The carp represents the control for our study. Being raised in captivity, this fish currently has no natural predators and special needs for locomotion or protection. The *Megalops atlanticus* (Atlantic tarpon) inhabits both fresh and salt waters of the Atlantic. With a top speed of near 7 kph it is one of the ten fastest fish of the world. Speed is important for evading predators and feeding. Lastly, the *A. gigas* is one of the largest freshwater fish in the world and inhabits the Amazon River Basin

in South America. In previous reports in this field the *A. gigas* has been identified as “arapaima”, and to maintain consistency it will be regarded as such here. The scales of the arapaima are credited with protecting this fish from attacks of the piranha [32] and have enabled it to survive for centuries.

All three of these fish are teleost and possess elasmoid scales. Carp scales were extracted from farmed fish marketed as East Asian carp. In comparison, the tarpon and the Arapaima were wild fish captured in the Caribbean Sea and the Amazon River, respectively. For the studied fish, no additional information was available for record. One of the differences between these three teleost is their overall size at maturity [68–70]. According to their weight (3.4, 5.5 and 20 kg, respectively) and length (53, 75 and 157 cm, respectively) the fish ranged between 3 to 6 years of age, indicating that each had reached maturity. In order to compare the scales objectively, it was necessary to have a similar reference system beyond size and weight. During the process of growth, a specific number of scales emerge from the epidermis covering the body of the fish. Afterwards, the existing scales increase their size during the maturation of the fish [70,71]. Thus, the scale count along the lateral line was recorded and served as a reference in the process of extracting the scales. There were 38, 45 and 55 scales on the lateral line for the carp, tarpon and Arapaima, respectively.

Scales were extracted from the body of each fish within three characteristic regions, including adjacent to the head, mid-length and near the tail (**Figure 4.1.A**). To be consistent, these regions were defined at distances from the gill plate of 15%, 40% and 80% of the total number of scales along the lateral line. In recognition of possible variations in the scale structure, four scales were obtained in each region as shown in **Figure 4.1.B**; scales 1 and 3 are along the lateral line of the

fish, and scales 2 and 4 were above and below the lateral line, respectively. After extraction, the scales were stored in Hanks Balanced Salt Solution (HBSS) at room temperature and were fixed within a week of harvesting the fish for further evaluation.

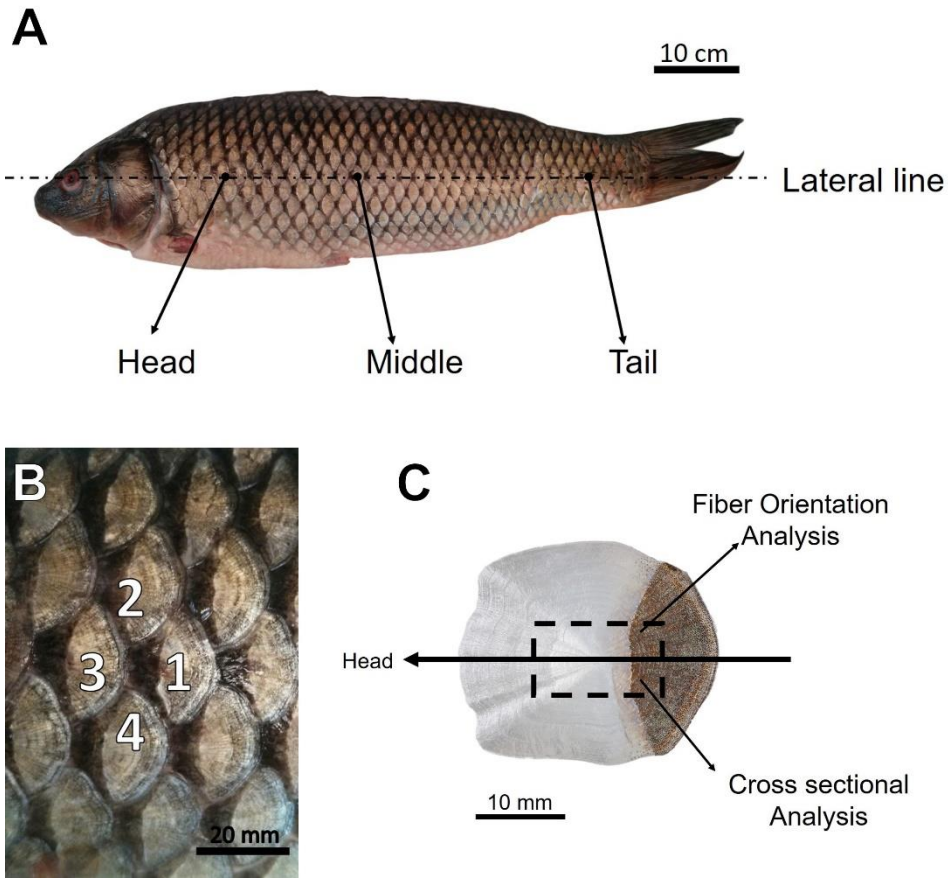

Figure 4.1. Details of the scale samples evaluated, including preparation and analysis. A) The three anatomical positions of the extracted scales (head, middle and tail). In each location, four adjacent scales were extracted (B, head region). Scale numbers 1 and 3 are on the lateral line of the fish. C) An extracted scale with description of the locations used for analyzing the fiber orientation and cross section. Note that the 0° fiber orientation corresponds to the longitudinal axis of the fish and all angles are defined according to clockwise rotations from this axis.

The comparison of scales from the three fish included an evaluation of the ply orientations, the lamination stacking sequence and the overall microstructure. Therefore, the scales were divided into two equal parts along the centerline. Half of the scale was used for conducting the ply rotation

measurement and the remaining half was used to evaluate the cross-section, including the overall thickness, number of plies, thickness of the individual sections (i.e. limiting layer and elasmodine), and the depth of mineralization from the limiting layer. In recognition of potential variations in thickness of the scales [29], cross sectional samples were cut where the thickness is most uniform as indicated in **Figure 4.1.C.** The scales were fixed by submerging them in 2% glutaraldehyde buffered with 0.1 M sodium cacodylate with pH=7.2 for 4 h. They were then rinsed in 0.1 M sodium cacodylate buffer followed by post-fixation in 1% osmium tetroxide buffered with 0.1 M sodium cacodylate for 2 h. After rinsing, the scales were dehydrated through an ascending ethanol series from 50 to 95%, followed by 100% of acetone and instant dehydration in 2,2-dimethoxypropane (DMP) for 5 h. Instant dehydration and rinsing with 100% acetone was followed by infiltration of the scales in Mollenhauer resin. To expose the microstructure, the cross-sectioned samples were trimmed and faced with a microtome using a glass knife (Leica EM UC6 Ultramicrotome, Vienna, Austria). To evaluate the ply orientations and rotations, the natural curvature of the scales after dehydration resulted in a bias angle that allowed the measurement of all the layers within a single viewing plane. The samples for fiber orientation measurement were polished with SiC abrasive paper from mesh numbers of #800 to #4000. Final polishing was performed with a liquid suspension of 3 micron diamond, followed by a liquid suspension of 0.04 micron Al_2O_3.

Samples were sputtered with Au/Pd and the microstructure of scales within each region of evaluation was examined with a scanning electron microscopy (SEM) in secondary electron imaging mode (JEOL, model JSM- 6010PLUS/LA, Peabody, MA). Final measurements of the ply rotation angles and distribution of ply thickness were obtained by post-processing of the SEM

images using cellSens (Olympus, Tokyo, Japan). All angles were measured clockwise (cw) from the longitudinal axis of the fish, which was defined as the reference (**Figure 4.1.C**).

4.4 RESULTS

A cross-section view of a representative scale from the tarpon is shown in **Figure 4.2.A**. The limiting layer and the individual plies of the elasmodine are clearly evident. There is also a gradient in the degree of mineralization that is apparent beneath the LL, which is reflected by the change in contrast in the micrograph with depth and divides the elasmodine into two distinct regions. A more detailed view of the lamination pattern of the elasmodine for representative scales from each fish is shown in **Figure 4.2.B**. According to a comparison of the micrographs in this figure, there are two important findings to highlight. Firstly, the average ply thickness in the three scales is not equivalent. For instance, the average ply thickness in the Arapaima is approximately 30 μm and is nearly five times that of the carp. Secondly, the carp and tarpon scales appear to share a similar arrangement of adjacent plies, resulting in a stacking sequence that repeats every five plies. In comparison, the Arapaima scales have a stacking sequence that repeats every two plies.

A quantitative comparison of important microstructural characteristics of the scales is presented in **Figure 4.5** and **Figure 4.4**. The overall total thickness of the scales is shown in Figure 4a and was found to be significantly different between the fish analyzed. Although the arapaima scales showed the greatest thickness overall, they did not exhibit the greatest thickness in all three regions of the body as the thickness changed with anatomical position. For the carp and the arapaima, the scales obtained from the head and middle regions were significantly thicker than the tail scales. In contrast, the head scales for the tarpon were significantly thinner than scales from the middle and the tail.

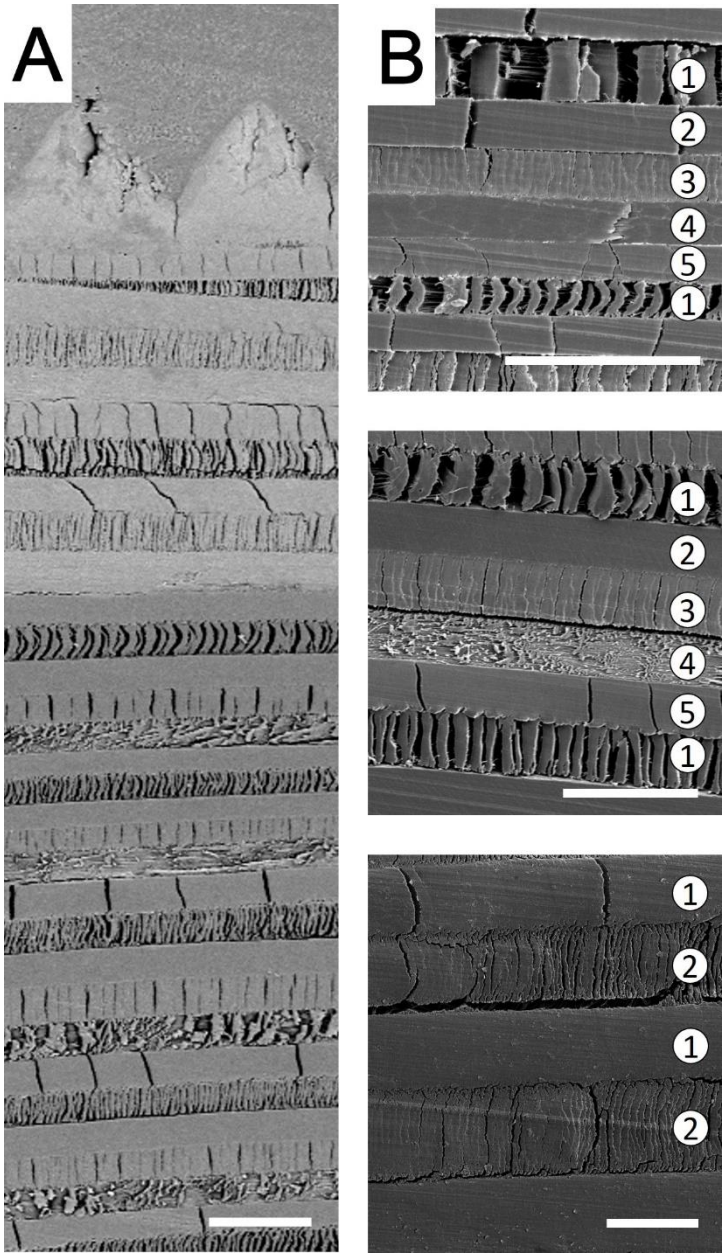

Figure 4.2. Evaluation of the collagen fiber ply orientations of the scales after fixation and dehydration. A) Backscattered SEM image from a tarpon scale from the middle region. As evident from the decrease in brightness from top to bottom, there is a reduction in relative mineral content from the limiting layer to the internal elasmodine. B) Stacking sequence of the plies for the carp, tarpon and arapaima (from top to bottom). The carp and tarpon share similar stacking patterns with an apparent replication every five plies, suggesting a Bouligand-type or a double twisted plywood structure. In contrast, for the arapaima scale the stacking pattern exhibits a replication every other ply. Scale bar = 50 μm.

The overall thickness of the scale is an important feature but the depth of mineralization is the unique characteristic that makes the elasmodine special. As shown in **Figure 4.2.A**, the macrostructure of the scales can be divided into three different regions (or layers) according to the differences in composition and mineral content. The thickness of the limiting layer (LL) is shown in **Figure 4.5.B**. It can be seen that the LL thickness of scales from the carp and tarpon is similar, and that it does not undergo large changes in thickness with anatomical position. The LL of the arapaima is the greatest of the three fish, and its thickness in the head and middle scales is greater than that of scales from the tail. Note that the LL of the arapaima scales is between 2 to 6 times thicker than that of the other two fish in all three regions of evaluation.

In a previous evaluation regarding the fracture resistance of scales from the carp it was found that the ratio of the external elasmodine to the total elasmodine thickness (EE ratio) was important [67]. The EE ratio represents the relative number of plies in the elasmodine that are more highly reinforced by apatite. In **Figure 4.5.C** the EE ratio is shown for each fish as a function of the anatomical position. As evident in this figure, the arapaima scales possess an EE ratio that is significantly greater than that of both the carp and tarpon. Note that scales from the head of the carp and arapaima have a much higher percentage of mineralized plies than scales of the middle and tail regions. In contrast, for the tarpon the greatest number of mineralized plies was found in scales of the tail, although the difference was not significant from the other anatomical regions sampled.

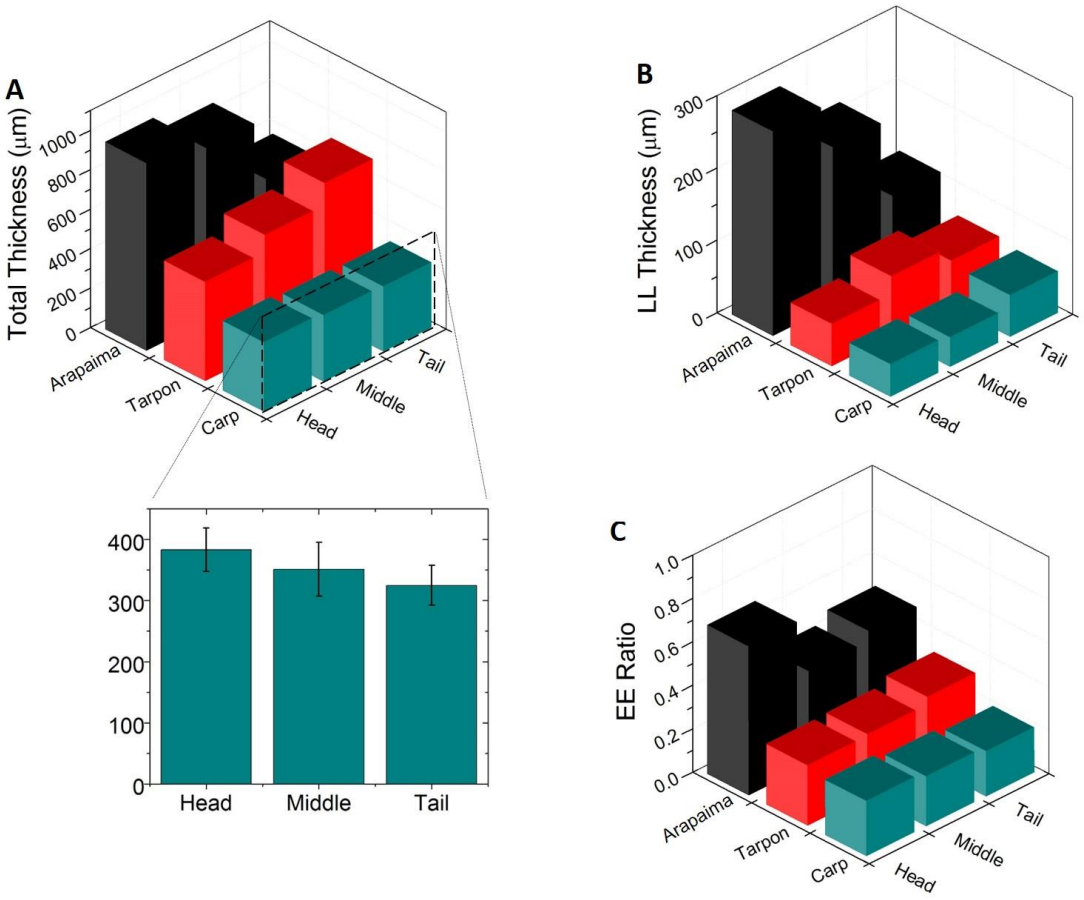

Figure 4.3. A comparison of the microstructural characteristics of the carp, tarpon and arapaima scales in the three anatomical positions. A) Total thickness, B) Limiting layer thickness and C) External elasmodine ratio, which represents the ratio of the EE thickness to the total elasmodine thickness. All measurements where conducted after fixation and dehydration of the scales

In engineered fiber reinforced composites the number of individual plies and their thickness are important to the mechanical behavior of the laminate [72]. Consequently, these qualities of the fish scales were evaluated and are shown in **Figure 4.4**. The total number of collagen fibril plies in scales of each fish is shown in **Figure 4.4.A**. Interestingly, although scales of the carp and tarpon were much thinner than those of the arapaima (**Figure 4.3.A**), they both possessed a larger number of plies (**Figure 4.4.A**). A comparison of the ply thicknesses within the external and internal elasmodine layers is shown in **Figure 4.4.B** and **4.4.C**, respectively. For both of these regions the average ply thickness was relatively similar over the entire body of each fish. Akin to the results

shown in **Figure 4.3.A**, the arapaima scales have the thickest plies overall within both the EE and IE. In addition, there was a significant difference in the ply thickness between the three fish studied. As evident from **Figure 4.4.B** and **4.4.C**, the plies of the arapaima scales are roughly 2 and 4 times thicker than those of the tarpon and carp scales, respectively. There are additional important features evident from comparisons of **Figure 4.4.B** and **C**. For example, the EE plies are generally thicker than those of the IE, except for scales of the head and middle regions of the arapaima and the scales of the tail in the tarpon, where there were no significant differences. The arapaima and carp had increases of nearly 50% and 150% in the EE ply thickness, respectively.

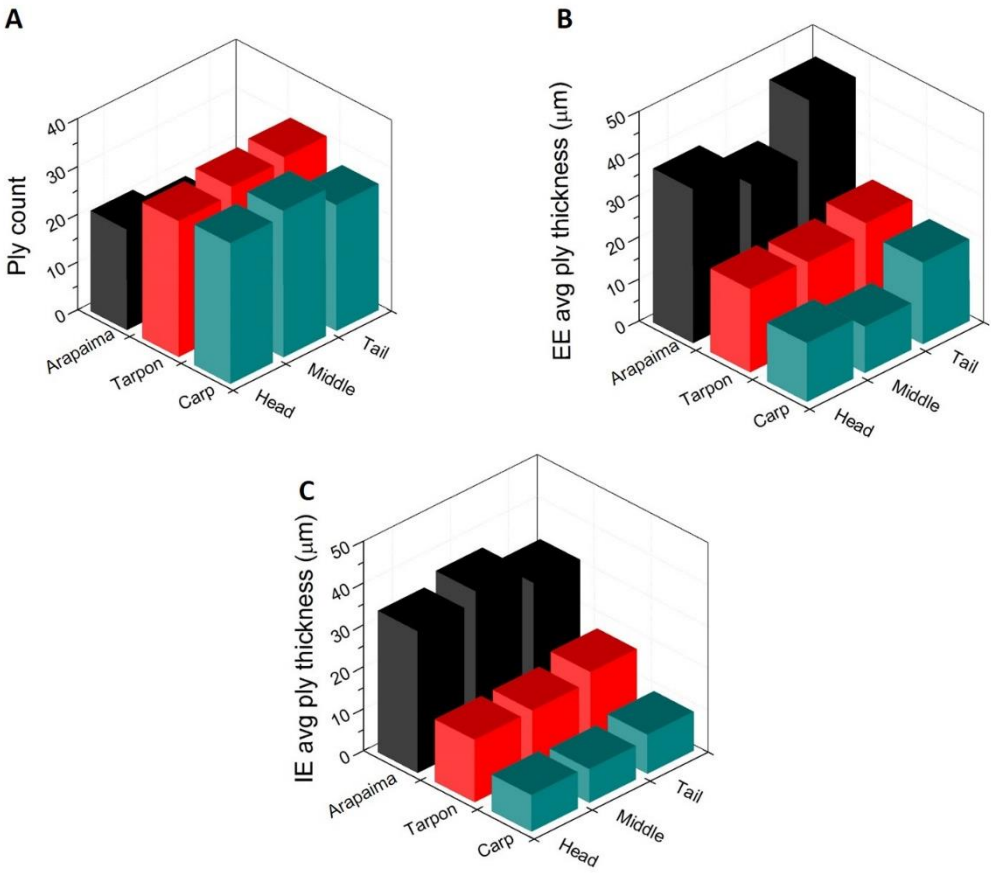

Figure 4.4. Qualities of the collagen fibril plies of the elasmodine for the carp, tarpon and arapaima fish. A) Number of plies in the elasmodine, B) Average ply thickness of the external elasmodine and C) Average ply thickness in the internal elasmodine. All measurements were conducted after fixation and dehydration of the scales.

Based on a comparison of the cross-sectioned scales (**Figure 4.2.A**) it was apparent that there are differences in the ply stacking sequence of the elasmodine for the three fish. The ply rotation angles were determined from a top view of the scales and sequential polishing. One of the major concerns to address was whether fiber orientations remained constant through the whole scale. To this end, measurements were performed over a large area of the scale with high and low magnification, and revealed that the fibers were primarily straight and parallel over the entire ply. In a previous report on the scales from striped bass a cross-ply evaluation was carry out on the elasmodine after removal of the mineralized layers [24]. If plies of the external elasmodine were revealed by a pull out method, that could result in disruption and artifacts. To avoid this concern, all of the layers where exposed through the thickness of the scales by the polishing approach. Results from this analysis can be seen in **Figure 4.5**. Specifically, micrographs of exposed plies for carp and tarpon scales are shown in **Figure 4.5.A** and **5.B**, respectively. For the scales of these two fish it was found that the fiber orientation of adjacent plies was rotated an average of 75° with respect to one another, which results in 5 increments of rotation to achieve a complete revolution. This Bouligand type structure forms a helix through the thickness of the scale. In comparison, adjacent plies in the arapaima scales exhibited a rotation of approximately 90°, which is equivalent to a cross-ply orthogonal laminate.

Figure 4.6 shows the primary ply orientations in the tarpon scales and relative angle of rotation in terms of the cumulative frequency distribution. The ply orientations are shown in **Figure 4.6.A** for the three regions of evaluation. This figure enables a visual comparison of the ply distribution with respect to the longitudinal axis of the fish (0°). Each polar plot presents results for the four scales evaluated in these regions. Interestingly, the ply orientations were not aligned with the longitudinal axis of the fish. Surprisingly, scales of the head and tail regions do not appear to

exhibit a preferential orientation. In contrast, scales from the middle region exhibited a preferential alignment with respect to the longitudinal axis of the fish. The average ply rotation angles for scales of the three regions are shown for all three fish in **Figure 4.6.B**. Although the tarpon scales did not share a common preferential orientation in the three regions of evaluation, the average ply rotation between adjacent plies was approximately the same. The average rotation angle for the scales of the carp and tarpon is 75° and in all three regions of the body. For the arapaima, the average ply rotation was approximately 90°.

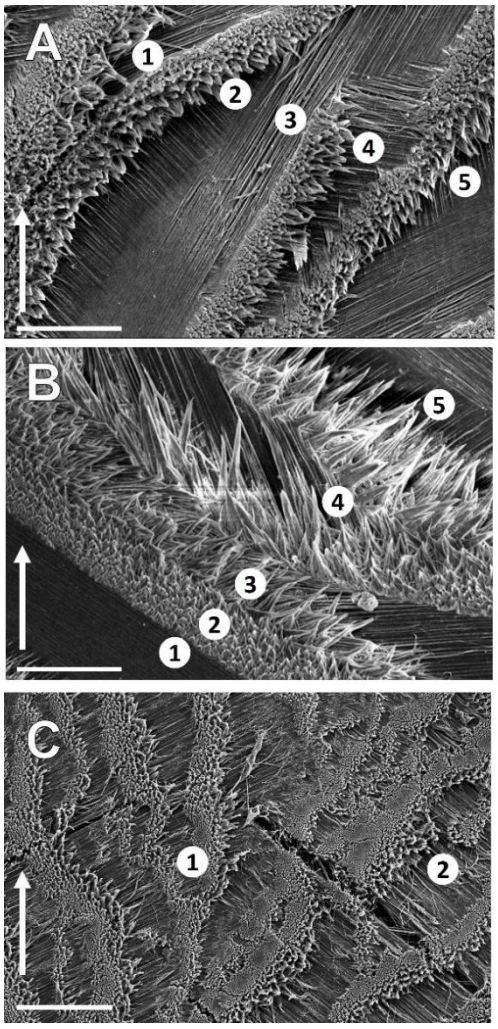

Figure 4.5. Fiber orientations of the individual plies. A) Carp. B) Tarpon, C) Arapaima. The arrow in the SEM images represents the direction of the lateral line of the fish and points towards the head of the fish. Scale bar = 50 μm.

A comparison of the cumulative frequency distribution of the ply orientations for scales of the three fish is shown in **Figure 4.7**. These results were obtained for the head scales and serve as an illustration that is representative of the other anatomical locations. The ply orientation distributions in **Figure 4.6.B** show that the carp and tarpon share the same rotation angle between adjacent plies. However, the distributions in **Figure 4.7** reveal that the plies of scales from the three regions have different preferred alignment with the longitudinal axis of the fish. Scales from the head and tail regions of the carp had a preferential offset angle from the longitudinal axis of the fish of 30° and 40°, respectively. In comparison, the tarpon scales did not exhibit a preferred alignment of the ply orientations for these same locations. In the case of the arapaima, the plies of scales from the head were aligned primarily with the 0°/90° orientation. However, in the remaining two locations, no preferred alignment of the plies was evident.

4.5 DISCUSSION

Over recent years the quest to develop tougher and more durable materials has led to explorations involving natural dermal armors. Elasmoid fish scales are an attractive candidate within this group of materials, particularly for applications that require both flexibility and resistance to penetration. Early efforts focused on the recreation of the mechanical response and structure have treated elasmoid scales as uniform plates imbricated in a soft substrate [11,73]. This assumption, although valid for an initial approach, do not reflect the complexity of the laminate structure. In a recent study [74], fabricated a biomimetic fish skin material where it was shown the importance of the overlapping of the scales and the mechanical properties of the constitutive materials to the overall mechanical behavior of these dermal armors. Numerical [11,75] and analytical [52,76] models have been used to analyze the flexural response of fish skin. However, no study has been reported

that explores the mechanical behavior of elasmoid scales where they are regarded as a composite material. For fish scales to inspire future generations of structural materials, a better understanding of the relationships between scale structure, mechanical behavior and their contribution to performance is essential. In this investigation elasmoid scales from three different teleost fish were evaluated, and a comparison of their microstructure was performed to identify important differences. Overall, results of the evaluation showed that the scales of the three fish exhibited unique characteristics, and that some of the differences between fish are dependent on the anatomical location.

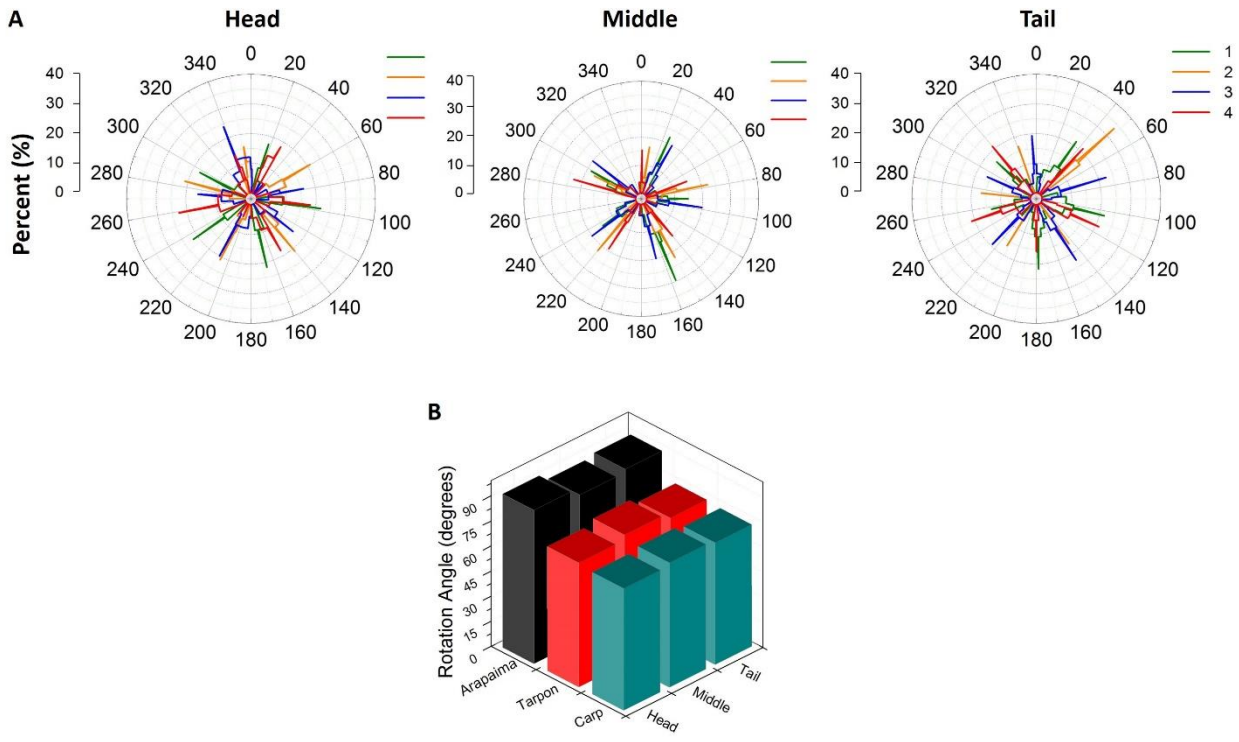

Figure 4.6. Primary ply orientations in scales of the tarpon. A) A comparison of the cumulative frequency distribution of the ply orientations for the head, middle and tail regions. Note that the 0° orientation is defined parallel to the lateral line of the fish. B) Average rotation angles between consecutive collagen fiber plies for the three fish and within the three regions of evaluation.

In addition to the unique size and shape of the scales, one of the most notable differences amongst the three fish was the change in scale thickness across the body. Scales of the carp and arapaima decreased in thickness from the head to tail, whereas those of the tarpon increased in thickness in this direction (**Figure 4.3.A**). Garrano et al (2012) noted that variations in the mechanical properties of carp scales over the body were related to the region-specific functional and protective needs. For instance, the strength and elastic modulus of the scales were greatest in the head and middle regions, which are areas with vital organs. The scale thickness was also greater in these regions, which would increase the level of protection achieved. A later study concerning the fracture resistance of carp scales suggested that the spatial variations in thickness could be due to the squamation sequence [67].

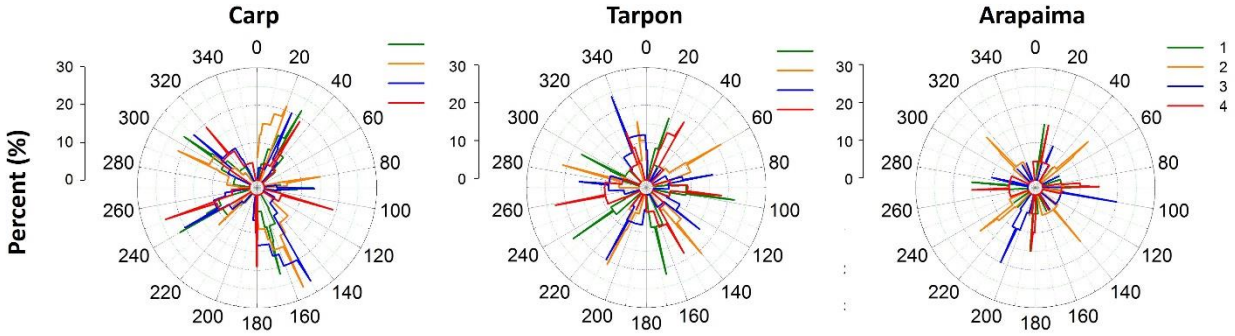

Figure 4.7. A comparison of the primary ply orientations of scales for the three fish. Each polar plot describes the cumulative frequency distribution of ply orientations for the head region. The 0° orientation is defined parallel to the lateral line of the fish. Note that the carp and tarpon scales have similar ply orientation distributions, while the arapaima scales have a rotation between plies of ~90°. Additionally, the carp scales show greater consistency in the alignment of the collagen fibers in consecutive plies with respect to the other fish.

Squamation refers to the generation of scales from the dermis and influences the relative period of time that the scales have undergone external growth. This process starts in different anatomical regions and follows a designated pattern over the body. A mechanical stimuli is apparently

responsible for the preferential development of scales in specific anatomical regions [53]. Once started, the growth process of the scales involves an increase in projected area and thickness to cover the body of the fish [24,77]. **Figure 4.8** shows a direct correlation between this two variables, were it can be seen that it's a process that is independent of fish species.

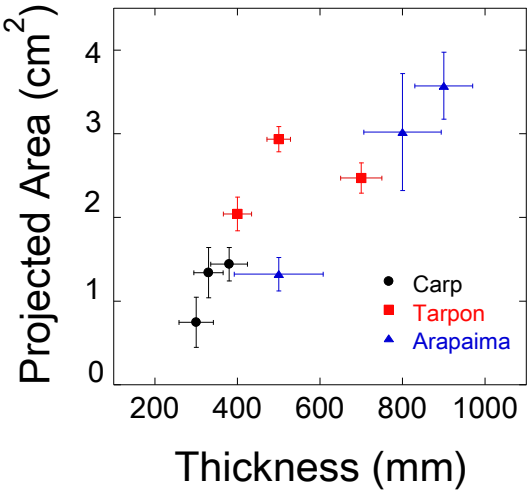

Figure 4.8. Correlation between the projected area of the scales with its respective measured thickness. As evident, scales with larger projected area are thicker as a consequence from the radial growth and top to bottom deposition of collagen plies during the development of scales.

The most common squamation sequence is from anterior to posterior, which occurs in the carp and arapaima. There are cases where the process starts from the posterior and progresses to the anterior, including the zebra fish [53] and the tarpon [56]. Indeed, the thickness of the tarpon scales follows that trend (**Figure 4.3.A**). One concern with this interpretation is that the entire squamation process (from head to tail) extends over roughly 40 to 80 days depending on the fish [55,56]. With the expected age of the three fish evaluated ranging over 3 to 6 years, it is difficult to attribute the entire anatomical variations in scale thickness to the range in number of days of squamation. Nevertheless, ontogenetic effects early in life can be carried forward for extended periods of time,

sometimes permanently [78]. Clearly the factors contributing to spatial variations in scale thickness and its importance to the performance of dermal armors will require further study.

Differences in scale thickness between fish are reflected in all three layers, but are most prominent in the LL (**Figure 4.3.B**). Zhu et al (2012) described the LL as the first barrier to penetration, highlighting that it dissipated contact energy by brittle fracture and mitigated the stresses transmitted to the elasmodine by redistributing them over a large area. Due to the relatively slow speed of the arapaima and the aggressiveness of its predators (including crocodiles and piranha), a larger LL thickness could be expected to achieve higher puncture resistance. Nevertheless, there was also a marked difference in the LL thickness in the arapaima with anatomical position, which was not reflected in this highly mineralized layer of the other fish.

One possible contribution to the unique spatial variations of the LL for the three fish is their body movements. Locomotion patterns in fish are classified according to which parts of the body are involved in propulsion and the degree of movement [79]. About a dozen general types of fish locomotion are recognized, but two are of interest here. Akin to the subcangariform species, the arapaima undulates its body into less than one full wavelength, but more than a half wavelength. In comparison, both the carp and tarpon are carangiform species and undulate their bodies into shallow waves less than one-half wavelength. They achieve faster locomotion by involving only posterior segments of the body in wave generation [80]. One major disadvantage in the subcangariform is that the attack angle of the tail changes constantly as the tail sweeps back and forth, producing less thrust at low angles and creating more drag at greater angles [79]. Perhaps the pronounced decrease in the LL thickness of arapaima scales from head to tail is related to the larger movement of the mid and tail sections during swimming. A lower LL thickness in the

posterior region would reduce the stiffness of the scales and facilitate this type of body motion. That would diminish the stored energy in the scales of these regions and its potential contribution to the energy needed for locomotion [52].

The elasmodine of the three fish possesses a laminated structure, and both the thickness and orientations of the plies were quantified. There was a significant increase in ply thickness from the internal to the external elasmodine in the scales of all three fish. Scales of the arapaima had the greatest average ply thickness overall (**Figure 4.4.B** and **4.C**). Furthermore, the EE ratio was substantially greater in scales of the arapaima than the other two fish (**Figure 4.3.C**). These characteristics are attributed to the degree of mineralization of the collagen plies and are important to the scale properties. For instance, in a comparison of reported mechanical properties for scales of the carp [23], arapaima [37] and tarpon [31], the maximum tensile strength is relatively similar for the three fish (~25 MPa). Scales of the carp and tarpon possess similar elastic modulus (0.4 vs 0.3 GPa, respectively), but less than half the value of scales from the arapaima (0.86 GPa). The elastic moduli measurements are very consistent with the trends in EE ratio (**Figure 4.3.C**); the carp and tarpon scales have EE ratios that are approximately only half that of the arapaima. The elastic modulus is clearly influenced by the number of more highly mineralized plies. The distribution in EE ratio for the arapaima (**Figure 4.3.C**) suggests that scales of the head region should exhibit substantially larger modulus than the middle and tail regions. Yet, an analysis of spatial variations in arapaima scales has not been reported.

Zylberberg and Nicolas (1982) studied the mineralization of scales and found that it primarily occurs in two stages. The LL is mineralized first and occurs by cellular processes, starting with the interfibrillar nucleation of crystals that cluster and form needle-shape crystals until a highly

mineralized matrix is formed. Crystals in the LL are arranged in a radiating manner [8,81] with pattern of mineral deposition that is regarded as spheritic mineralization [82]. The mineralization of the elasmodine follows the LL and is dependent on the fiber organization and contributing mechanisms. The mineralization front progresses from the LL within the elasmodine and its extent is reflected by the EE ratio (**Figure 4.3.C**). The depth of mineralization is a consequence of the distribution of the elasmocytes (mineralizing cells similar to the osteocytes) into the elasmodine, as well as species-specific differences in mineralization [14,82]. The elasmodine of the arapaima and tarpon have elasmocytes that extend along the collagen fibers. That results in a more uniform progression of the mineralizing front [82]. Elasmocytes are present throughout the whole scale thickness in the arapaima, whereas in the tarpon they are only located in the first few layers. Thus, the elasmodine of the arapaima scales appears to be mineralized more extensively due to the distribution of the elasmocytes throughout the thickness.

In cyprinidae or carp, additional thin collagen (TC) fibers (≤ 30 nm) can control the depth of mineral deposition [83]. The TC fibers are oriented perpendicular to the scale surface and connects the dermis of the fish with the interior of the scale from the LL to the elasmodine [14]. With the presence of TC fibers, minerals are first found at the mineralization front and later the crystallites are located alongside the collagen fibrils but they do not penetrate into the intrafibrillary matrix [83]. TC fibers are mineralized more rapidly than the rest of the fibers due to the presence of mucosubstances around them creating a mineralization front that resembles inverted trees. Hence, the limited EE ratio of the carp can be related to the difference in mechanisms of mineralization and limited penetration depth of the TC fibers in the elasmodine.

A comparison of the ply orientations within the elasmodine showed that there were unique characteristics of the lamination sequence amongst the three fish. Mandl (1839) was the first to describe how fish scales are stratified by layers of aligned collagen fibers whose directions change from one layer to the next. In general, the lamination pattern of fish scales is usually described as either orthogonal [24,30], twisted [82], or double twisted plywood [26,84]. The orthogonal plywood structure has alternating layers of aligned fibrils that are oriented roughly orthogonal to one another. In contrast, the twisted plywood collagen fibrils rotate progressively through successive layers, forming a Bouligand type structure. The double twisted plywood structure is described as a modified orthogonal plywood, where every second layer is rotated by a small angle, so that the orthogonal system is just slightly twisted [26]. Earlier studies on the arapaima [85] and carp [82] described the laminate system as more or less orthogonal, but an accurate measurement of the fiber rotations was not given. More recent studies have characterized the laminate system of the arapaima as either an orthogonal [32] or a twisted Bouligand type with a rotation close to 70° [8,37,39]. These different interpretations appear to arise from the measurement approach and fiber rotation resulting from prior deformation incurred by testing.

In the present study, direct measurement of the fiber rotation was performed on scales without prior deformation and after chemical fixation, thereby eliminating uncertainty. Our results show that regardless of location, the arapaima scales have a double twisted plywood structure as subsequent plies are roughly orthogonal to one another; there is a small rotation in every couple of layers that can change the fiber orientation just slightly ($\leq$10°). After removal of the offset angle from the lateral line, the average rotation between adjacent plies of the arapaima is 90° (Figure 10). These results agree with those of [82]. Both the carp and tarpon scales clearly exhibited a

twisted plywood structure with an average rotation angle of 75° (**Figure 4.9**). That distribution results in a stacking sequence that repeats every 5 plies as indicated in **Figure 4.5**.

The complex distribution of collagen fiber plies of the elasmodine stimulates questions regarding what controls the development and organization of these structures [82] concluded that rather than a sequential assembly process that results automatically, the fiber organization could be a "long distance order" that develops from simultaneous crystallographic and biological control processes. From a mechanics perspective, the unique ply thickness and orientations of the three fish could be attributed to the body shape and stress states generated during locomotion. Subcarangiform ancient fish with body shape similar to the arapaima, including the *Latimeria chalumnae* and several species of *Dipnoi* (lungfish), also have elasmodine with double twisted plywood structure [82]. Less primitive species with small scales like *Poecilia reticulate* (guppy) have an orthogonal plywood structure [84]. In comparison, evolved carangiform families similar to the carp and tarpon including *Hemichromis bimaculatus* (African jewelfish), *Leporinus friderici* and *Carassius auratus* (gold fish), have a twisted plywood structure with angle of rotation that varies between 25° and 35°. The ply rotation frequency in the scales of these smaller fish is much greater than found for the carp and tarpon, which could imply that the rotation angle is at least partly related to the fish growth rate.

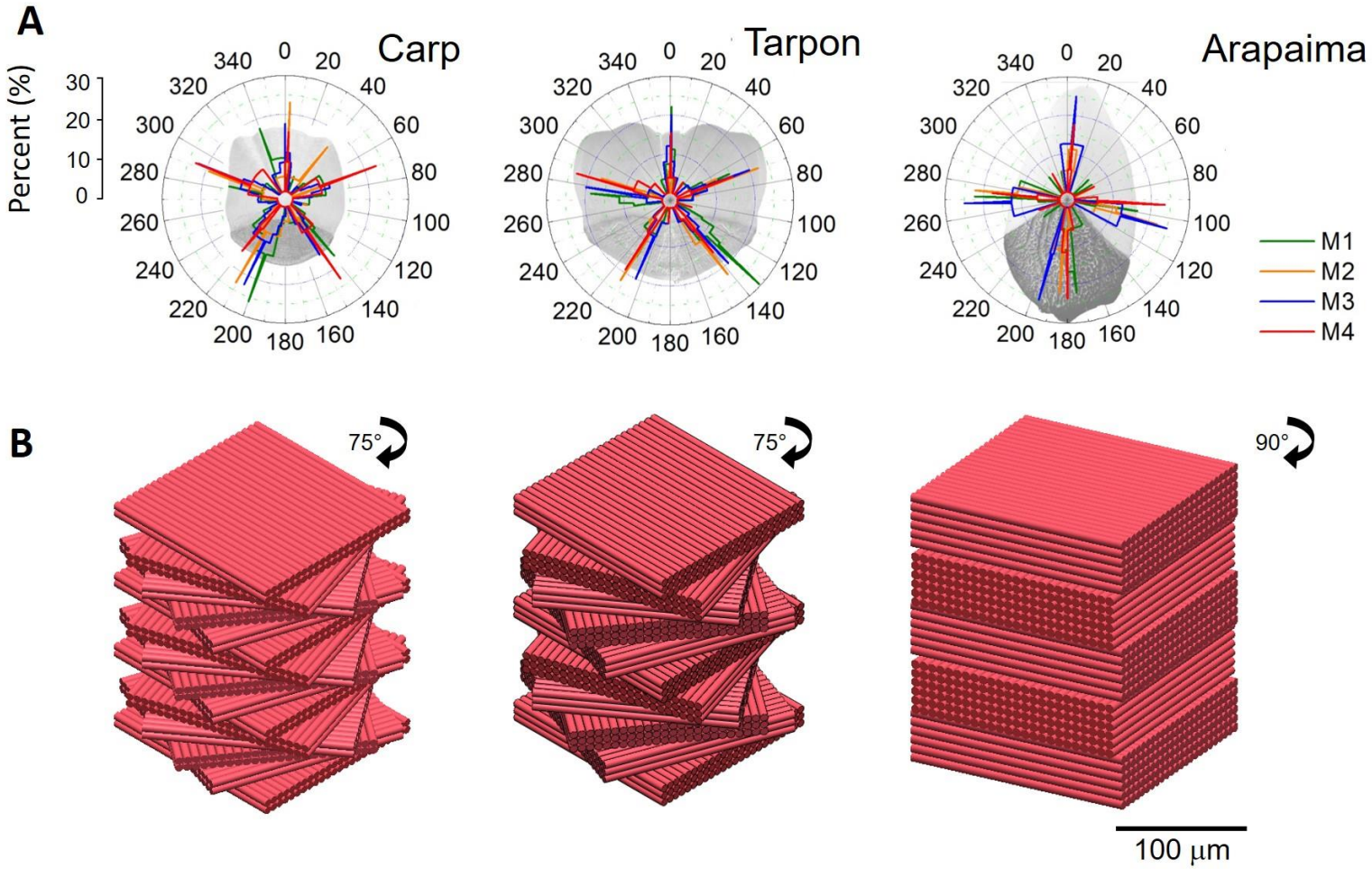

Figure 4.9. Rotation angles between consecutive plies. A) Polar plots for the cumulative frequency distribution of scales from the middle region of each fish. Each plot represents the ply rotations from four scales after aligning the plies to the same initial offset. B) Schematic representation of the stacking sequence and average ply thickness for the carp, tarpon and arapaima (left to right). Note the differences in the lamination sequence and thickness. Fibril diameters are not to scale.

Although the collagen fibril orientations and ply stacking sequence are expected to influence the mechanical properties of the scales, these qualities are seldom considered in investigations of the structural behavior [39] commented that the collagen matrix undergoes rotation (along with other mechanisms) under tension and is dependent on fiber direction. Plies with fiber offset angles between 15 and 30° from the tensile axis rotate towards the tensile direction and deform in tension, whereas fibers at an angle > 60° rotate away from the tensile axis. That increases the importance of an offset between the ply directions and the lateral axis of the fish, as well as with respect to the specimen orientations used in evaluating the mechanical behavior. Results for the ply stacking sequence analysis showed that the plies could have an initial offset angle with respect to the lateral axis of the fish (**Figure 4.6** and **Figure 4.7**) that contributes to the relative fiber orientations and mechanical properties of specimens obtained with respect to the principal coordinates of the body. In addition, while the offset angle may be consistent amongst scales of an anatomical region, it is not necessarily consistent over the entire length of the fish. For example, scales from the head region of the tarpon had an offset angle of approximately -20°, whereas that angle changes to +20° and then +40° in the middle and tail regions (**Figure 4.6.A**). The consistency of this offset angle is greater for the middle region than in scales from the head and tail regions. For the tarpon evaluated, scales of the middle region would appear more likely to exhibit anisotropic behavior than those of the head and tail regions due to the consistency in offset angle.

In order to fully understand the anisotropy reported in previous evaluations on the mechanical behavior of scales it is necessary to know the ply orientations as well as the offset angle. Unfortunately, that information has not been included in previous studies of scales. And based on

the regional variations in these parameters (**Figure 4.6.A**) it is also important to know the spatial variations in these qualities. For instance, due to the double twisted plywood structure of the arapaima scales, similar strength would be expected parallel and transverse to the primary ply directions (**Figure 4.9.A**). However, Yang et al. (2014) found that specimens with longitudinal orientation were stronger than those with transverse orientation. For the arapaima scales evaluated in the present study, the head scales had an offset that preferentially aligns with the 0 and 90° directions as shown in **Figure 4.7**. The consistency in orientations was greater when the offset angles were aligned (**Figure 4.9**). But these values are not necessarily indicative of the offset angles and consequent ply orientations in all locations, enabling differences in strength in the axis defined by Yang et al (2014). Therefore, to understand sources of anisotropy in the mechanical behavior of the scales it is necessary to know the preferential orientations of the fibers and offset angles.

Results from this investigation provide new understanding concerning the microstructure and laminations patterns of fish scales, as well as the potential contribution of these qualities to their mechanical behavior. Despite the importance of these findings, there are concerns and limitations to consider. There were biological variables that were not controlled, like growth conditions, environment and age. In addition, the thickness of the LL or the EE ratio could vary depending on the age of the scale irrespective of the fish if the scales were regenerated due to prior events. Therefore, further study involving environmental control of the fish growth would be desirable. Perhaps the largest limitation is that scales from only a single fish were evaluated from each species, which included four samples per anatomical region. Although the investigation was designed to compare results of structure and lamination patterns between the three fish, it is not clear how consistent these qualities are amongst fish of the same species. There are variations in

the mechanical behavior of scales from different fish of the same species [67], which appears to be a reflection of the variations in structure. Furthermore, while the rotation angles are expected to be consistent amongst fish of the same species, it is not known if the offset angles are as well. Hence, a full characterization of the structure is recommended in evaluations of mechanical properties of scales from each fish, even for fish of the same species. The spatial variations in microstructure of the scales from the three fish highlight the importance of recording the anatomical position in future studies on fish scales. Important differences in the LL thickness, EE ratio, fiber rotation and preferential orientation of the scales with respect to the longitudinal axis appear to be important parameters to the performance of natural armored systems.

4.6 CONCLUSION

A comparison of the lamination pattern and microstructure of scales from the *Cyprinus carpio* (carp), *Megalops atlanticus* (tarpon), and the arapaima *gigas* was conducted. Important differences were found in the scales between the three fish and with respect to anatomical position. For example the thickness of scales varied with location and was unique amongst the three fish. The differences in thickness were associated with the degree of mineralization reflected in the dimensions of the limiting layer (LL) and external elasmodine (EE). For the carp the LL thickness is essentially uniform over the fish length, whereas in the arapaima and tarpon the LL decreased and increased from head to tail, respectively. Furthermore, the thickness of mineralized plies in the EE is substantially greater than that of the non-mineralized collagen plies, and the arapaima exhibit an EE ratio nearly twice that exhibited by the carp and tarpon scales. Thus, the arapaima scales have a larger proportion of their total thickness occupied by more highly mineralized plies, which appears essential for achieving puncture resistance.

An evaluation of the lamination sequence of the elasmodine showed that the scales of the three fish possess spatially dependent characteristics. The carp and the tarpon have a twisted plywood structure with average ply rotation between adjacent plies of 75°, resulting in a repetition of the stacking sequence every 5 plies. In comparison, the arapaima was characterized as a double twisted structure with average rotation of 90° and slight rotation (<10°) offset between adjacent plies. Furthermore, the scales of each fish exhibited a unique preferential offset angle of the ply orientations with respect to the lateral line of the fish. This characteristic appears to be important to the direction dependence in the mechanical behavior of fish scales and in quantifying the degree of anisotropy. The preferred rotation and offset also appeared location-dependent. As such, experimental evaluations concerning the mechanical properties of fish scales should account for the potential importance of anatomical position.

4.7 ACKNOWLEDGEMENTS

This research was supported in part by a seed grant from the University of Washington, by Colciencias through contract 0210-2013 and from a laboratory directed research and development funding associated with Chemical Imaging Initiative at Pacific Northwest National Laboratory. Part of this work was conducted at the Molecular Analysis Facility, which is supported in part by funds from the University of Washington, the Molecular Engineering & Sciences Institute, the Clean Energy Institute, the National Science Foundation and the National Institutes of Health.

Chapter 5. The limiting layer of fish scales: structure and properties

5.1 SYNOPSIS

Fish scales serve as a flexible natural armor that have received increasing attention across the materials community. Most efforts in this area have focused on the composite structure of the predominately organic elasmodine, and limited work addresses the highly mineralized external portion known as the Limiting Layer (LL). This coating serves as the first barrier to external threats and an important role in resisting puncture. In this investigation the structure, composition and mechanical behavior of the LL were explored for three different fish, including the arapaima (*Arapaima gigas)*, the tarpon (*Megalops atlanticus*) and the carp (*Cyprinus carpio*). Features of the LL were evaluated with respect to anatomical position to distinguish site-specific functional differences. Results show that there are significant differences in the surface morphology of the LL from posterior and anterior regions in the scales, and between the three fish species. The composition of the LL is also unique among the three fish. Results from nanoindentation showed that the LL of tarpon scales is the hardest, followed by the carp and the arapaima and the differences in hardness are related to the apatite structure, possibly induced by the growth rate and environment of each fish.

Keywords – Apatite; Armor; collagen; fish scales; hardness; ionic substitution, limiting layer; nature; scale morphology,

5.2 INTRODUCTION

Structural materials in nature have been increasingly studied over the last decade and they are serving as a source of inspiration in the generation of new engineered materials with advanced properties [9,65,66]. Nature utilizes minerals and proteins as the primary building blocks for hard tissues and largely controls the mechanical behavior through modulation of the mineral content [41]. However, for some structural biological materials there are unique qualities of the microstructure that yield additional qualities.

Within the theme of bioinspiration, scientists have been fascinated by natural armors, which exhibit high specific strength and toughness [12]. These materials are a special class of natural composites consisting of a matrix of collagen [10,41] or keratin fibers [86]. Fish scales have drawn considerable attention due to their laminated composite structure, their flexibility and their specific strength and toughness [87]. These qualities appear to have evolved to meet the specific requirements of each fish according to its habitat and predator/prey relationships.

Elasmoid scales can be divided into a posterior or exposed region, and an anterior region that is mostly embedded in the skin of the fish (**Figure 5.1**). The posterior area of the scale has a high roughness related to hydrodynamic properties during swimming [88]. In comparison, the anterior area consists of grooves in the radial direction (radii) and ridges that form circular rings (circuli) around a central area called the ‘‘focus” [89]. The radii and circuli of scales possibly provide increased flexibility and a means of maintaining the scale attachment, respectively [24]. While these morphological features would be expected to possess geometry important to function, a quantitative comparison of the external features between fish of different species has not been reported.

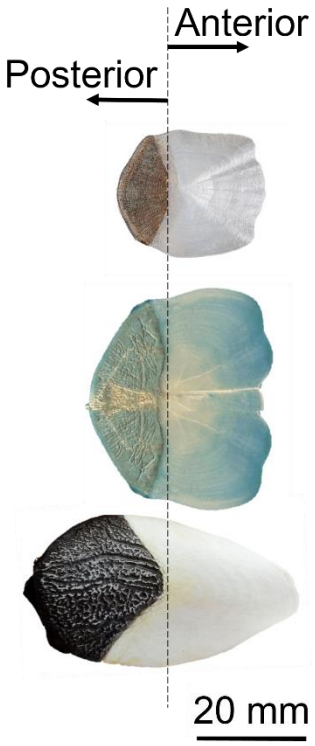

Figure 5.1. . Relative geometry, size and identification of the anterior and posterior regions of the carp, tarpon and arapaima scales.

The LL is clearly a key layer of the structure of elasmoid scales. It is also in direct contact with the environment and would be expected to have additional functions beyond simply contributing to the penetration resistance [24]. However, there is limited detailed knowledge on the structure and properties of the LL from elasmoid scales. In addition, no study has compared the composition and properties of the LL for scales of fish across species or from different habitats. Therefore, the objective of the present study is to characterize the LL of scales from selected species of fish for the first time, and to extend the current knowledge of this mineral system.

5.3 MATERIALS AND METHODS

Elasmoid scales were harvested from the bodies of three different fish including the *Cyprinus carpio* (i.e. freshwater carp), the *Megalops. atlanticus* (i.e. tarpon), and the *Arapaima gigas* (i.e. pirarucú). To be consistent with previous reports, the *latter* is identified as the "arapaima". Each fish inhabits a different natural environment, which can be important to the elemental composition and the potential for substitutions in the apatite structure. Furthermore, the protective requirements and locomotion of each fish could contribute to the development of unique structure and properties of the LL. The carp represents the control for this study as they are raised within a controlled aquatic environment. In comparison, the tarpon and the arapaima were wild fish captured in the Caribbean Sea and the Amazon River, respectively. One difference worth noting between the three fish was their size. According to their weight (3.4, 5.5 and 20 kg, respectively) and length (53, 75 and 157 cm, respectively), the fish ranged between 3 to 6 years of age, indicating that each had reached maturity.

The scales were extracted from the body of each fish within three characteristic regions, namely the head, middle and tail regions. These regions corresponded to distances from the gill plate of 15%, 40% and 80% of the total number of scales along the lateral line, respectively. The extraction was performed by hand and achieved by gentle pulling of the scale. After extraction, the scales were stored in Hanks Balanced Salt Solution (HBSS) at room temperature. The scales from each fish were divided into two groups, including one for evaluating external features of the LL (topography), and one for evaluating properties over the cross-section including chemistry and hardness.

The external topography of the limiting layer was evaluated using a surface profilometer (MarSurf XR 20, Göttingen, Germany) with skidless contact probe and 2 μm diameter. Surface profiles were obtained perpendicular to the circuli length in zones corresponding to the anterior and posterior regions. These profiles were acquired using a traverse length of 10 mm. The surface profiles were used in calculating the peak to valley height (Ry) and wavelength of the circuli within selected windows of evaluation distributed across the total length of the scales. In addition, the microscopic features of the surfaces were evaluated via scanning electron microscopy (SEM) in secondary electron imaging mode (JEOL, model JSM- 6010PLUS/LA, Peabody, MA). The samples were sputtered with Au/Pd to assist in the evaluation.

Within a week of extraction the scales selected for cross sectional analysis were fixed in 2% glutaraldehyde buffered with 0.1 M sodium cacodylate with pH=7.2 for 4 h. They were then rinsed in 0.1 M sodium cacodylate buffer followed by post-fixation in 1% osmium tetroxide buffered with 0.1 M sodium cacodylate for 2 h. After rinsing, the scales were dehydrated through an ascending ethanol series from 50 to 95%, followed by 100% of acetone and instant dehydration in 2,2- dimethoxypropane (DMP) for 5 h. Instant dehydration and rinsing with 100% acetone was followed by infiltration of the scales in Mollenhauer resin.

To evaluate the structure and composition across the thickness, selected scales were cross-sectioned and then faced with a microtome using a glass knife (Leica EM UC6 Ultramicrotome, Vienna, Austria). Raman spectroscopy was performed with a renishaw inVia system equipped with a Leica DMIRBE inverted optical microscope (Renishaw, Wotton-under-Edge, United kindom) utilizing a 785 nm Diode laser (50% power) in backscattering configuration to quantify the chemical composition and the distribution of mineral content. The instrument was calibrated

to the Stokes Raman signal at 785 cm^{-1} using a bulk single crystal of Si with the direction oriented normal to the laser. A 50 aperture was used with pinhole, resulting in an approximately 2 μm diameter sampling cross section. The spectral samples were collected over 20 s exposure time and were carried out through the thickness of the limiting layer of head scales for a total of 4 evaluation points. The Raman peaks were used to determine the modes of vibration of the phosphate and collagen. To quantify the mineral stoichiometry, X-ray photoelectron spectroscopy (XPS) experiments were performed using a Kratos Axis Ultra DLD photoelectron spectrometer (Manchester, UK) operated with a monochromatic Al Kα X-ray source (*HV*=1486.6eV) at 20mA and 15kV. The surfaces were briefly sputtered with 5 keV argon ions prior to analysis. High resolution imaging was performed in parallel imaging mode at field of view 1 or 2 (800 or 400 mm) with single point background corrections recorded at binding energies 10 eV below the corresponding peak. High-resolution O 1s, N 1s, C 1s, P 2p and Ca 2p spectra were acquired with an analyzer pass energy of 160 eV with a data point spacing of 0.5 eV/step at field of view 2. Measurement locations where distributed across the LL of each fish with a spot size of 15 μm.

Preliminary information on the atomic distribution of trace elements in the LL layers was also detected by Atom Probe Tomography (APT). Samples were prepared using the dual-beam SEM/FIB instrument (Helios Nanolab, FEI, Hillsboro, Oregon) using established protocols [90]. A rectangular coating of platinum (FIB-Pt) of roughly 2 x 15 μm was deposited over a region of interest on the polished cross-section using the ion beam (30kV, 46pA). A wedge of material below the Pt coating was cut out and sequentially affixed to the tops of Si posts in an array (Cameca Scientific Instruments, Madison, WI) with FIB-Pt and a final width of 1-2μm. Each tip was shaped and sharpened using annular milling patterns of increasingly smaller inner and outer diameters. The majority of the amorphized surface region and implanted gallium in the tip surface was

removed by milling at 2 kV, 24 pA. The APT analyses were conducted in a Cameca local-electrode atom-probe tomograph (LEAP 4000XSi, Cameca, Madison, WI) using a pulsed laser (λ = 355 nm, 100 kHz, 100 pJ per pulse). The DC potential on a microtip during APT was controlled to maintain an evaporation rate of 0.0025 or 0.005 ions per laser pulse. The base temperature of the microtip was maintained at 60 K and the ambient vacuum pressure was below 10^{-8} Pa.

Nanoindentation experiments were performed using an Ubi1 nanomechanical test instrument (Hysitron, Inc., MN) and a Berkovich indenter with 150 nm tip radius. Indentations were performed after ascending ethanol treatment using a conventional trapezoidal scheme including a 10 s loading period, 5 s hold at maximum load and 10 s unloading. Hardness values were obtained from the maximum load and the reduced elastic modulus was obtained from the indentation stiffness at unloading versus indentation depth curve following the Oliver and Pharr method [91]. Indents were made over the LL thickness in increments of 10 µm for the carp and every 15 µm for the tarpon and arapaima. An array of 6 indents were performed at each point to obtain the average hardness and elastic modulus values. In addition, scanning probe microscopy (SPM) images of the cross-sectional topography were obtained using the in situ scanning capability of the nanoindenter to ascertain the quality of indents and features of interest identified using the optical microscope.

5.4 RESULTS

The surface morphology of the limiting layer from scales of the three fish is shown in **Figure 5.2**. Differences in both the geometry and spacing of the circuli are evident between the three species

in both the anterior and posterior regions. In general, the posterior region exhibits protrusions with no particular pattern. For the carp (**Figure 5.2.A**), an array of irregular shaped protrusions covers the exposed region of the scales, which transitions to denticles (i.e. ridges) after the posterior/anterior (P/A) interface. For cycloid scales, including scales of the carp, it is common for dispersed denticles to begin around the focus of the scale [92]. Anterior to the focus, progressive agglomeration and fusion form longer and more uniform ridges that form the circuli in the anterior region. In the tarpon scales, the posterior region is uniformly covered by tightly packed circular protrusions (**Figure 5.2.B**). At the P/A interface, the circular protrusions transition into ridges; with proximity to the anterior edge, the separation distance between the ridges increases, with each protrusion becoming more clearly distinguishable. For the arapaima (**Figure 5.2.C**), protrusions are also evident and have a rounded morphology that changes from the posterior to anterior regions. In the posterior region, the protrusions are rounded and randomly dispersed. After the P/A interface the protrusions have a tear shape and are arranged in rows. In comparing the LL morphology of the three fish, it is interesting that the tarpon scales have the most continuous ridges, whereas the circuli of the arapaima are limited to individual protrusions.

Selected optical micrographs for representative cross-sectioned scales of the three fish are shown in **Figure 5.3**. These images are focused on the LL within the anterior region to accentuate details of the circuli geometry. For the carp (**Figure 5.3.A**) and the tarpon (**Figure 5.3.B**), the cross sectioned LL exhibits a serrated pattern due to the distribution of the circuli and their geometry. The average LL thickness of the carp and tarpon scales from the LL/EE interface to the circuli peaks is roughly 40 μm and 70 μm, respectively. For the arapaima, the LL exhibits a much more irregular cross section geometry due to the tear shaped protrusions (**Figure 5.2.C**). Nevertheless, the average LL thickness is roughly 300 μm.

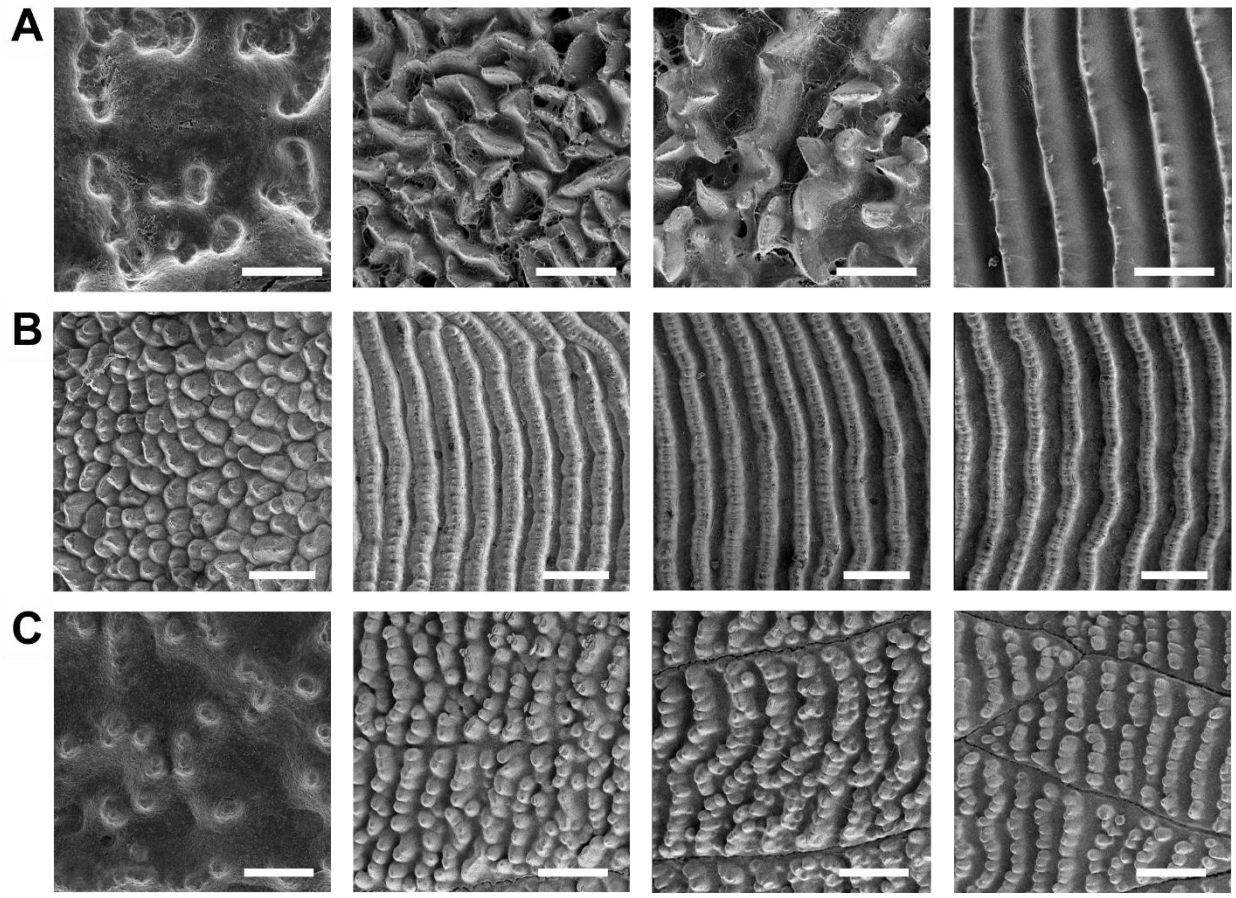

Figure 5.2. . The surface morphology of the limiting layer seen from top (external) view. The images were obtained at normalized distances from the posterior edge of the scale including (from left to right) 15%, 30%, 50%, and 70% of the total length. A) Carp scales, scale bar = 50 μm; B) tarpon scales, scale bar = 200 μm, C) arapaima scales, scale bar = 500 μm.

There are unique features of the LL from the three fish. For example, in the carp scales there is a transition zone between the highly mineralized LL and the EE (**Figure 5.3.A**). This zone is located nearest the EE and follows a serrated pattern that is in phase with the circuli. As evident in **Figure 5.3.A**, both the external circuli and the transition are inclined towards the anterior direction, having an inclination of approximately 70° with the surface. Notably sharper than the carp, the circuli of

the tarpon were not inclined, and the apparent depth of the valleys in the circuli is smaller than in the carp. The LL of the arapaima scales is much more irregular (**Figure 5.3.C**) in circuli height distribution. In addition, there are wave-like features in the cross section that resemble the marks generated by waves on a beach. These features, can be better appreciated in the transmitted light image in **Figure 5.3.D** from a section of approximately 400 μm thickness. The distance between these wave-like features decreases with increasing proximity to the LL/EE interface. Near the outer edge of the LL the average separation spacing of the waves is roughly 10 μm, and that decreases to almost no distinct wavy features near the beginning of the EE.

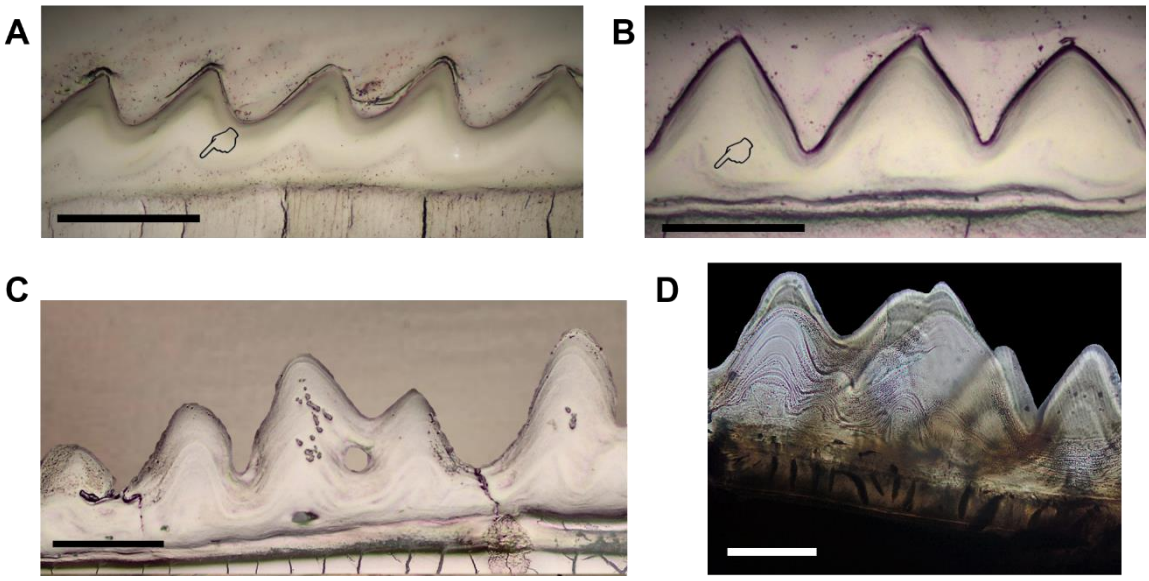

Figure 5.3. . Optical images of the limiting layer for the three fish for A) carp (scale bar 50 μm), B) tarpon (scale bar 50 μm) and C) arapaima (scale bar 2000 μm) scales. Note that the LL of the arapaima scales has a cross sectional wave pattern that is clearly seen in D) transmitted optical light image of the arapaima LL (scale bar 100 μm). Transition zones indicated in Figures A and B (pointers) were noted between the mineralized limiting layer and the mineralized collagen matrix for the carp and tarpon scales.

According to the cross-section images in **Figure 5.3**, the LL exhibits an interesting external topography. The surface topography of the scales was quantified in terms of the circuli depth and

circuli spacing. Results for the Circuli Depth (CD) are presented in **Figure 5.4** for scales from the three regions of each fish. For the carp scales (**Figure 5.4.A**) there is a significant decrease in CD from the posterior region to the P/A interface, after which the CD remained constant in the anterior region of the scales. The CD of the tarpon scales is shown in **Figure 5.4.B** and shows the significant increase in CD from posterior to anterior regions. Results for the CD for the arapaima scales are shown in **Figure 5.4.C** and show that there is a general decrease in CD from the posterior to the anterior regions. Although there were no differences in the CD with respect to anatomical position for the carp and tarpon, the LL of the arapaima exhibited significant differences with location, especially for the posterior zone of scales of the middle region. (**Figure 5.4.C**). The LL of scales from the head and middle regions decreased from the posterior to the anterior regions, whereas there was no spatial variation in the LL for the circuli of scales from the tail. It is important to note that there were substantial differences in the maximum CD between the three fish. The maximum CD in order of decreasing depth was found in scales of the arapaima (~800 μm), carp (~100 μm) and tarpon (~50 μm).

Results for the Circuli Spacing (CS) measurements of scales from the carp, tarpon and arapaima are shown in **Figure 5.5.A** to **Figure 5.5.C**, respectively. Clearly evident in this figure, there are differences in the CS between the three fish. For the carp and tarpon the smallest circuli spacing was identified in the posterior region, while for the arapaima scales it was found in the anterior region. Yet, no significant differences were found with respect to the anatomical region of the scales. Trends in CS spacing for scales of the tarpon (**Figure 5.5.B**) are similar to those of the carp, i.e. the CS increases towards the anterior edges. However, in the case of the tarpon a local maximum is found at 80% of the scale length, followed by a sharp decrease at the end of the anterior edge. The trend in CS spacing of the arapaima scales (**Figure 5.5.C**) contrast that of the

tarpon, with largest CS near the posterior edge and decrease with distance towards the anterior region. In general, the values range from roughly 400 μm to 200 μm, which agrees with the earlier findings [32].

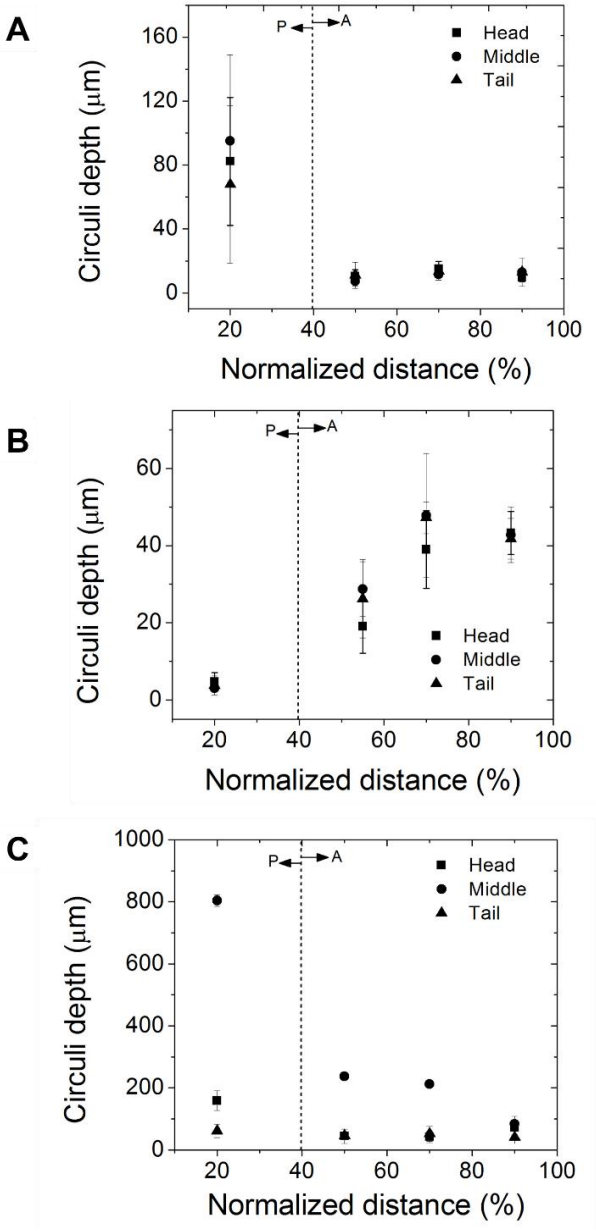

Figure 5.4. . A comparison of the average circuli depth for the LL over the total length of scales from the posterior edge. The distributions are shown for the three anatomical positions of the A) carp, B) tarpon and C) arapaima scales. There are significant differences between the anterior (A) and posterior (P) regions of the scales for all three fish. Note that scales of the arapaima have the highest peak to valley height in their surface profile.

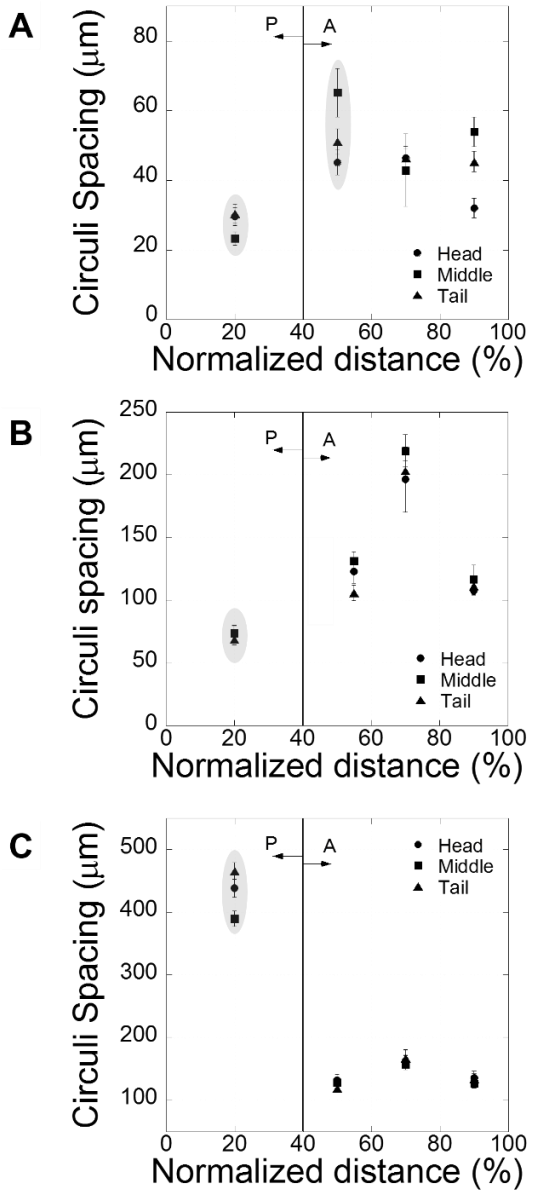

Figure 5.5. . A comparison of the circuli spacing on the LL surface of scales from the A) carp, B) tarpon and C) arapaima in the three anatomical positions. There are significant differences in the spacing between the three fish and also between regions. The highlighted data represents spacing distinguished from the protrusions and not continuous circuli.

Results for the Circuli Spacing (CS) measurements of scales from the carp, tarpon and arapaima are shown in **Figure 5.5.A** to **Figure 5.5.C**, respectively. Clearly evident in this figure, there are

differences in the CS between the three fish. For the carp and tarpon the smallest circuli spacing was identified in the posterior region, while for the arapaima scales it was found in the anterior region. Yet, no significant differences were found with respect to the anatomical region of the scales. Trends in CS spacing for scales of the tarpon (**Figure 5.5.B**) are similar to those of the carp, i.e. the CS increases towards the anterior edges. However, in the case of the tarpon a local maximum is found at 80% of the scale length, followed by a sharp decrease at the end of the anterior edge. The trend in CS spacing of the arapaima scales (**Figure 5.5.C**) contrast that of the tarpon, with largest CS near the posterior edge and decrease with distance towards the anterior region. In general, the values range from roughly 400 μm to 200 μm, which agrees with the earlier findings [32].

Figure 5.6 shows a summary of the elemental composition of the LL from scales of the head region from each fish. These results are representative of those for the entire fish as there are no significant differences in the mineral composition of the LL with respect to anatomical position of the scale [40]. Chemical distribution maps including calcium (Ca 2P), carbon (C1s) and nitrogen (N1s) across the LL thickness are shown in **Figure 5.6.A**. There was a decrease in the concentration of calcium from the outer surface of the LL to the LL/EE interface for all three fish examined. For the arapaima scales, the volume percent of apatite decreased from 60% to 40%, while the tarpon and carp scales showed a decrease from 70% to 20%. Representative Raman spectra for each fish are shown in **Figure 5.6.B** and a summary of the spectra identified is listed in Table 5.2. The Raman peaks with greatest intensity are attributed to phosphate, carbonate and collagen and the secondary peaks are related to amino acids [93–95]. The ν_1 phosphate stretching vibration at 961 cm^{-1} is the strongest marker for the apatite. The ν_2 and ν_4 phosphate bending vibrations were also visible at 431 cm^{-1} and 589 cm^{-1}, respectively. As evident from the review of spectra, there are differences

in the apatite structure, crystallinity and collagen in the LL between the three fish. Most evident, the arapaima has a different apatite structure in comparison to the carp and tarpon, which have a strong band at 1075 cm^{-1} indicating type B carbonate substitution (carbonate substituting for phosphate in the apatite lattice). Furthermore, there are important changes with respect to the collagen structure represented by the amide I (~1677 cm^{-1}) and amide III (~1256 cm^{-1}) peaks. Broad bands were observed in the amide III (~1253 and 1325 cm^{-1}) [96–101] for the arapaima, while for the carp and the tarpon these peaks were narrow and well-defined. Preliminary results from APT regarding the atom scale composition of the LL is shown in **Figure 5.6.C**. APT has high resolution at low concentrations, allowing the detection of trace elements like fluorine with the expected phosphates and carbonates that correspond to apatite. Interestingly, magnesium was only found in the tarpon scales, while sodium and chlorine were identified in the carp scales.

Nanoindentation was performed to evaluate the mechanical properties of the LL and results are shown in **Figure 5.7**. The distribution in reduced modulus with normalized distance across the LL of the three fish is shown in **Figure 5.7.A**; the modulus decreases with increasing distance from the surface for all three fish. In recognition that the LL is a biological material, the LL could exhibit spatial variations within a scale. To address possible variations, multiple indentation scans were made across the thickness of the LL in adjacent circuli ridges and results are shown for the reduced modulus in **Figure 5.7.B**. As evident in this figure, there were no significant differences between measurements at the same relative depth, indicating a high degree of repeatability. A comparison of the hardness distribution over the normalized LL thickness is shown in **Figure 5.7.C** and the distributions with physical distance are presented in **Figure 5.7.D**. Interestingly, the LL hardness of the arapaima is lower than that of the tarpon and carp scales, which is most evident from the normalized distribution (**Figure 5.7.C**). The largest hardness for the arapaima was 1.4 GPa, which

is comparable to previous results that range between 1 GPa and 2 GPa [8,33]. Furthermore, the gradient in hardness across the thickness is equivalent for the three fish in normalized distance, but very unique when examined in physical distance. Clearly the gradient in hardness distribution is inversely proportional to LL thickness and therefore greatest in the carp and tarpon.

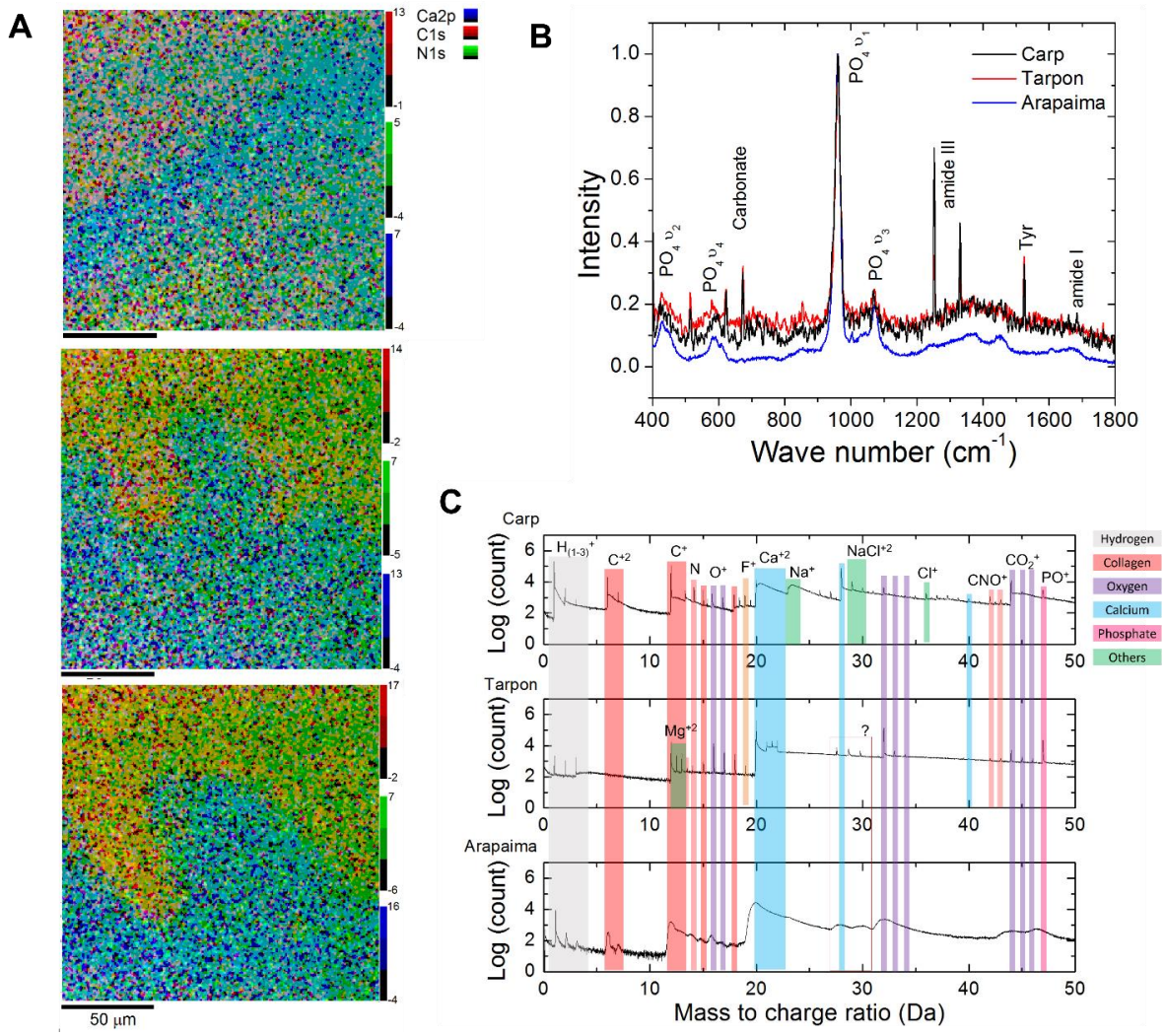

Figure 5.6. . Evaluation of the limiting layer composition in head scales A) Element distribution across the thickness of the LL from XPS analysis. Shown, top to bottom are the carp, tarpon and arapaima. The areas with high concentrations of nitrogen (green) correspond to resin used for the scale mount. B) Raman and C) APT spectra of the limiting layer at 0.5 normalized distance. Differences in B) are related to the changes in the apatite structure. The atomic scale evaluation of the elemental composition in C) detected small amounts of Mg in the tarpon scales and ions of NaCl on the carp, elements that facilitate the mineralization process.

Table 5.2. Raman lines and their assignments. ν: stretching coordinate; d: deformation coordinate; γw: wagging coordinate; γt: twisting coordinate; s: strong; m: medium; w: weak; sh: shoulder; vw: very weak.

Arapaima	**Tarpon**	**Carp**	**Assignment**
	383 s	385 s	
394 vw	397 s	397 s	Pro[21]
431 s	431 m	431 m	PO_4 ν_2 [28]
	512 m	513 m	ν(SS); cysteine [26]
584 s	580 vw	581 w	PO_4 ν_4 [27]
609 sh m			PO_4 ν_4 [28]
	621 m	622 m	PO_4 ν_4 [28[
		647 w	Phe[21]
	671 m	672 m	ν_4 $CO_3^{2-;}$ carbonate [24,29]
851 m sh	853 vw	853 vw	Pro [21]
960 s	960 s	961 s	PO_4 ν_1 [24]
1002 w		1002 vw	ν(cc); Phe [26]
1039 vw	1033 vw	1035 w	PO_4 ν_3 [29]
	1068 m sh	1068 m	CO_3 [24,28]
1071 m	1071 m	1071 m	PO_4 ν_3 [28]
1111 m sh			ν(C-N) [21]
1187 m sh			Tyr[21]
1245 m sh			amide III [26]
	1251 s	1252 s	amide III [26]
	1330 s	1331 s	Desmosine [27]
1345 m sh			γw (CH_3,CH_2)[21]
1376 m	1376 w	1374 vw	Proteoglycans (PGs)[25]
1450 s	1450 w	1447 m	C-H bending [27]
	1525 s	1524 s	Tyr[22]
1608 s		1605 vw	amide I [26]
1673 s	1674 w	1670 w	amide I [27]

5.1 DISCUSSION

Recent investigations concerning the mechanical behavior of fish scales have established that the puncture resistance[24] and toughness[28,67] are largely dependent on the contribution of the

more highly mineralized layers, namely the LL and EE. Although the distribution in mineral content over the whole scale thickness has been studied [30,92,102], to the authors' knowledge a corresponding detailed evaluation of the limiting layer has not been reported. Furthermore, no study has compared the LL of scales from different fish species to explore differences in structure and properties related to their habitats or the multi-functional requirements of the scales. Here, the morphology, chemical composition and mechanical properties of the limiting layer of three different fish species were evaluated and compared for the first time.

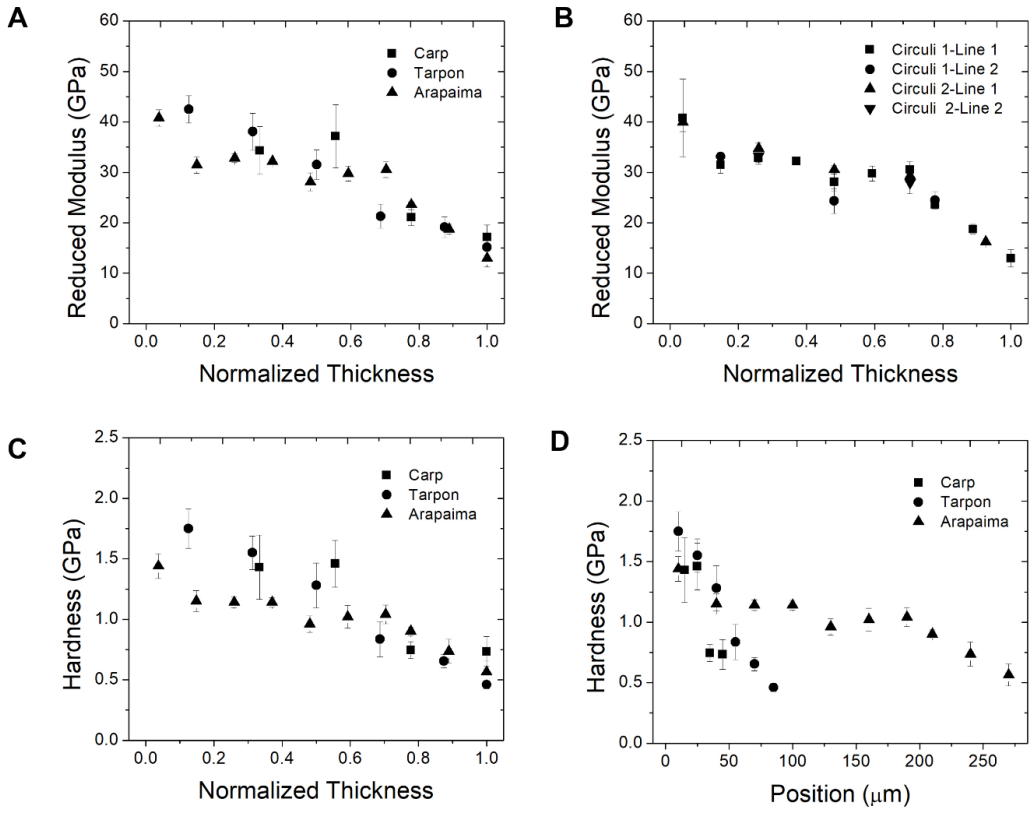

Figure 5.7. . Mechanical properties across the LL thickness for representative scales from the head region of the carp, tarpon and arapaima. A) Distribution of reduced modulus over the normalized thickness for the three fish and B) reproducibility of measurements for the Arapaima along different circuli. These results represent the degree of the consistency in measurement for all three fish. C) Distribution of hardness over the normalized thickness. The hardness distribution for the three fish are shown in terms of the actual thickness in D). The normalized thickness starts at the outer surface of the LL (Norm. Thickness = 0) and proceeds to the inner surface (LL/EE interface (Norm. Thickness= 1))

Important differences in scale structure have been found across the body of fish, which are potentially attributed to the body motion during undulatory propulsion [87,103]. Previous studies have identified a rough pattern of mineral on the surface of the scales formed by protrusions in the posterior region and by radii and circuli in the anterior region. Significant differences in the roughness have been related to the hydrodynamic characteristics and the flexibility the fish needs for its locomotion [24,31,32,52,103]. For instance, scales from the bluegill sunfish (*Lepomis macrochirus*) were found to have the highest radii counts from regions of the body that are either naturally curved (dorsal) or experience higher lateral curvature during swimming [104]. Circuli depth in the posterior area of scales is closely related to the boundary layers that can be formed during swimming. Due to the high amplitudes during the undulatory motion of the tail at high speed, a change from a laminar to a turbulent boundary layer can occur. Furthermore, turbulent boundary layers can form closer to the head as fish become larger [105]. The presence of protuberances in the posterior regions can help to control the turbulence intensity near the body [104]. When flow becomes turbulent, the protuberances could concentrate fluid shear stress, while experiencing a drop in shear stress over valleys, which imparts a decrease in frictional drag overall. For the arapaima, a fish with subcarangiform locomotion (undulation of the body involves less than one full wavelength)[80] and significantly larger body length, the presence of higher protuberances in the posterior region acts to reduce drag and the potential for acoustic noise (**Figure 5.3**). Furthermore, as the natural undulatory movement of the arapaima involves a larger portion of the body, a higher tendency to form a turbulent boundary layer is expected in mid-body of the fish. This could explain the significant increase in the circuli depth for middle scales in the posterior region in the arapaima.

Following the same principles, previous authors have proposed that circuli depth is important to reducing drag [32,104]. However, the epidermis and mucus that cover the body and scales can obscure the differences in CD, rendering the anterior region to be smooth. Sire [88] interpreted the circuli to help anchor the scales within the epidermis. That provides an alternate manner of interpreting the different geometries of the protrusions (**Figure 5.2**), differences in CD in the anterior region (**Figure 5.3**) and the cross sectional shapes of the circuli (**Figure 5.5**). Based on the geometry of the circuli it is possible to separate the fish in two groups. Although the carp circuli consist of uniform inclined ridges (**Figure 5.2**.**A**) and the arapaima circuli is formed by tear shaped protrusions (**Figure 5.2**.**C**), in both cases there is an inclination that could enhance mechanical interlock of the scale within the epidermal pocket. For the tarpon, the circuli consist of individual conical protrusions (**Figure 5.2**.**B** and **Figure 5.5**.**B**) that increase in height towards the mid-anterior region of the scale, and then remain constant to the anterior edge of the scale (**Figure 5.3**.**B**). Since there is no inclination, anchoring has to be provided by a change in height of the protrusions.

The presence of radii and circuli spacing has been also related to an increase in the flexibility of the scales and to limit tensile stresses to the valleys between circuli during bending of the scale by reduction of the material [32,88,104]. An earlier study showed that the thickness of the LL varies within species and for instance, in the case of the arapaima scales, it also differs when compared between anatomical areas [87]. However, the flexibility of the scale is not only influenced by the thickness of the limiting layer and the circuli. The external elasmodine ratio, or the amount of mineralized plies in the scales must also be taken into account. Using simple mechanics of material [106], and the previously reported data[87], it's possible to demonstrate the effect of microstructural changes in the flexibility of the scales (**Figure 5.8**). There are spatial changes in the moment of inertia of the scales, as shown in **Figure 5.8**. The carp and arapaima scales undergo a

decrease in the moment of inertia from the head to the tail, with 15% and 67% decrease, respectively. Meanwhile, the tarpon scales undergo an increase in moment of inertia of 15% from the head to the tail. Some of this change is related to the LL thickness and the neutral axis shift, and the remainder is attributed to the presence and shape of the protrusions. These spatial variations influence the scale stiffness significantly, and undoubtedly contribute to the fish propulsion. They are something to consider in the transition of efforts from characterization of scales to the development of bioinspired analogues and the corresponding methods of manufacturing.

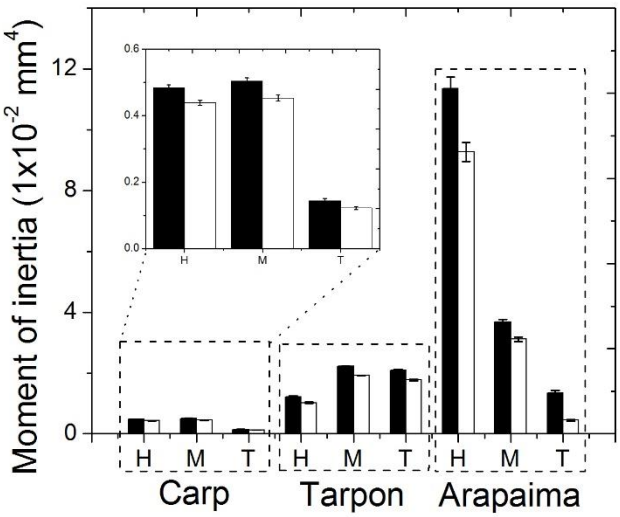

Figure 5.8. . Comparison of the moment of inertia for scales of the carp, tarpon and arapaima scales from the three regions. Note the differences in spatial variations between the tarpon with respect to the carp and arapaima, which are related to the protrusions of the limiting layer.

Optical images of cross-sectioned scales from the arapaima showed wave-like patterns in the LL similar to beach marks (**Figure 5.5.D**). The images in Torres et al [107] also showed evidence of these wave-like features at low magnification images [35]. The mineralization of scales is a cellular

process that begins at the LL with the interfibrillar nucleation of crystals that cluster following a spheritic mineralization until a highly mineralized matrix is formed [25,82]. Then, mineralization progresses to the EE, where apatite platelets organize in the c direction of the collagen fibers, creating a reinforcement similar to the one in bone [108,109]. Whether the wave-like pattern represents a change in the environment, age, or both is unclear. However, the wave pattern represents a seasonality of apatite accretion by virtue of the wide vs. narrow bands that have formed. Since arapaima are tropical fish, it could reflect dry vs. wet seasons, and the seasonal changes in growth. Differences in the apatite as a consequence of seasonal growth, would be reflected in a systematic variation of elemental concentrations from the top to the bottom of the LL. However, our current results does not show such variation (**Figure 5.6**). Since the wave-like pattern can only be seen using optical microscopy, seasonal changes could result in a modification of the apatite crystals. Ultrastructure studies of fish scales have shown that mineralization of the LL occurs by agglomeration of crystals, but there is no evidence of preferential orientations of apatite crystals in the LL [25,110,111].

Apatite accommodates chemical substitutions changing the structure of a mineral. As a consequence, there are critical effects on mineral properties, such as solubility, hardness, brittleness, thermal stability, and optical properties like birefringence. Among the substituting ions reported in bone and tooth mineral are F, Cl, Na^{+}, K^{+}, Fe^{2+}, Zn^{2+}, Sr^{2+}, Mg^{2+}, citrate, and carbonate [112]. Although, not common, analyzing the mineral composition in fish scales as a non-lethal substitute for otoliths analysis has been used to obtain life history profiles during their migratory patterns. The use of spectroscopy techniques that allow high resolution profiles of elements in the cross section of scales, like laser ablation ICP-MS, demonstrated that is possible to detect changes in Mg, P, Ca, Mn, Sr and Ba in the mineral of tarpon scales [102]. Although

preliminary, the results from the APT on the LL of scales revealed differences in elements that can form ionic substitution in the apatite structure (**Figure 5.6.A**). The APT mass spectra were consistent with previous studies of HAP [90,113,114], however C ions and CN ions were also detected in the LL due to the presence of collagen and non collageneous proteins. The mass spectra for the arapaima shows signs of attenuation, for instance in the C^{+} and the Ca^{2+} regions, which demonstrate differences in the energy absorption with respect to the carp and tarpon. The attenuation renders the analysis for the arapaima non-conclusive since the presence of elements like Mg, Na and F could be masked. Nonetheless, clear differences were found between the carp and tarpon that could be related to their growth environment. Wild tarpon were found to have presence of Mg in their scales [102], similar to the results in **Figure 5.6.A**. Previous APT studies on enamel have shown the presence of interfaces enriched with Mg and Na between HAP nanowires [114], which have an effect on the solubility at the periphery and result in anisotropic etching [113]. Furthermore, the presence of Na and Cl in carp scales could be a result of the brackish environment related to its farming.

Recent studies of scales from the carp [40] and tarpon [31] have shown that there are progressive decreases in the mineral content from the LL to the IE. In scales of the arapaima, this decrease was responsible for spatial changes in hardness and elastic modulus throughout the thickness of the scale [8,33]. There are also changes in these properties over the thickness of the LL. **Figure 5.9** shows the distribution in hardness, mineral/organic ratio and Ca/P ratio over the LL thickness for head scales from the three fish. The mineral to organic ratio was estimated from the areas of the peaks corresponding to $\nu_1 PO_4$ and Amide I. The distributions in **Figure 5.9** reveal that the gradient in LL hardness is most correlated with the relative decrease in the degree of mineralization, as expected.

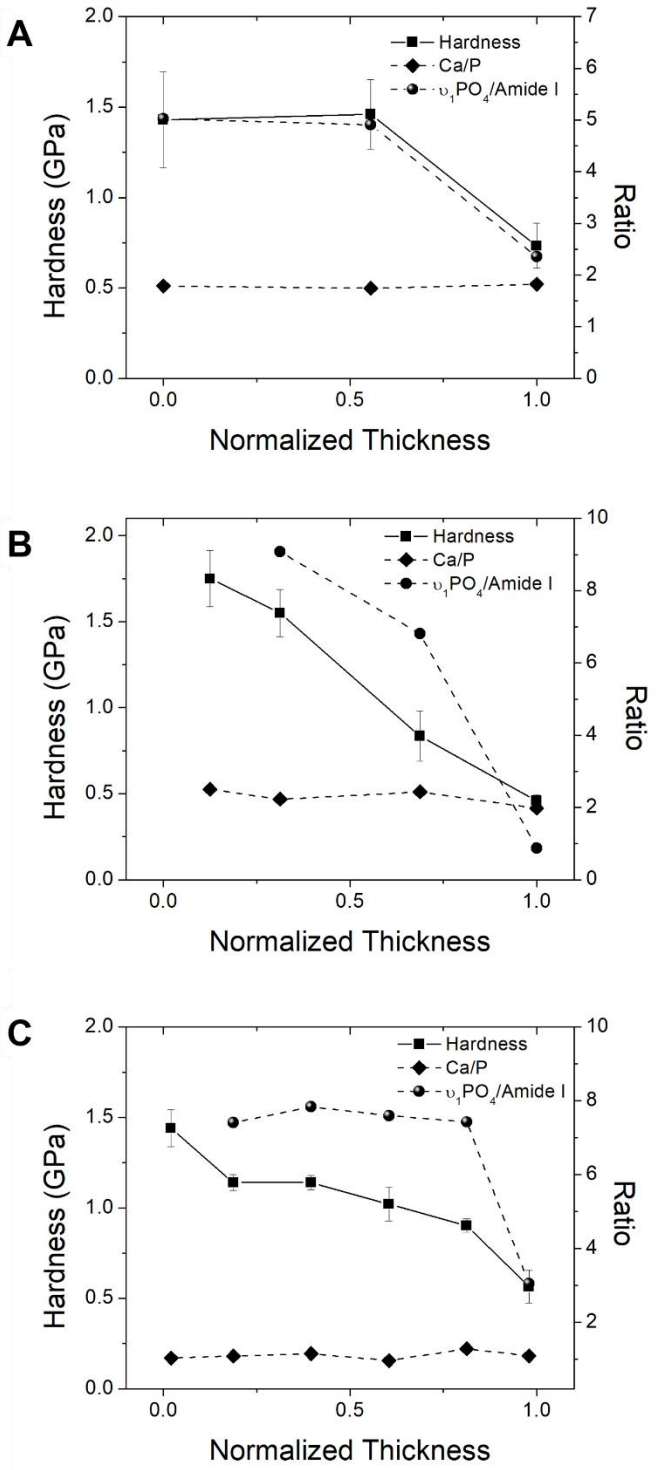

Figure 5.9. . Variation in the hardness, calcium to phosphate ratio (Ca/P) and phosphate/collagen ratio (ν_1PO4/ Amide I ratio) of the limiting layer across its thickness defined in terms of the normalized thickness. A) Carp, B) Tarpon and C) Arapaima. The decrease in degree of mineralization is reflected by the decrease of the phosphate/collagen ratio as defined by the ν_1PO4/ Amide I ratio.

Further exploration of the LL hardness and dependence on composition in **Figure 5.10** show that while a lower mineral to organic ratio results in a reduction in hardness of the LL, similar values of hardness can be achieved by significantly different values of mineral to collagen ratio (**Figure 5.10.A**). In order to understand the differences in the LL hardness between fish (**Figure 5.7**), it is necessary to analyze if the LL is composed by the same type of apatite crystals. A comparison between the Ca/P of the three fish with the measured hardness is presented in **Figure 5.10.B**. Theoretical stoichiometric HA has a 1.67 Ca/P ratio [100,112,115] with an average hardness of 1.5±0.5 GPa [116]. This values become important as higher Ca/P are related to higher hardness. A higher Ca/P implies a higher strain in the crystal lattice which will have a direct effect on the physical properties of the apatite. It is evident that the tarpon has the highest Ca/P, being followed by the carp and arapaima. An increase or decrease in the Ca/P with respect to stoichiometric hydroxyapatite (HA) is a reflection of ionic substitutions [92,113]. According to the Ca/P ratio each fish is composed of different apatites, being respectively calcium deficient carbonated apatite, tetracalcium phosphate (TetCP) and tricalcium phosphate (TCP) for the carp, tarpon and arapaima scales, respectively [100,112]. Therefore, an ascending contribution from TCP, HA, calcium deficient carbonated apatite and TetCP is expected on hardness.

Previous Raman studies on arapaima scales found the presence of carbonate anions in its apatite structure[8,32]. Nevertheless, in the present results, peaks related to the vibration of carbonates were only found only in carp and tarpon scales. The presence of carbonates is probably related to the fish habitat. Carbonated HA has also been found in the scales of *C. argus* and *Pagrus. Major,* fish that similar to the tarpon are found in the sea [92,95]. In contrast, investigations on the gold fish or *Carassius auratus,* a fresh water fish, found no presence of carbonation in the scales [92], similar to the arapaima. However, carp usually lives in fresh or brackish water and in comparison

to the *Fundulus heteroclitus* [92] that is found mainly in brackish water and estuaries, showed evidence of carbonation. **Figure 5.6.C** revealed the presence of Na and Cl in the composition of the carp's LL, an indication that it was farmed in an environment that tried to mimic brackish water. A possible increase in the salt levels of the water could have fomented the formation of carbonated apatite in the carp. This highlights the possibility of modifications in the apatite properties by changes in the growth environment of the fish.

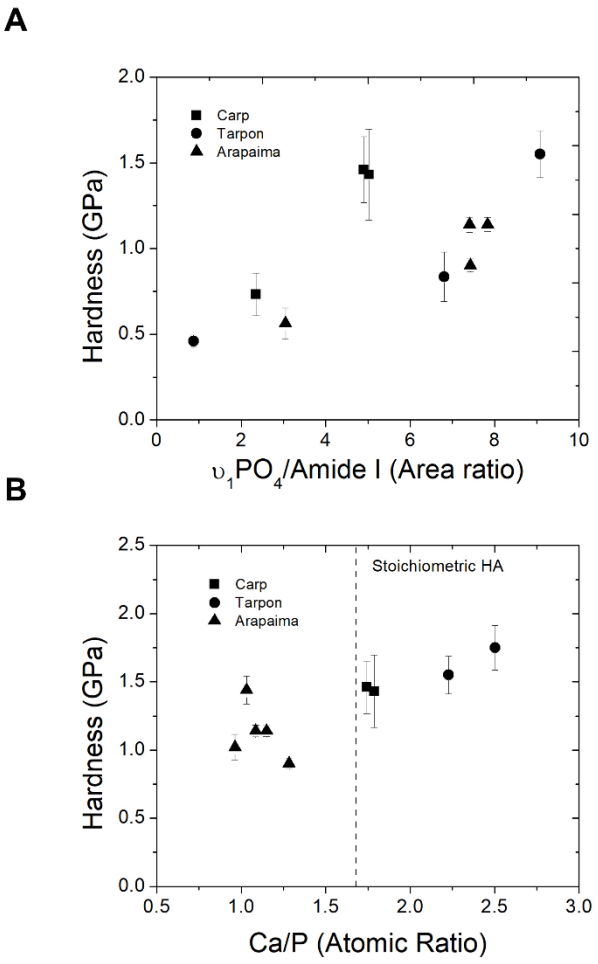

Figure 5.10. . Hardness of the limiting layer and its changes with the degree of mineralization and apatite structure for the carp, tarpon and arapaima scales. A) Hardness variation with mineralization reflected by the phosphate to collagen ratio, and B) Hardness variation with apatite structure reflected by the calcium to phosphate ratio.

Results from this investigation provide new understanding concerning the mineral structure of the limiting layer and how the growth environment can contribute to changes in properties. Additionally, important morphological features in the limiting layer of carp and arapaima scales were seen for the first time. To better understand the wave-like pattern in the circuli of arapaima scales, a characterization enabling high-resolution elemental variations across the LL thickness is needed. Furthermore, one of the most intriguing aspects of natural composites is how materials with such different elastic modulus can be so strongly integrated without undergoing separation. The exciting discovery of a transition zone between the LL/EE in the carp warrants further exploration of this suture-like interface and its function.

5.2 Conclusion

An experimental evaluation of the morphology, chemical composition and mechanical properties of the limiting layer was performed for scales of three different fish species. Significant differences in the surface morphology of circuli between the posterior and anterior regions were found in the carp, tarpon and arapaima scales. Higher protrusions were found in the posterior region of the arapaima scales in comparison to the rest of the fish, which appear related to the locomotion pattern and size of this ancient fish. A decrease in hardness and elastic modulus was identified with increasing proximity to the LL/EE interface for all three fish, and was found related to the spatial variation in the degree of mineralization. The LL of the tarpon scales was the hardest, followed by the carp and the arapaima. A positive correlation between the hardness and Ca/P ratio was identified. Results suggest that the growth environment can induce carbonate substitution of the

phosphate in the apatite structure, changing the Ca/P ratio and causing differences in the mechanical properties.

5.3 Acknowledgements

This research was supported in part by a seed grant from the University of Washington, by Colciencias of Colombia through contract 0210-2013 and from a laboratory directed research and development funding associated with Chemical Imaging Initiative at Pacific Northwest National Laboratory. Furthermore, part of this work was conducted at the Molecular Analysis Facility, a National Nanotechnology Coordinated Infrastructure site at the University of Washington which is supported in part by the National Science Foundation [grant ECC-1542101], the University of Washington, the Molecular Engineering & Sciences Institute, the Clean Energy Institute, and the National Institutes of Health.

Chapter 6. Contributions of the layer topology and mineral content to the elastic modulus and strength of fish scales.

6.1 SYNOPSIS

Fish scales are an interesting natural structural material and their functionality requires both flexibility and toughness. Previous studies have reported that there are spatial variations in the elastic properties of fish scales corresponding to the anatomical regions of the fish, and that they appear to be attributed to changes in the microstructure. In the present study, a model is proposed that describes the elastic behavior of elasmodine fish scales in terms of the relative contributions of the limiting layer and both the internal and external elasmodine. The mechanical properties of scales from the *Megalops atlanticus* (i.e. tarpon) were characterized in tension and compared with predictions from the model. The average error between the predicted and the experimental properties was 7%. It was found that the gradient in mineral content and aspect ratio of the apatite crystals in the limiting layer played the most important roles on the elastic modulus of the scales. Furthermore, misalignment of plies in the external elasmodine from the longitudinal direction was shown to reduce the elastic modulus significantly and is one approach that the fish scale flexibility can be moduluated for a specific mineral content.

Key words: Fish scales, elastic properties, rule of mixtures, collagen, apatite.

6.2 INTRODUCTION

The Limiting layer (LL) serves as the outermost coating of elasmoid scales and as such is regarded as the first barrier against penetration [24]. Based on earlier reports [14,25,83], the mineralization front extends from the LL into the underlying collagen matrix of the elasmodine. According to the distribution in mineral content, the elasmodine is further divided into external (EE) and internal (IE) regions, with the EE possessing the larger mineral content of the two.

Previous studies on the mechanical behavior of fish scales have revealed that the strength and elastic modulus of the scales are largely dependent on the number of mineralized plies of the EE, and the ratio of the elasmodine thickness to the total thickness of the scale (i.e. elasmodine ratio) [40,67]. The rule of mixtures is commonly adopted as a first approach to describe the elastic behavior of composite materials based on the contributions of the constituent layers. Although, a model for the elastic properties of scales has been presented, it was not based on an explicit description of the contributions from the LL, EE and IE of the scales [24]. Owing to the differences in mineral content of these three layers and their distribution, these factors should be considered in descriptions of the elastic behavior. Furthermore, the lamina orientations in the elasmodine is not the same for all fish [87] and is potentially an important contributor to the elastic properties as well.

Earlier studies concerning the contribution of the individual layers of scales to the mechanical properties have evaluated the strength and elastic modulus of the IE and mineralized layers separately. A summary of the tensile properties from these investigations is listed in Table 6.3. The elastic modulus of the mineralized layers is significantly larger than that of the whole scale, which apparently results from the large mineral gradient. Whereas properties of the IE are largely

controlled by the stretching of unidirectional collagen fibrils, the properties of the EE and LL have not been reported individually due to the difficulty in achieving separation. For the *M. saxatilis,* the properties of the mineralized layers were estimated using the rule of mixtures assuming the volume fraction of the IE is equal to the sum of the volume fractions of the EE and LL. However, it is not clear that this ratio is constant over the length of the fish.

Table 6.3. Elastic modulus (E) and strength (S) of scales reported for the arapaima, tarpon and striped bass in the longitudinal direction. The properties are defined in terms of the whole scale thickness, as well as the contribution of the individual layers. The properties on the mineralized layers are marked as (*) since they correspond to estimations using the rule of mixtures assuming the volume fraction of the IE is equal to the sum of the volume fractions of the EE and LL. All quantities are listed in MPa.

	Entire Scale		**IE**		**EE+LL**	
Fish	**E**	**S**	**E**	**S**	**E**	**S**
Arapaima gigas *(Yang et al., 2014)*	860±320	23.6 ± 7.2	470 ± 250	36.9±7.4	----	----
Megalops atlanticus *(Gil et al.,2016)*	300±59	24.37 ± 7.1	170	40±8	----	----
Morone saxatilis *(Zhu et al., 2012)*	~860±150	~30± 10	~450±150	~65± 15	~1250*	~45*

Understanding the relative contributions of the mineralized layers and IE to the mechanical behavior of fish scales is necessary to distinguish the principles that guide the scale development and its ability to achieve the multifunctional performance. According to the results of previous studies, the tensile properties and Mode III tear resistance of elasmoid scales are highly correlated

with the EE ratio [40,67]. However, a detailed analysis of the importance of spatial variations in the scale microstructure on mechanical behavior was not conducted. To the authors' knowledge, no study has developed a microstructure-based model that quantitatively details contributions of the microstructural characteristics to the tensile properties of scales. Therefore, the objective of this study is to develop new knowledge regarding the contributions of the layer topology and the layer composition to the elastic modulus and strength of elasmoid fish scales.

6.3 EXPERIMENTAL EVALUATION

Scales from a wild captured *Megalops atlanticus* (i.e. tarpon) were extracted from the body of a single tarpon within three characteristic regions including adjacent to the head, mid-length and near the tail, following established procedures [87]. After extraction, the scales were stored in Hanks Balanced Salt Solution (HBSS) at 4°C and evaluated within a week of harvesting the fish. Conventional dog-bone shaped tensile samples were sectioned from the scales using a punch and stamping process [117]. In recognition of the variation in thickness of the scales [29], a single sample was stamped from the center of each scale where the thickness is most uniform; the specimens possessed a gage section length and width of 5 mm and 3 mm, respectively (**Figure 6.1**). The thickness was measured over the length of the gage section to assess the variation, and in general varied by less than 50 μm over the gage section length. The lowest value was used in calculating stress. All of the specimens were obtained with alignment parallel to the fish length, in recognition that the scales may exhibit anisotropy due to the different alignment of the collagen fibers [24,37,67,87].

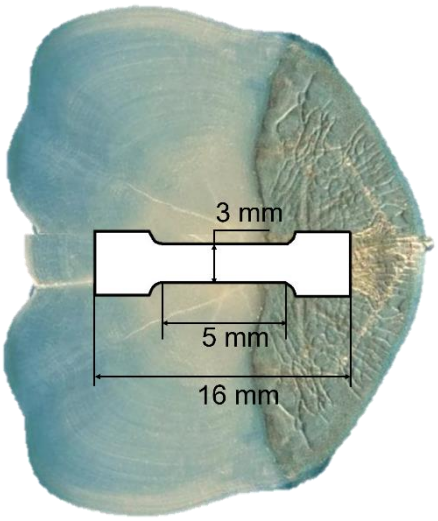

.

Figure 6.1. Location and geometry of the stamped tensile specimens from a representative tarpon scale.

After sectioning, the specimens were maintained in an HBSS bath at room temperature. Subsequently, the remaining area of the scales outside of the stamped tensile specimen was used for microstructural analysis. The fixation process started with submersion in 2% glutaraldehyde buffered with 0.1 M sodium cacodylate with pH=7.2 for 4 h. They were then rinsed in 0.1 M sodium cacodylate buffer followed by post-fixation in 1% osmium tetroxide buffered with 0.1 M sodium cacodylate for 2 h. After rinsing, the scales were dehydrated through an ascending ethanol series from 50 to 95%, followed by 100% acetone and instant dehydration in 2,2-dimethoxypropane (DMP) for 5 h, and then followed by infiltration of the scales in Mollenhauer resin. The microstructure and fiber orientation of individual lamina were analyzed following established procedures [87]. The fixed samples were sputtered with Au/Pd and the microstructure within each region of evaluation was examined with a scanning electron microscopy (SEM) in secondary electron imaging mode (JEOL, model JSM- 6010PLUS/LA, Peabody, MA). Final

measurements of the distribution of ply thickness were obtained by post-processing of the SEM images using cellSens (Olympus, Tokyo, Japan).

Tensile testing was performed under displacement control loading using a universal testing machine (Instron ElectroPuls E1000, Norwood, MA). The instrument's load cell has a full-scale range of 250 N and precision of 0.01%. A stroke rate of 0.2 mm/min was utilized, which corresponded to a strain rate of roughly $5x10^{-4}$ 1/s according to the specimen gage length. Five specimens were prepared from each anatomical region (head, middle and tail), which resulted in a total of 15 specimens prepared and evaluated. Mechanical properties of the scales were determined from results of the tension tests using the engineering stress-strain definitions. The elastic modulus (E) and strength (S) were determined for each specimen. The elastic modulus was determined using the tangent method for strains less than 1% and the strength was defined by the first significant drop in stress.

Results from the microstructural analysis were used to estimate the volume fraction of each layer for the individual scales (**Figure 6.2**). As evident from the distributions, the IE is the most prevalent component of the tarpon scales, being followed by the EE and the LL. The overall average volume fraction of these three layers – considering all three regions - was 0.58±0.07, 0.30±0.05 and 0.12±0.03, respectively. The largest variations in the volume fractions were noted in the EE and LL for scales of the head and middle regions. It is important to highlight that specimen H3 in **Figure 6.2** and M4 (not shown) exhibited distributions outside of a single standard deviation of the mean response, which could be reflected in the mechanical properties. Scales from the tail exhibited a constant LL volume fraction of about 11%; the largest variation among specimens in this region was in the EE volume fraction. Further information concerning the first ply orientation,

number of EE and IE plies, as well as the EE and IE ratios for the scales evaluated are presented in

Table 6.4.

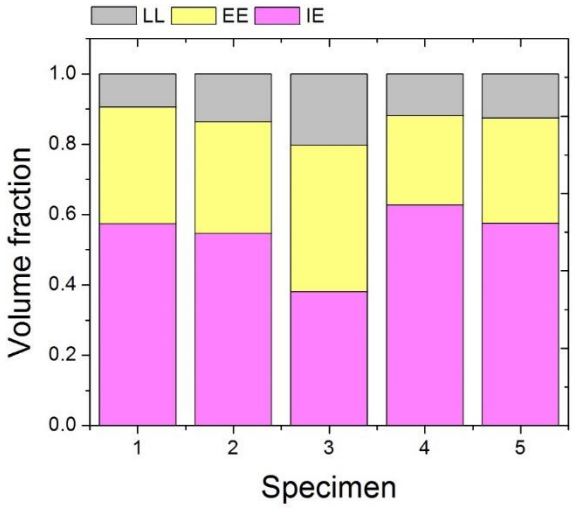

Figure 6.2. Distribution of the volume fraction of the limiting layer (LL), external elasmodine (EE) and internal elasmodine (IE) for tarpon scales of the head region. The average volume fraction of these three layers averaged over the head, middle and tail regions was 0.12±0.03, 0.30±0.05, and 0.58±0.07, respectively.

Results of the tensile tests performed on the scales are presented in **Figure 6.3**. Specifically, the elastic modulus and strength of the individual specimens are shown in **Figure 6.3A** and **Figure 6.3B**, respectively. These results are consistent with previous reported values for the elastic modulus and strength of tarpon scales. The maximum elastic modulus was obtained for scales of the head region (~350± 75 MPa), which was significantly higher than that from the middle and tail regions, and agrees with results of a previous study [31]. There is a comparatively higher variation in the strength as evident in **Figure 6.3B**, especially for scales of the head and middle regions; the coefficient of variation is greater than 0.35. While there are less pronounced variations

in the elastic modulus of the scales within a region (**Figure 6.3A**), there are significant differences across the anatomical locations.

Table 6.4. Microstructural characteristics of the tarpon scales. The first ply angle was measured CW with respect to the direction of the head of that fish.

Specimen	First ply angle	EE plies	IE plies	Number of plies	EE ratio (%)	IE ratio (%)
H1	163	7	16	23	30	70
H2	140	10	18	28	36	64
H3	19	6	4	10	60	40
H4	19	8	21	29	28	72
H5	180	9	17	26	35	65
M1	15	8	14	22	36	64
M2	69	8	38	46	17	83
M3	40	12	30	42	29	71
M4	27	3	9	12	25	75
M5	21	15	31	46	33	67
T1	48	5	6	11	45	55
T2	141	9	20	29	31	69
T3	145	11	32	43	26	74
T4	121	7	24	31	23	77
T5	55	5	21	26	19	81

Owing to the higher degree of mineralization of the collagen matrix of the samples H3 and M4, they would be expected to have higher strength and elastic modulus than the other scales in their respective anatomical groups. Indeed, the elastic modulus and strength of specimen H3 is the largest of that for scales of the head group (**Figure 6.3A**) and overall. However, specimen M4 exhibited an elastic modulus and strength that was lower than the average of these properties.

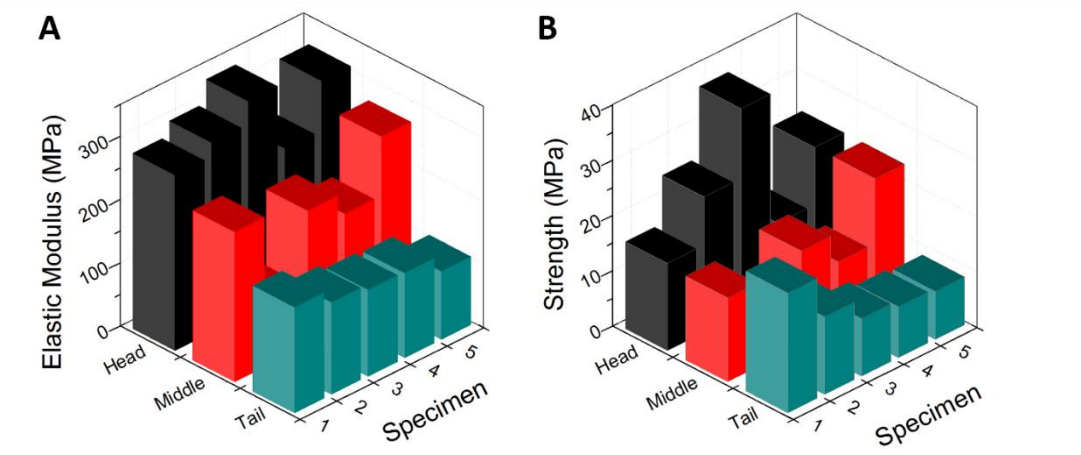

Figure 6.3. Mechanical properties of tarpon scales from the head, middle and tail regions. (A) Elastic modulus; (B) Strength. The strength is defined as the stress at first axial ply failure of the elasmodine.

The EE ratio was estimated for each of the scales using the measures of the relative layer thickness. Figure 4 shows the distribution of elastic modulus (**Figure 6.4A**) and strength (**Figure 6.4B**) in terms of the EE ratio of scales from the three regions. Clearly, a larger proportion of mineralized plies in the elasmodine results in a higher elastic modulus and strength. These trends agree with the recent findings of previous studies reported on carp scales [40,87]. Nevertheless, to understand the role of each layer on the mechanical behavior, further exploration is necessary

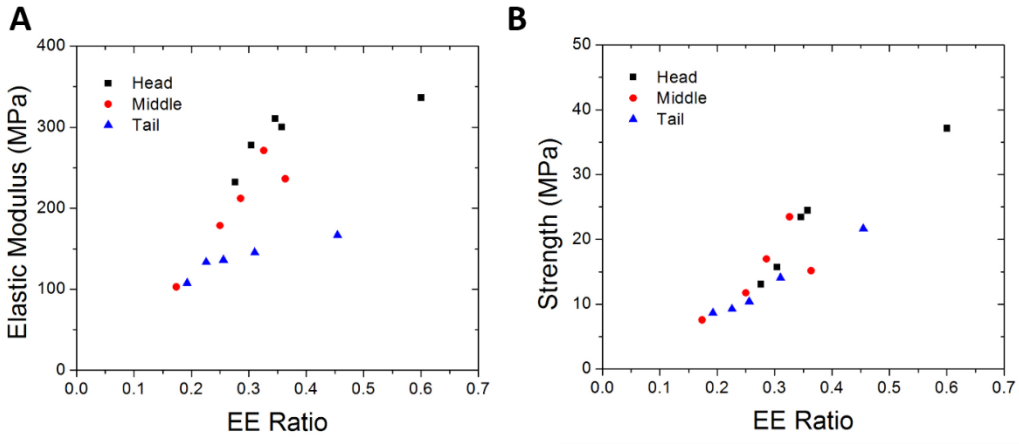

Figure 6.4. Mechanical properties of the tarpon scales from the three regions plotted in terms of the external elasmodine (EE) ratio: (A) elastic modulus, (B) strength.

6.4 MODEL

The elastic response of a fish scale under in-plane uniaxial tension can be treated as a system of springs in parallel. Due to the layered nature of the scales, the resulting stiffness of the composite can be represented by the contributions of the LL, EE and IE. For a material under uniaxial tension, the restoring force per unit cross-section of material is directly proportional to its stiffness (k) as well as the spring displacement (ΔL) according to

$$\frac{F}{A} = k\frac{\Delta L}{L} \tag{6.3}$$

where F is the total force applied to the material, A is the cross sectional area and L is the initial length. When defined for a material, the proportionality constant k is an intrinsic property of the material. For a material maintained in the elastic region, Hooke's law can be used to describe the relationship between the stress (σ) and strain (ε) according to

$$\sigma = E\varepsilon \tag{6.4}$$

As can be seen in 6.4, the spring stiffness in 6.3 is the elastic modulus of the material. In the case of springs in parallel, the total force of the system is equal to the summation of the response of each component. Therefore, for a material system with n springs, the total axial force (F_T) to achieve a deformation of magnitude ΔL is given by

$$F_T = \sum_{i=1}^{n} A_i E_i \frac{\Delta L_i}{L_i} \tag{6.5}$$

Since the configuration requires equivalent strain of all components of the system, the effective elastic modulus of the material E_T can be obtained by rewriting Eq 6.5 for the modulus as

$$E_T = \sum_{i=1}^{n} \frac{A_i}{A_T} E_i \tag{6.6}$$

where A_i and A_T are the cross-section areas of the individual layer and total, respectively. If all of the components in the system share the same depth, the area fraction can be reduced to a thickness ratio. Then, accounting for the thickness of the three primary layers (**Figure 6.1**) of the scales, the elastic modulus of the scales (E*) can be described as:

$$E^* = \frac{t_{LL}}{t_T} E_{LL} + \frac{t_{EE}}{t_T} E_{EE} + \frac{t_{IE}}{t_T} E_{IE} \tag{6.7}$$

If the distribution of the LL, EE and IE is known as well as their elastic moduli, then the effective elastic response of the scale can be estimated according to Eq. 6.7.

A previous study on the mineral content of fish scales from different teleost fish found that the volume fraction of mineral in tarpon scales decreases from the LL to the IE. The mineral content was maximum at the surface of the LL (70%), and then decreased linearly to 17% at the LL/EE interface. The mineral content remained constant within the EE and then decreased abruptly to negligible content within the IE [118]. Thus, the IE can be treated as layers of unidirectional type I collagen without mineral reinforcement. Both the EE and LL, however, consist of type I collagen

reinforced by apatite crystals. As such, the elastic modulus of these layers will be dependent on the volumetric fraction of the reinforcement according to [72]

$$E_c = v_r E_r + v_m E_m \tag{6.8}$$

where v_r and v_m are the volumetric fractions of the reinforcement and the matrix respectively. This form of the rule of mixtures is widely used for the prediction of properties of continuous, unidirectional composites. However, the reinforcement of the LL and EE does not comply with this condition. The elasmodine of teleost fish scales has been characterized as a laminate structure consisting of lamina of unidirectional collagen fibers that undergo a rotation from ply to ply [25,26,87] In the EE, the minerals are oriented along the axis of the collagen fibrils [14,25,111] Similarly, bone minerals are oriented along the axis of the collagen fibrils creating a preferred direction (longitudinal axis) [108,109]. However, Currey showed that misalignment of the fibrils in bone reduces the elastic modulus due to the corresponding change in the mineral direction [119] In the case of fish scales, particular plies of the twisted plywood structure undergo rotation and translation under the applied tensile stress. Specifically, plies oriented 15°-30° from the tensile axis or less undergo rotation and a reorientation towards the applied force, whereas plies oriented between roughly 60°-90° orient themselves away from the tensile axis [39]. Consequently, the collagen fiber orientation of lamina in the EE is an important factor to account for in a prediction of the elastic modulus.

The effect of the misalignment between the loading axis and the reinforcement orientation was studied by Nielsen and Chen in 1968. The ratio of elastic modulus between the aligned and misaligned unidirectional composite is described by

$$\frac{E_0}{E_\theta} = \cos^4\theta + \frac{E_0}{E_{90}} sin^4\theta + \left(\frac{E_0}{G} - 2\upsilon\right)\cos^2\theta sin^2\theta \qquad (6.9)$$

where E_θ is the elastic modulus of the plies with reinforcement misalignment of θ, and E_0 and E_{90} are the values of E for alignment angles of 0° (i.e. aligned) and 90° (i.e. orthogonal), respectively. The quantities G and ν are the shear modulus of the composite and ν is the major Poisson's ratio. Using representative values for the parameters in Eq. 6.9, Currey showed that E_θ of bone decreases sharply with increasing misalignment, which emphasizes the importance of accounting for misalignment in the prediction of properties of mineralized tissue. Therefore, predictions for the elastic modulus of elasmoid fish scales should account for the ply orientations when accounting for the contribution of the EE. The elastic modulus of the EE (E_{EE}) can then be estimated as

$$E_{EE} = \sum_{i=1}^{EEplies} \frac{t_i}{t_T} E_{\theta_i} \qquad (6.10)$$

where the $E_{\theta i}$ is the elastic modulus of the *ith* ply according to its misalignment angle (θ), and t_i is the ply thickness.

To estimate the elastic response of scales according to Eq 6.10 it is necessary to have values for the parameters in Eq. 6.9. Several studies have characterized the elastic modulus of hydrated tendon using X-ray diffraction techniques, with values ranging between 0.15 and 1 GPa [120–122]. For the present study, the lower limit was used to represent E_0 of hydrated collagen of the IE (E_{IE}). Using an elastic modulus for hydroxyapatite (HA) of 80 GPa [123], and volume fracture mineral of 17%, the E_0 for the EE was estimated to be 13.7 GPa according to Eq. 6.8. Then, using the inverse rule of mixtures [72], E_{90} for the EE was calculated to be roughly 180 MPa. Similarly,

using values for the shear moduli of HA and collagen as 17.3 GPa [124] and 2.9 MPa [125] respectively, the G_{EE} was found to be 3.49 MPa. The effect of collagen fibril orientation on the elastic modulus of plies of the EE is shown in **Figure 6.5**. As evident from this distribution, plies with a misalignment from the longitudinal direction greater than 7° contribute only minimally to the in-plane elastic modulus of the scales.

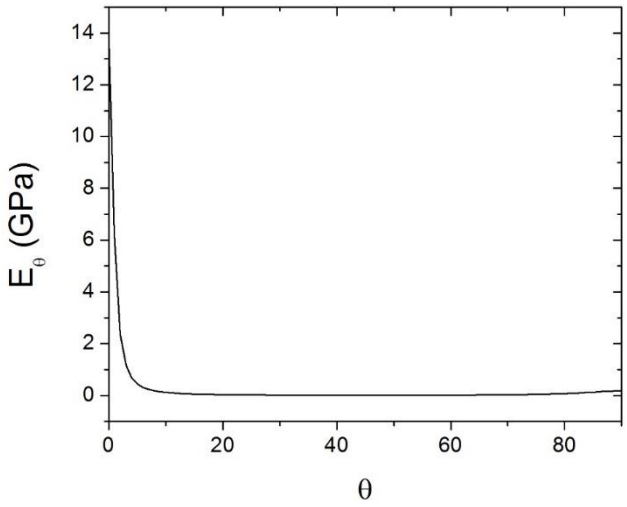

Figure 6.5. The effect of crystal misalignment on the elastic modulus of the EE. The orientation represents the deviation of the collagen fibers from the longitudinal direction (i.e. tensile axis) in the plies of the elasmodine.

According to a recent study, the mineralization of the LL follows a downward gradient from the outer surface to the LL/EE interface [118]. For tarpon scales, the level of mineralization decreased from 70 ± 3 % to 17 ± 2 %, which should be accounted for in predictions of the elastic modulus of the whole scale. **Figure 6.6** shows an optical image for the LL of a tarpon scale with a discretization scheme used to account for the mineralization gradient. If the gradient in mineral content is known over the unit cell geometry, then the elastic modulus of the LL (E_{LL}) for in-plane tension can be calculated according to

$$E_{LL} = \frac{t_{LL}}{t_T} \sum_{j=1}^{m} \frac{a_j}{a_T} E_j \tag{6.11}$$

where t_{LL} and t_T are the thickness of the LL and scale, respectively. Here, a_T is the total area of the unit cell and j represent the number of divisions (m) of the cell. Therefore, a_j represents the area of the division j, and E_j is elastic modulus of the slice a_j, which is discussed below.

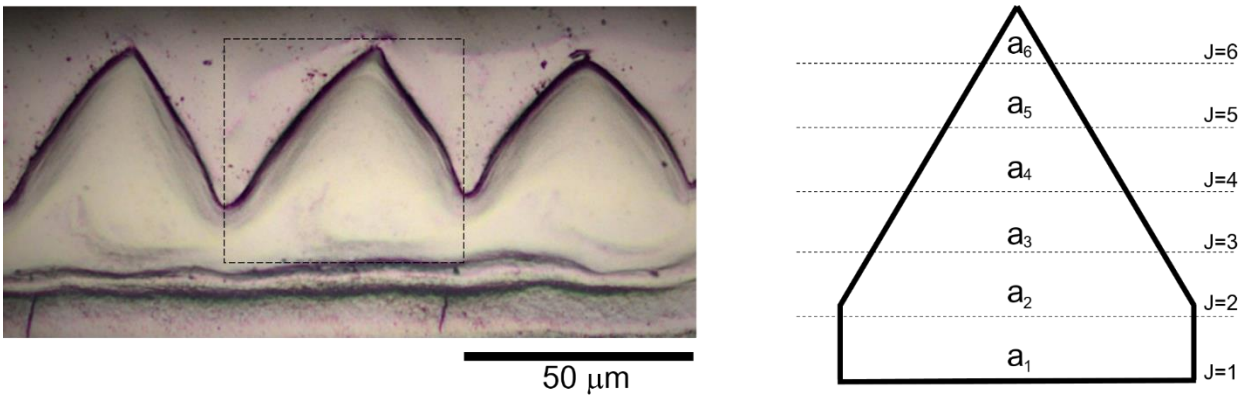

Figure 6.6. Geometry of the limiting layer for a representative tarpon scale. As evident from the image (left), the LL has a ridge geometry that repeats over the scale and the ridges can be further discretized into j individual sections (right).

A previous evaluation of the LL mineralization revealed that it has a random distribution of mineral crystals [81]. Therefore, Eq. 6.8 should not be used in predicting its elastic modulus. Instead, models that account for the shape and distribution of the reinforcement are more appropriate. The Halpin-Tsai equations are often used to predict the properties of mineralized tissues [126] but they assume a continuous reinforcement. Nielsen proposed an alternative model for predicting the elastic modulus of random, discontinuous fiber composites (E_{c*}) according to [127,128]

$$E_{c*} = E_m\left(\frac{1+A\eta v_r}{1-\eta\psi v_r}\right) \tag{6.12}$$

where

$$\psi = 1+\left(\frac{1-\phi}{\phi^2}\right)v_r \tag{6.13}$$

$$A = 2\frac{l}{d} \tag{6.14}$$

and

$$\eta = \frac{\frac{E_f}{E_m}-1}{\frac{E_f}{E_m}+A} \tag{6.15}$$

Here E_f and E_m are the fiber and matrix moduli, respectively and v_r is the volume fraction of mineral. The l/d is the fiber aspect ratio. Finally, the parameter ϕ is packing fraction or the maximum reinforcement fraction possible while still maintaining a continuous phase, which for random fibers is usually taken as 0.82. The parameter ϕ should not be confused with volume fraction [129].

In previous evaluations of fish scales, the strength of the IE has been demonstrated to be higher than the strength of the whole scale when it includes the EE and LL layers [24,31], as evident from Table 6.3. Mineralization of the collagen matrix reduces the propensity for plastic strain [40,61,63]. As a consequence, the strength of the scales is limited by the strain to failure of the mineralized

layers (EE) and would be expected to depend on the EE ratio, as well as the relative mineral content of the EE. Indeed, there is a strong correlation between the experimental strain to failure (ε^*) and the EE ratio as shown in **Figure 6.7** for the tarpon scales. That dependence can be defined in terms of a linear relationship according to

$$\varepsilon^* = k_1 * EE_{ratio} - k_2 \tag{6.16}$$

where k_1 and k_2 are constants determined experimentally that are dependent on fish species and level of mineralization. A best fit of the experimental results from **Figure 6.7** for tarpon scales result in k_1 as 0.384 and k_2 as -0.019.

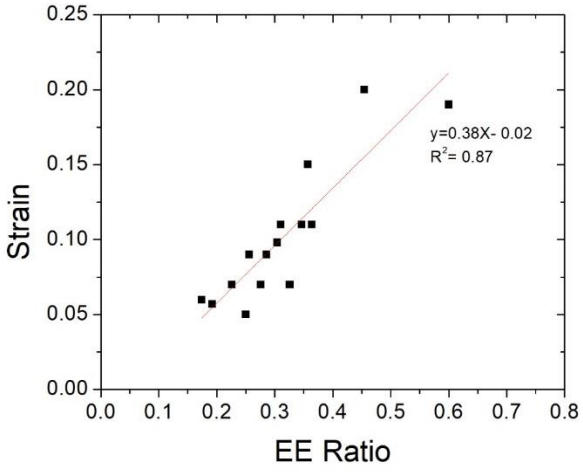

Figure 6.7. Linear correlation between the strain to failure and the External Elasmodine (EE) ratio for scales from the three regions of the tarpon.

In previous studies the tensile strength of fish scales has been defined as the maximum stress recorded just prior to the first significant drop in stress [23]. Stress vs strain curves for selected

tarpon scales obtained from the three regions of evaluation are shown to the first major load drop in **Figure 6.8A**. For scales of the head and middle regions, the curve can be divided into two zones as shown in **Figure 6.8B**. The initial portion of the curve is linear and defines the elastic response, which quantifies the elastic modulus of the composite (E^*). The response is linear, until failure of the LL, which was identified by the change in slope. Although this behavior was common for scales from all the regions, it was most distinct for scales of the head and middle regions. In addition, the strain at failure of the LL varied between regions. For scales of the head and middle regions, failure of the LL occurred at a strain of roughly 0.04 ± 0.01, as indicated by the dotted line in **Figure 6.8B**. After this point, the scales exhibited a second linear regime that reflects the elastic modulus of the elasmodine (E'), including contributions from both the EE and IE. This second regime of linear behavior ends at the first major load drop, which corresponds to the first axial ply failure of the elasmodine. Using this event to define "failure", the strength of scales from the head and middle regions can be modeled as:

$$S = 0.042E^* + \varepsilon^* E' \tag{6.17}$$

where ε* represents the predicted strain at first ply failure according to the EE ratio and relationship defined by Eq. 14. For scales of the tail, changes in the integrity of the LL with strain were not evident, and failure was defined at the first load drop, as evident in **Figure 6.8A**. Therefore, for tail scales the strength, can be estimated by multiplying the predicted strain to failure (ε^*) by the elastic modulus of scales from this area.

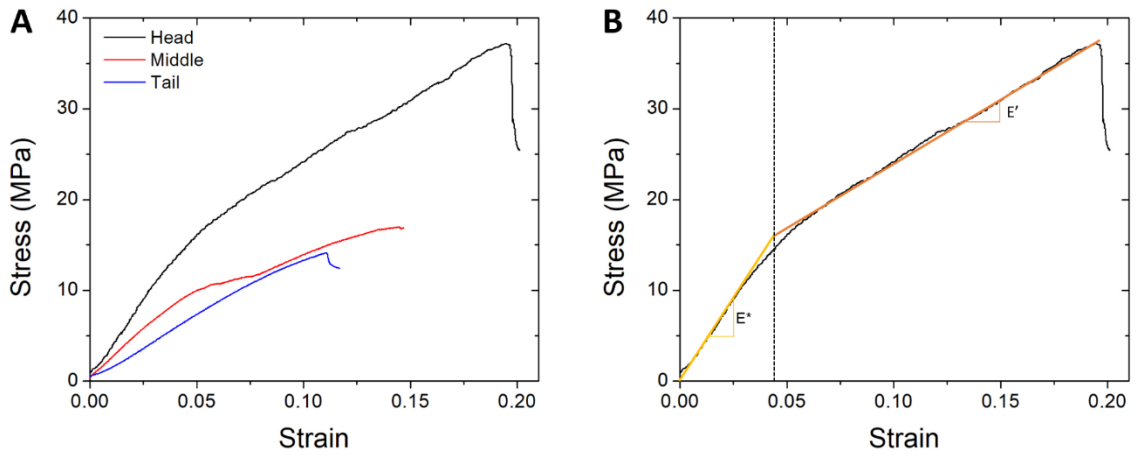

Figure 6.8. Stress vs strain responses for the tarpon scales. (A) Representative head, middle and tail scales of the tarpon. The initial response of head and middle scales was divided into two regions as shown in (B). An elastic modulus of the scales was defined (E*) according to the initial linear region. After failure of the limiting layer, the response transitions into a second region defined by the elastic response of the elasmodine (E'). On average, the transition from E* to E' occurred at a strain of 0.041 ± 0.01 m/m for the head and middle scales. Contrary to the head and middle regions, scales from the tail showed the first significant change in slope after failure of the elasmodine as shown in (A).

4. DISCUSSION

Over the past decade a number of evaluations have reported on the structural behavior of fish scales, which have established their potential to serve as a model for the design of new multi-functional engineering materials. Surprisingly, very few of the studies performed in this area have explored the properties of scales over the anatomical regions of the fish [23,31,67]. As evident from results describing the elastic modulus and strength in **Figure 6.3**, there are distinct differences in scale properties across the body of the tarpon. Possible explanations include selective reinforcement to protect areas with vital organs [23], the differences in time from scale eruption to maturity that has regulated the degree of mineralization achieved [87], or simply Nature's response to the location-specific multi-functional requirements. All of these reasons are plausible.

In the present work, a semi-empirical model is presented for predicting the elastic properties of fish scales and to further understand the relationship between scale structure and properties.

The thickness of the LL is significantly lower than that of the EE and IE, regardless of the anatomical location (**Figure 6.2**). Nevertheless, it is the mostly highly mineralized layer and possesses an elastic modulus that is several orders of magnitude higher than that of the IE. While the EE is also highly mineralized, its overall contribution to the in-plane scale stiffness is limited by the misalignment of the plies (**Figure 6.5**). The mineral content of the individual layers of the scales is not significantly different between anatomical locations in fish of the same species [40]. As such, the significant differences in E* of the scales between anatomical regions (**Figure 6.3A**) is expected to be primarily attributed to the variations in LL thickness. Nevertheless, the spatial variations in the elastic modulus in **Figure 6.3A** could also be related to specific qualities of the mineral crystals.

Mineralization of fish scales is driven by a cellular process and there is evidence suggesting that the aspect ratio of the apatite crystals among species is different [87,110,111]. Under that condition, the scale stiffness is not simply a function of the LL thickness. For instance, the aspect ratio and packing fraction of the mineral crystals are important to consider in estimating the elastic modulus of the LL. In previous studies of bone and dentine, an aspect ratio between 25 and 30 was selected [119,126]. Deproteinization of *Arapaima gigas* scales revealed a randomly oriented mineral phase with a platelet morphology. The plates showed average dimensions of 50 nm thickness and 500 nm diameter [8], which results in an aspect ratio of 10. The packing fraction of the reinforcement has been suggested to have a maximum value of 0.82 for random fibers. The importance of crystal aspect ratio and its packing fraction to the elastic modulus of the LL is shown

in **Figure 6.9**. Values of packing fraction higher than 0.82 result in a decrease of the elastic modulus of the LL. Clearly, variations in the aspect ratio have greater influence on the elastic modulus than variations of the packing fraction. To the authors' knowledge, a comparison of the apatite crystal dimensions among fish species and its influence on scale stiffness and other components of the structural behavior has not been reported. This is an interesting consideration and extends the possibilities for bioinspiration. There may also be spatial variations in the crystal aspect ratio, which would enable further modulation of scale stiffness over the body of the fish.

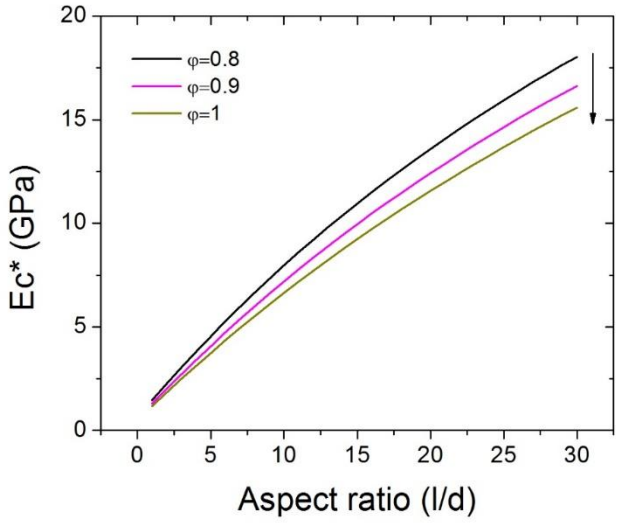

Figure 6.9. Effect of the mineral crystal aspect ratio (l/d) and the packing factor (□) on the elastic modulus of limiting layer.

Using the models for each layer, an estimate for the individual layer contributions to the overall elastic modulus of scales from the three regions is shown in **Figure 6.10A**. Contrary to earlier interpretations [67], the elastic modulus of the scales is heavily dependent on the LL, and is most important to scales of the head region. Contribution of the EE is limited due to its lower total

volume fraction than the IE across anatomical regions. The EE could have a greater contribution if more plies of the elasmodine are aligned with the loading axis. A comparison of the predicted elastic modulus of the scales with the experimental results is presented in **Figure 6.10B** in terms of the volume fraction of the LL. For best agreement between the predicted and experimental responses, the average aspect ratio of the mineral crystals in the head, middle and tail scales were 3.0, 2.4 and 1.0, respectively. Excluding the response of specimen M4, which failed prematurely and resulted in a difference >100%, the maximum "error" between the prediction and experimental result is 25%. The average difference is 7%. This range lies well within the extent of natural variation in mechanical properties of the scales within a specific region [8,23,24,31,40,67].

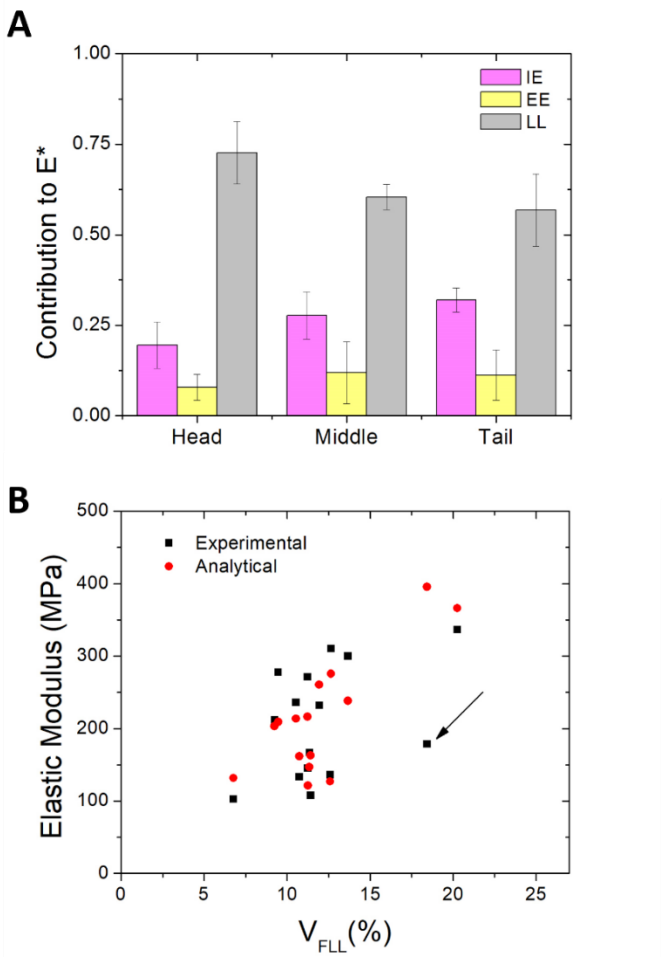

Figure 6.10. Elastic modulus of the scales and predictions from the proposed model. (A) Average contribution of the LL, EE and IE to the elastic modulus of the scales within the three regions. (B) Comparison of the experimental and predicted values and their dependence on the volume fraction of the LL (VfLL). The arrow highlights specimen M4, which failed prematurely and resulted in a difference between experiment and prediction of over 100%.

Thus far the spatial variations in scale properties have been interpreted to be related to the mineral content. An additional contribution to differences in the elastic modulus across regions could be from cross-linking of the collagen in both the IE and EE. Cross-linking has been shown to have an effect on the mechanics of collagen [130] and could be an important factor to the structural behavior of scales, especially considering the volume fraction of the IE (**Figure 6.2**). An

increase in cross-linking would resist sliding and stretching of the tropocollagen molecules, thereby increasing both the stiffness and strength of the collagen, as well as of the scales overall.

The constitutive behavior of the scales was described using a simple bi-linear model as shown in **Figure 6.8B**. The initial linear regime defines the elastic modulus of the pristine tri-layer composite, which was modeled as a material system of springs in parallel. The initial linear response is dictated by the elastic moduli of the more highly mineralized layers, i.e. the LL and EE. In response to the axial deformation, the highly mineralized LL fails first, which transfers its load share to the elasmodine. According to the tensile response in **Figure 6.8**, failure of the LL occurs at approximately 4% strain, and the elasmodine continues to undergo linear inelastic deformation thereafter until first ply failure of axial plies of the EE. A comparison of the predicted strength of the tarpon scales (Eq. 6.17) with the experimental results are shown in **Figure 6.11** for the three anatomical regions. The predicted tensile strength of head and middle scales (**Figure 6.11A** and **Figure 6.11B**, respectively) was within an average error of 16%. Meanwhile, the predicted strength of the tail scales (**Figure 6.11C**) was predicted with an average error of 2%.

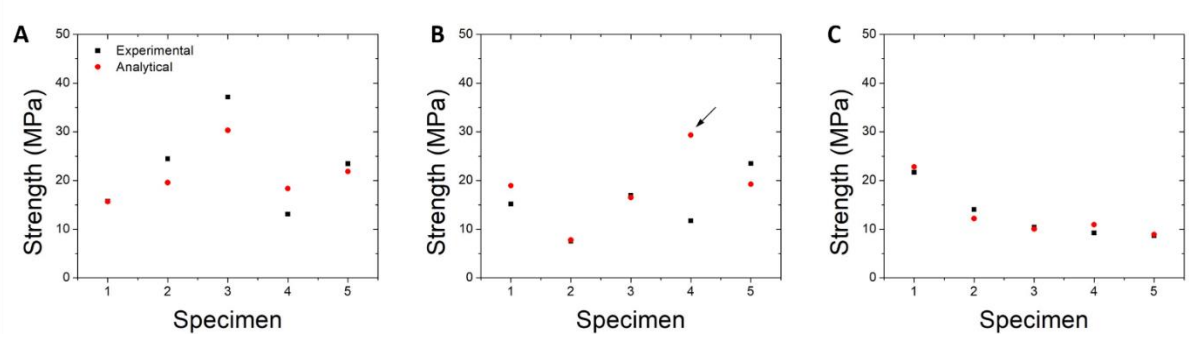

Figure 6.11. Prediction of the strength of the tarpon scales from the three regions. (A) head, (B) middle, (C) tail. Note the arrow in (B), which highlights specimen M4. This scale failed prematurely resulting in a prediction error of over 100%.

Similar to the comparison of experimental and predicted elastic moduli, the predicted strength of specimen M4 did not agree with the experimental measurement (difference > 150%). Previous studies performed on tarpon scales reported large variations in strength, even within anatomical regions [31]. Although some variation is undoubtedly a consequence of the unique layer distribution through the thickness of the scales (**Figure 6.2**), a more probable contribution is that the the scale possessed defects in the EE that resulted in significantly lower elastic modulus and strength. Liu et al [131] recently characterized tensile failure of scales as a three step process that involves fracture of the LL, followed by an increase in deformation until delamination of the mineralized layers from the IE. Premature failure of the LL and EE initiating from defects can cause variations in the elastic modulus and strength. Of course, the introduction of defects during the stamping process of the tensile specimens could facilitate premature failure and early transition from the first to the second region of deformation defined in **Figure 6.8B**. It is important to highlight that the predicted strength of the tail scales agreed very well with the experimental results (**Figure 6.11C**). The tail scales did not appear to be influenced by defects in the mineralize layers, as expected, due to the lower number of mineralized plies. The surface of the LL is populated by the presence of circuli and radii, which are important to the scale flexibility [24,31,118]. The radii

extend within the elasmodine and are the most likely contribution to premature failure of the scales under an axial loading configurations.

Results from this study have provided quantitative descriptions for the relative contributions of the layered structure to the mechanical behavior of elasmoid fish scales. The structural behavior of the scales was shown to depend on contributions from the microstructural features of each layer and that there are spatial variations in the relative contributions of the layers. Although the EE ratio is important to the elastic modulus and strength of scales (**Figure 6.4**), the primary contribution to these properties comes from the LL (**Figure 6.10A**). In scales of the tarpon, up to nearly 75% of the scale stiffness is attributed to the LL; the largest contribution of this layer is in scales of the head region. Due to misalignment of the minerals with respect to the loading direction, an increase in the mineralization of the elasmodine has less influence on the tensile response overall.

Although the results provide additional understanding of fish scales as a structural material, there are some concerns and limitations that are necessary to address. The strength of the scales was defined in terms of the first axial ply failure of the external elasmodine. That definition is appropriate for engineering applications, but may not be the most appropriate for the multi-functional performance required by the fish. Additional consideration of the definitions used for the strength of fish scales is recommended, especially if a comparison between species will be performed. Furthermore, as a result of the analytical modeling it was found that the scale properties potentially depend on other aspects of the scale microstructure, which have not been explored in detail experimentally. For instance, there is strong evidence that the aspect ratio of mineral crystals of the LL contribute to its elastic modulus, which is critical to the scales overall. Consequently,

future work concerning the mineral crystals of the LL is warranted. In additional, collagen crosslinking was not considered in the modeling, but could contribute substantially to the elastic modulus and strength, especially near the tail where the mineralized content plays a lesser role. These details are at the heart of the materials science of fish scales, and are ripe topics to be explored in future work.

6.5 CONCLUSIONS

A semi-empirical model was developed to quantify the elastic behavior of elasmoid fish scales in terms of the relative contribution of the three primary layers, including the limiting layer (LL) and the external (EE) and internal elasmodine (IE). Due to the limited information for the elastic modulus of the EE and LL, estimates were obtained from a rule of mixtures approach that accounts for the geometry of the mineral reinforcement. The findings show that although the elastic modulus of individual plies of the EE can be orders of magnitude higher than that of non-mineralized collagen, the ply rotations of the twisted plywood structure result in a significantly lower elastic modulus of the scale, and hence lower stiffness overall. The LL plays the largest role on the elastic response, followed by the internal elasmodine (IE), which has a significant contribution that varies with anatomical location. Results for predictions of the elastic modulus were within 7% average error with experimental results for tarpon scales, and well within the variation in properties of natural fish scales. Experimental variations of strength across scales within a single anatomical region were found to be potentially related to brittle failure due to the presence of defects in the LL and EE.

Chapter 7. Flexural behavior of laminated materials inspired by fish scales: contributions of profile and interface design

7.1 SYNOPSIS

The strength and toughness of natural materials have identified them as a source of inspiration in the design and development of advanced engineering materials. In our previous evaluation of elasmoid scales, a suture-like feature was identified within the limiting layer (LL), which is the most external and heavily mineralized layer of the scales. In the present study, the effect of the LL profile and suture line geometry on the structural behavior of these scales and bioinspired analogues was studied using complementary experimental and numerical efforts. Results showed that the bending stiffness and work to fracture of the scales in flexure are reduced with increasing amplitude and decreasing wavelength of the LL profile. Furthermore, the gradient in elastic modulus of the suture region is instrumental in the scale flexibility. The structural behavior of the scales can be tuned by the suture line shape, its relative position in the LL and the LL profile. The results establish the potential for tailoring the mechanical response of flexible composite laminates by carefully adjusting the layer architectures and their interfaces. The suture line geometry of elasmoid scales appears to be key to its multi-functionality, and can help expand the possibilities for bioinspiration derived from this material system well beyond applications for body protection.

Keywords – bending stiffness; DIC; finite element simulation; fish scales; natural sutures

7.2 INTRODUCTION

In the search for advanced engineering materials, structural biological materials have a combination of strength and toughness that have inspired scientific interest. This combination of properties results largely from a hierarchical organization of the principle building blocks, namely the organic and mineral components. Through this organization and modulation of the mineral content, Nature has developed materials with a wide range of properties, including bone[108,126], the dentin and enamel of teeth [132,133], sea shells[134], turtle carapace[7] and fish scales [8,20,23,30].

By virtue of their high degree of mineralization, hard natural materials are generally considered as brittle and not capable of undergoing large deformation. However, these materials achieve toughness by the presence of weak interfaces, which play an important role in their mechanical response [135,136]. In general, the microstructure of natural structural materials incorporates weak interfaces that increase their toughness by deflecting and guiding cracks that enable larger deformation and exhaust strain energy [135,137]. There are multiple examples of interfaces in Nature, and a variety of different interface geometries, including straight, triangular or wavy sutures and interlocked shapes [138]. Apparently, the interface geometry is important to the overall mechanical response. For instance, brittle sinusoidal sutures were found to be up to three times tougher than straight interfaces made of the same bonding material [139,140]. In addition, periodic triangular sutures were identified to homogenize the stress distribution across the interface, which is beneficial to overall structural performance [134,141]. In the majority of biological composites, these interfaces involve the integration of two materials with very similar mechanical properties. However, fish scales have multiple interfaces that are at the intersection of materials with equivalent and also very different mechanical properties.

The Limiting layer (LL) is the most external and highly mineralized region of the scale and has been regarded as the first barrier against penetration [24]. Based on earlier studies [14,25,83], the mineralization front extends from the LL into the underlying collagen matrix of the elasmodine. Explorations of the tensile properties[131] and fracture resistance of elasmoid scales[67] have revealed that delamination occurs at the EE/IE interface, which appears to initiate from the abrupt change in mineralization. However, delamination surprisingly does not occur at the LL/EE interface despite the large gradient in mineral content [40]. The mechanisms contributing to this behavior have potential for a very large number of applications.

In our previous evaluation of scales of the *Cyprinus carpio* (carp) and *Megalops atlanticus* (tarpon) a suture-like feature was identified within the LL and near the LL/EE interface (**Figure 7.1**). At first glance it resembles that found in teeth[142], tortoise shells[7] and ammonite fossils[141], but appears to have some unique characteristics that have not been elucidated. Based on the knowledge acquired from other natural systems, the sutures and their geometry are expected to play an important role on the multi-functional qualities of fish scales. To facilitate the design of materials inspired by the structure of elasmoid scales, an understanding of the importance of the sutures and their geometry on the structural behavior of these materials is needed.

One of the most intriguing aspects of natural composites is how they can incorporate materials with very different elastic moduli, and achieve multi-functional structural behavior without delamination. With respect to the natural armors of fish, finite element [11] and analytical [52,76,143] models have been used to study the flexural response of fish skin where the scales were treated as uniform plates imbricated in a soft substrate. Finite element models have also been developed to understand the stress distribution in ganoine scales during puncture [144] and to

consider the evolution of fracture involving delamination at the interface of the ganoine layer.[145] Apart from these efforts, no study has explored the importance of the LL and suture designs on the mechanical behavior of elasmoid scales. Therefore, a combined experimental and numerical evaluation of the LL and suture geometry in elasmoid scales was conducted to understand their importance and function.

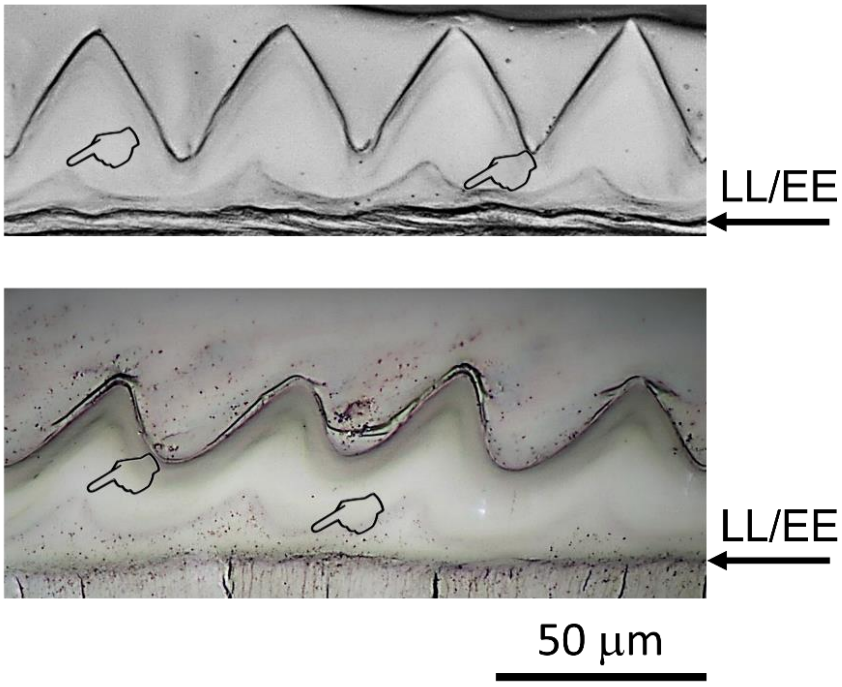

Figure 7.1. Optical images of the LL and the LL/EE interface for the tarpon (top) and carp (bottom). For each scale, the suture and interface are indicated by the pointer and arrow, respectively.

7.3 MATERIALS AND METHODS

Scales were obtained from the bodies of the *Cyprinus carpio* (i.e. freshwater carp) and the *Megalops atlanticus* (i.e. tarpon). The carp scales were extracted from farmed fish marketed as East Asian carp and the tarpon was a wild fish captured in the Caribbean Sea. No additional

information was available regarding the specific fish studied. Scales were extracted from the head and middle regions from both the carp and tarpon fish. These characteristic regions were selected since they have been shown to exhibit less flexible scales than the scales of the tail [118]. The scales were stored in Hanks Balanced Salt Solution (HBSS) at room temperature and tested within a week of extraction.

To characterize the suture geometry with respect to the LL/EE interface (**Figure 7.1**), representative scales from both fish were fixed by submerging them in 2% glutaraldehyde, post-fixated in 1% osmium tetroxide and dehydrated in 2,2- dimethoxypropane (DMP) following procedures outlined in previous studies [87]. Thereafter, the scales were infiltrated in Mollenhauer resin to expose the microstructure, and the potted samples were polished with SiC abrasive paper from mesh numbers of #800 to #4000. Final polishing was performed with a liquid suspension of 3 μm diamond particles, followed by a liquid suspension of 0.04 μm Al_2O_3. The exposed interface was evaluated with an optical microscope (Model BX51, Olympus, Tokyo, Japan) over a control volume of approximately 100x100 μm^2. For evaluation of the three-dimensional (3D) interface geometry, consecutive interface images were obtained by polishing to remove material in incremental depths of approximately 12 μm. Reconstruction of the images was performed in using a commercial software (Solid Works 2016, Educational edition, Dassault systems, Johnston, RI, USA), which enabled visualization of the suture morphology as shown in **Figure 7.2**.

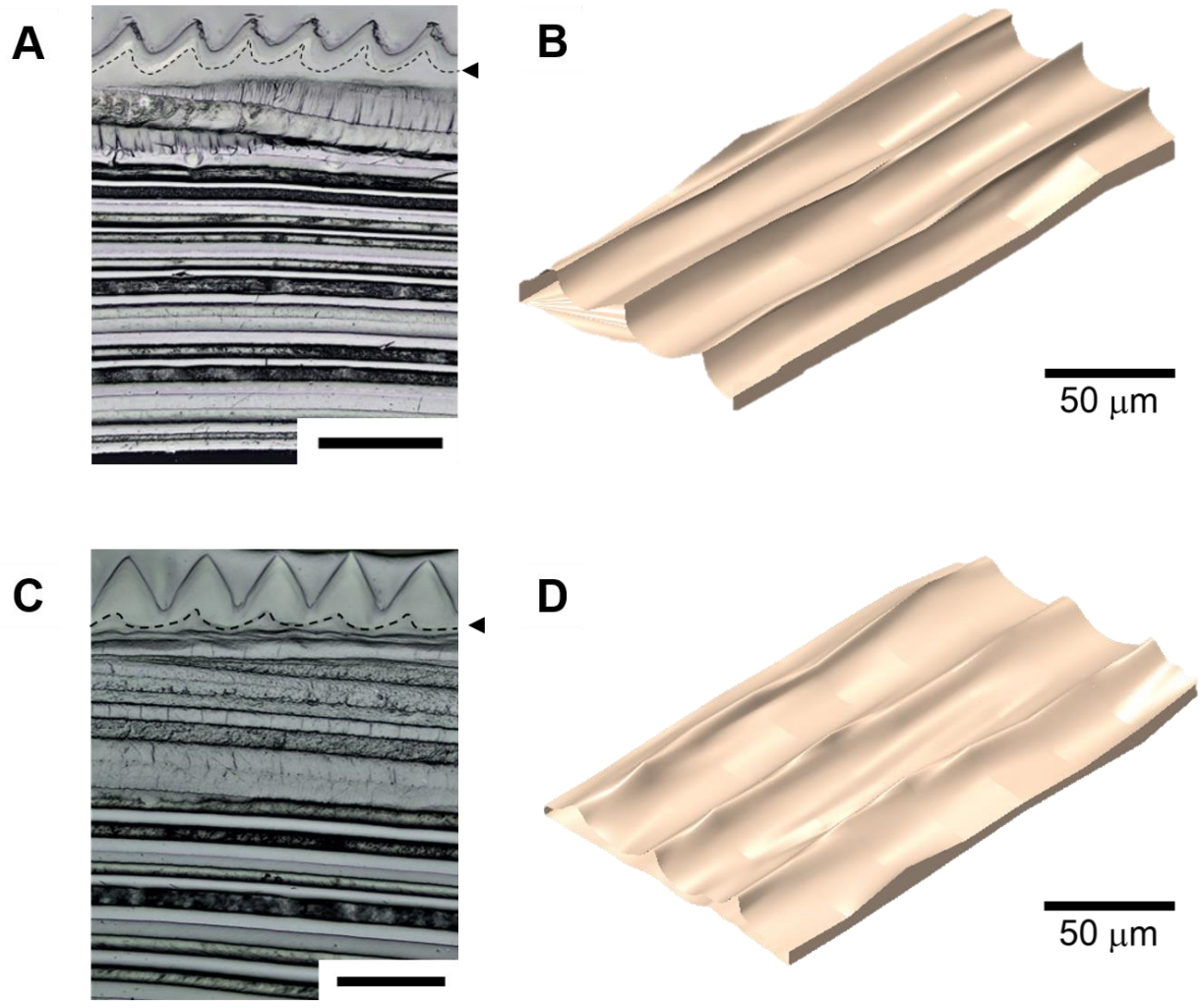

Figure 7.2. Geometry of the suture geometry for carp (A, B) and tarpon (C, D) scales. The 2D profile of the suture is outlined with a dotted line in A and C. The 3D representations of the suture line across the width of the scale (B, D) show that the geometry is continuous through the width of the scale.

The mechanical behavior of the carp and tarpon scales was evaluated under in-plane bending. Each scale was deformed to conform to the surface of steel mandrels with diameters that ranged from 50 mm down to 3 mm. The curvature resulted in specific levels of flexural strain. The strain distribution was evaluated using microscopic Digital Image Correlation (DIC) using the optical microscope. Although surface preparation is generally required for measurements of displacement or strain using DIC, the natural variation in grayscale resulting from the surface topography has

been demonstrated to be sufficient for microscopic measurements using proper surface illumination.[146] To prepare for DIC strain measurements, the scales were polished in the hydrated condition with SiC abrasive paper from mesh numbers of #1200 to #4000, followed by immersion in a 30 vol% aqueous ethylene glycol solution to prevent dehydration over the period of acquiring images. Previous studies have demonstrated that the use of ethylene glycol solution does not affect the mechanical properties of collagen based materials over short duration [147]. The images were obtained with a spatial resolution of 2048×1532 pixels and were processed using Ncorr [148]. a dedicated software developed for DIC, which supports the analysis of large deformation and introduces the necessary corrections for image distortion attributed to the lenses used. A validation of the strain measurements was performed by displacement controlled flexure of a polycarbonate thin sheet over the steel mandrels and comparing the experimental strain fields with those obtained by analytical and numerical estimates. Results of the experiments were in agreement with the analytical and numerical results within 10% average error.

In addition to the experimental component of the evaluation, a finite element analysis was performed to understand the importance of suture geometry and material parameters on the structural behavior of the scales. Numerical models were developed using commercial software (Abaqus CAE 2016, v6.19, Dassault Systems Simulia Corp., Johnston, RI, USA) to evaluate the in-plane bending and transverse tension responses of the scales. A unit cell model was developed that included the IE, EE, Suture and LL as described in **Figure 7.3**. Both the IE and EE were treated as continuum with isotropic properties as a simplification for the twisted plywood arrangement of the elasmodine in the scales of these two fish [87]. Due to the high mineral content of the LL (~70%), it was modeled as a linear elastic material [149]. The remaining layers were modeled as

elastic-plastic, with the inelastic behavior defined according to the results of previously reported tensile tests [23,31,40]. Table 7.5 contains the mechanical properties used in the models for each layer.

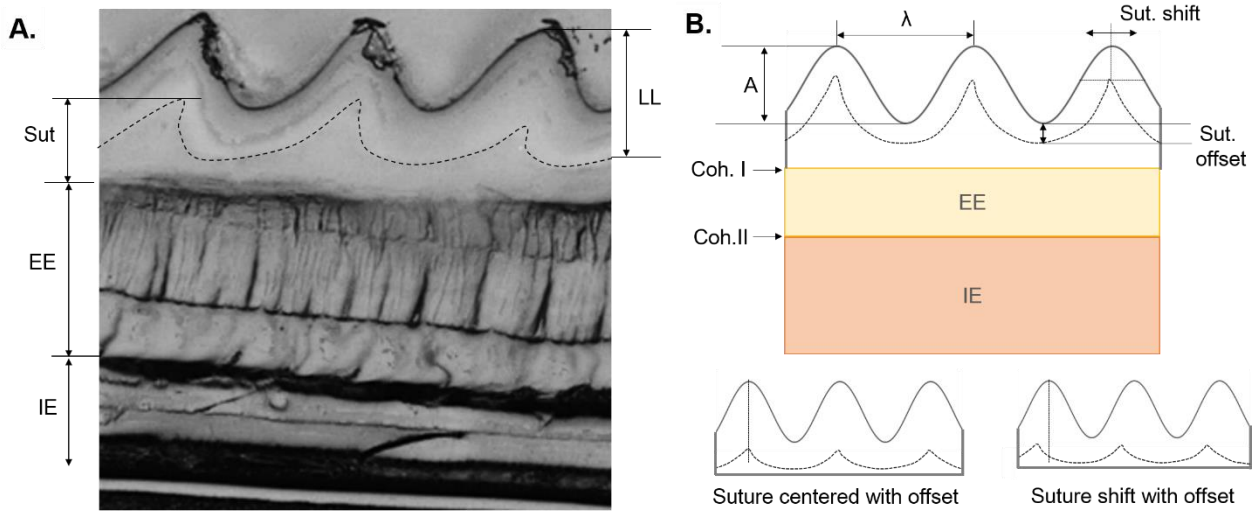

Figure 7.3. Unit cell of the layered system used in the numerical model. A) Optical image of a carp scale showing the external elasmodine (EE), the suture (Sut) and the limiting layer (LL). For simplicity, the LL and Sut geometry were idealized with sinusoidal wave geometry as shown in B. The amplitude (A), wavelength (λ), suture shift and suture offset were evaluated parametrically in the model. Variation of these parameters allowed the natural geometry of the tarpon scales to be replicated by having a suture offset followed by a suture shift as shown. Mechanical properties of the cohesive interfaces (Coh. I and Coh. II) were also varied to account for the influence of mineralization or collagen fibers.

Table 7.5. Mechanical properties of the layers used in the numerical simulations.

LAYER	**ELASTIC MODULUS (GPa)**	**POISSON'S RATIO**	**σ_y (MPa)**
Internal Elasmodine	0.45	0.27	9.6
External Elasmodine	2.0	0.28	15.4
Suture	21.0	0.28	15.4
Limiting Layer	30.0	0.30	------

Preliminary experiments involving flexure loading of the scales revealed that delamination of outer plies of the internal elasmodine occurred prior to the initiation of cracks in the LL (**Figure 7.4A**). A higher degree of flexure caused crack initiation in the valleys of the circuli of the LL, and propagation into the thickness as shown in **Figure 7.4B**. Separation or delamination along the suture was not observed, even under magnification. Therefore, the apparent interface at the suture line was defined with tied condition, whereas cohesive elements were used to model the IE/EE and the LL/EE interfaces. The definition of cohesive elements allowed separation of the bonded layers. The cohesive zone model follows a trapezoidal traction-separation law, which assumes that the cohesive elements have an infinitesimal thickness. The material properties of the cohesive elements were defined to simulate type I collagen, with an axial and shear modulus of 500 MPa and 29 MPa [121], respectively. Damage of the cohesive elements was defined when the maximum normal or maximum shear stress exceeded 16 MPa and 9 MPa [150], respectively. Damage evolution was defined by a normal displacement (transverse to the interface) of 45 μm, which is a critical distance observed experimentally were the collagen fibers no longer served as connective ligaments (**Figure 7.4A**).

Carp and tarpon scales have a diameter at least 100 times larger than its thickness. In addition, the sutures extend predominately along a single axis, as shown in **Figure 7.2**. Therefore, a 2D plain strain simulation was chosen to represent the scale response. A portion of the total scale was modeled that consisted of a segment length of 5 mm. Displacement control loading was performed to simulate flexure about a rigid mandrel with frictionless interaction. The required finite element mesh size was defined by the characteristic length (l_{cz}) of the cohesive zone according to

$l_{CZ} \propto E \cdot G_{coh} / \sigma^2_{max}$ where E, G_{coh} and σ_{max} are the elastic modulus, cohesive energy or work of separation and strength of the cohesive material. Similar to a previous study where the bonded interface is defined to simulate collagen, the characteristic length is 23 μm [151]. For all cases, the nominal element size (h_e) along the bonded interfaces was chosen to satisfy the requirement that $h_e \leq l_{cz}/5$. Given the detailed geometry of the scales and results of a mesh sensitivity study (Appendix B), values of $h_e \approx 2\ \mu$m at the cohesive interfaces and a $h_e \approx 0.5\ \mu$m for the suture and LL were determined sufficient.

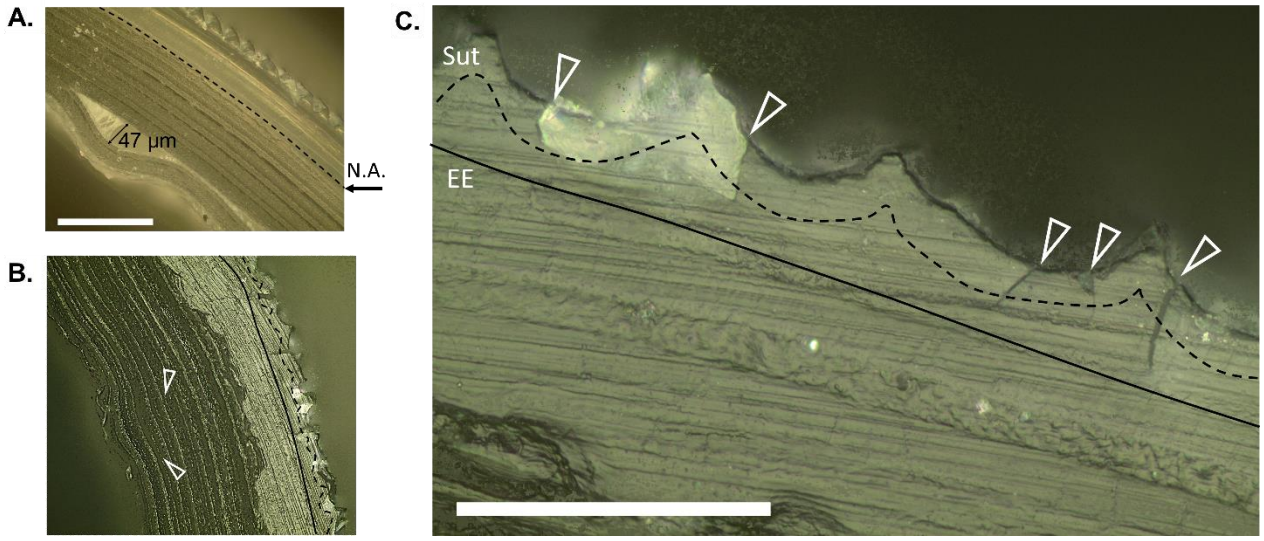

Figure 7.4. Deformation behavior of the scales. a) Tarpon scale deformed to a radius of curvature of 16 mm. The neutral axis (N.A.) is shown as calculated and is close to the IE/EE interface. Note the delamination of internal elasmodine (IE) plies due to buckling of the most interior laminae. Scale bar = 200 μm. b) Carp scale deformed to a radius of curvature of 1.5 mm, where buckling of the internal elasmodine is indicated. Fracture of the limiting layer was observed within the valleys of the LL, which is highlighted in c. c) Cracks in the LL and propagation towards the external elasmodine (EE). Scale bar = 50 μm.

Failure of the scale was defined by the experimental strain that caused the initiation of cracks in the LL. The relative scale performance, and the influence of the geometric parameters of the LL

and suture geometry, were assessed in terms of the bending stiffness of the scale (κ), the work to the onset of fracture (i.e. crack initiation), defined as the area under the load load-line displacement response until failure of the LL occurred, and the stress at fracture. The normal (σ_{CZ}) and shear (τ_{CZ}) stresses at the cohesive interfaces, were also evaluated.

A parametric evaluation of the contributions from the LL profile and suture geometry to the structural behavior of the scale was performed. As shown in **Figure 7.3**, the LL and suture were defined with sinusoidal wave geometry. The amplitude (A) and wavelength (λ) of the LL were varied to represent ¼, ½, 2 and 4 times the natural values of the LL for the carp (**Figure 7.3B**). These amplitude modifications also result in changes to the LL thickness. Furthermore, separation between the valleys of the LL and suture line was defined as the suture offset (Sut), which was varied from 0 to 100%. The definition of 0% corresponds to the when the suture is at the valleys of the LL, and 100% corresponds to sutures in contact with the LL/EE interface. The suture line is closer to the LL/EE interface in the tarpon scales (**Figure 7.1**), and the suture is not directly in phase with the LL in either scale. Therefore, a suture offset was explored by comparing a centered suture with a suture shift (translation) of 25% the wavelength. Finally, the properties of the cohesive elements were also included in the parametric evaluation. As shown in previous work, the alignment of the collagen fibers to the loading axis has a strong effect on their stiffness and effective strength[119]. Therefore, the elastic modulus was modified following the model proposed by Nielsen and Chen in 1968 [127] where the elastic modulus varies from 500 MPa for vertically aligned collagen to 63 MPa for collagen fibrils aligned with the interface. Since mineralization of the elasmodine is a downwards process [53,82,88,111], the cohesive interfaces can be subject to different degrees of mineralization. As such, the E_{coh}/E_{EE} was evaluated from

0.25 representing a non-mineralized interface to 1.0 assuming that the cohesive layers are mineralized to an equal degree as the EE.

7.4 RESULTS

The strain distribution across the thickness of a carp scale resulting from flexure loading is shown in **Figure 7.5**. Results from DIC showed that the overall strain increased with decreasing radius of curvature, as expected, and that the highest strain developed in the valleys of the LL due the geometric stress concentration. **Figure 7.5A** shows the strain distribution from experimental evaluation of a selected scale when deformed to a radius of curvature of 1.5 mm. At this extent of flexure, cracking within the LL layer was observed. A strain map corresponding to the numerical results for flexure is shown in **Figure 7.5B**. Results from the FEM simulations indicate that the highest strain in the scale occurs at the suture line, with a maximum of 7.5% strain, that the strain at the valleys of the circuli reached an average maximum of 3.3%. Previous studies have demonstrated that highly mineralized collagen matrices, like dentin, undergo microstructural cracking and that a strain-controlled failure criterion is most appropriate [152]. Based on the DIC results, a strain of 3.3% was defined as the critical strain corresponding to the initiation of failure at the valleys of the LL. This value was used in all further parametric analysis concerning the effects of suture and LL geometry on the structural behavior in the numerical model.

The effect of the LL and suture line geometry on the bending stiffness of the scales is shown in **Figure 7.6**. The average bending stiffness of the carp scales was found to be approximately 4

N/mm. That did not change with simplifying the suture from its natural shape to a symmetric sinusoidal wave profile (**Figure 7.6A**). Similarly, an offset of the suture to the center of the LL thickness and a shift of the suture line (25% of the wavelength) increased the bending stiffness by up to 40% as evident in **Figure 7.6A**. Variation in the suture offset over the LL thickness caused substantial changes in bending stiffness as shown in **Figure 7.6B**. The natural suture offset in **Figure 7.6A** represents a displacement of 10% from the LL/EE interface. Further displacement of the suture line towards the LL/EE interface increased the bending stiffness to its maximum of roughly 50%. In contrast, movement of the suture line closer to the LL decreases the stiffness, with nearly 70% decrease at the 0% offset position.

Changes in bending stiffness of the scales with LL amplitude and wavelength are shown in **Figure 7.6C** and **Figure 7.6D**, respectively. The bending stiffness increases with a decrease in amplitude and an increase in wavelength. The largest increases occurs for a flat LL, regardless of the presence of a suture, which promotes well over 100% increase in the bending stiffness with respect to that of the natural carp scale LL profile. An increase of the wavelength was also found to cause an increase in the bending stiffness as evident in Figure 6d. In comparison to the influence of the LL and suture geometry, changes in properties of the LL/EE and IE/EE interfaces did not contribute to the bending stiffness substantially (not shown). The maximum increase in scale stiffness occurs when the interface is mineralized and the collagen fibers are parallel to the interface, but the increase is limited to less than 10%.

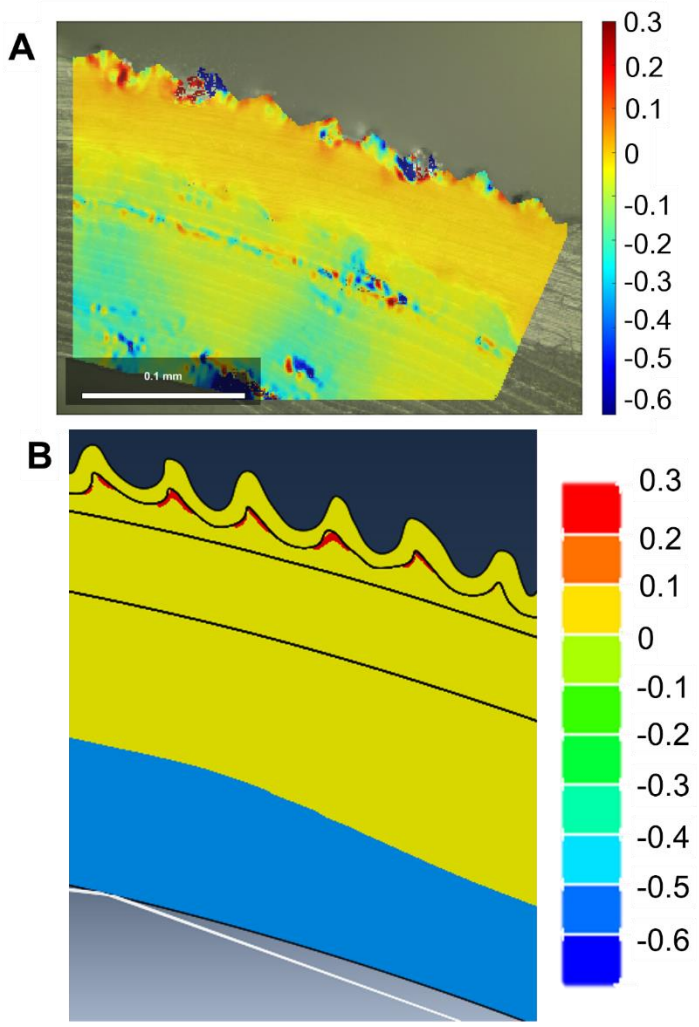

Figure 7.5. Strain field in a section of carp scale conformed to a 1.5 mm radius mandrel. A) Experimental strain map obtained using DIC, and B) results from the finite element model.

The effect of parametric variations of the LL and suture line geometry on the work to failure of the scales is shown in **Figure 7.7**. The influence of suture profile is shown in **Figure 7.7A**. The work to fracture of the natural carp scales was roughly 1.6 kJ, which increased by 40% by simplifying the suture profile geometry to a sinusoidal wave. In comparison, an offset corresponding to that observed in the tarpon scales resulted in over 100% increase in the work to fracture; further increase occurred with suture shift to the left by a distance of 25% of the LL wavelength. Similar to the changes in bending stiffness, an increase of the suture offset increased

the work to fracture (**Figure 7.7B**) and nearly 500% increase occurred with the suture line displaced to the LL/EE interface (100% offset). Conversely, over 100% decrease occurred when the suture line was displaced closest to the LL surface (0% offset). The importance of changes in the amplitude and wavelength of the LL on the work to fracture are shown in **Figure 7.7C** and **Figure 7.7D**, respectively. First, the work to fracture increased with a decrease in LL profile amplitude as shown in **Figure 7.7C**, and the work to fracture was greatest for a flat LL. The influence of LL wavelength is presented in **Figure 7.7D**, which shows that the work to fracture increases with increasing wavelength. An increase in wavelength to 4λ caused an increase in the work to fracture of over 200% and further increase occurred with change to a flat LL profile. Note, however, that these changes cause an increase in stiffness. The influence of collagen fiber alignment and interface mineralization are shown in **Figure 7.7E** and **Figure 7.7F**, respectively. As evident, variations in the properties of the interface also had a substantial contribution to the work to fracture. The maximum increases were observed when the collagen fibers are parallel to the interface (49%), and when the interfaces is highly mineralized (170 %) and compatible with that of the EE.

The stress at failure corresponding to the initiation of cracks in the LL that resulted from flexure loading during the experiments was estimated to be 105 MPa. Using the same definition of critical strain in the simulations, the influence of interface and suture geometry on the corresponding maximum stress at failure are shown in **Figure 7.8**. Simplification of the suture geometry to a sinusoidal profile had essentially no effect on the stress at failure as evident in **Figure 7.8A**; the same was true for suture shift. Suture offset was the most important, and caused a 10% reduction in the failure stress when the offset is minimum (0%) and close to the LL surface. A vertical offset

of the suture to the maximum (100%) at the LL/EE interface had limited effect on the stress at failure (**Figure 7.8B**). The amplitude (**Figure 7.8C**) and wavelength (**Figure 7.8D**) of the LL profile had opposite effects on the stress at failure. Specifically, an increase in the amplitude resulted in an increase in the stress failure, but was limited to less than 10%. Conversely, a decrease in the amplitude caused a small reduction in stress. In regards to wavelength, the failure stress decreased with increasing wavelength as evident in **Figure 7.8D**. Variations in the fiber alignment and mineralization of the cohesive interface had negligible contributions to the failure stress (not shown).

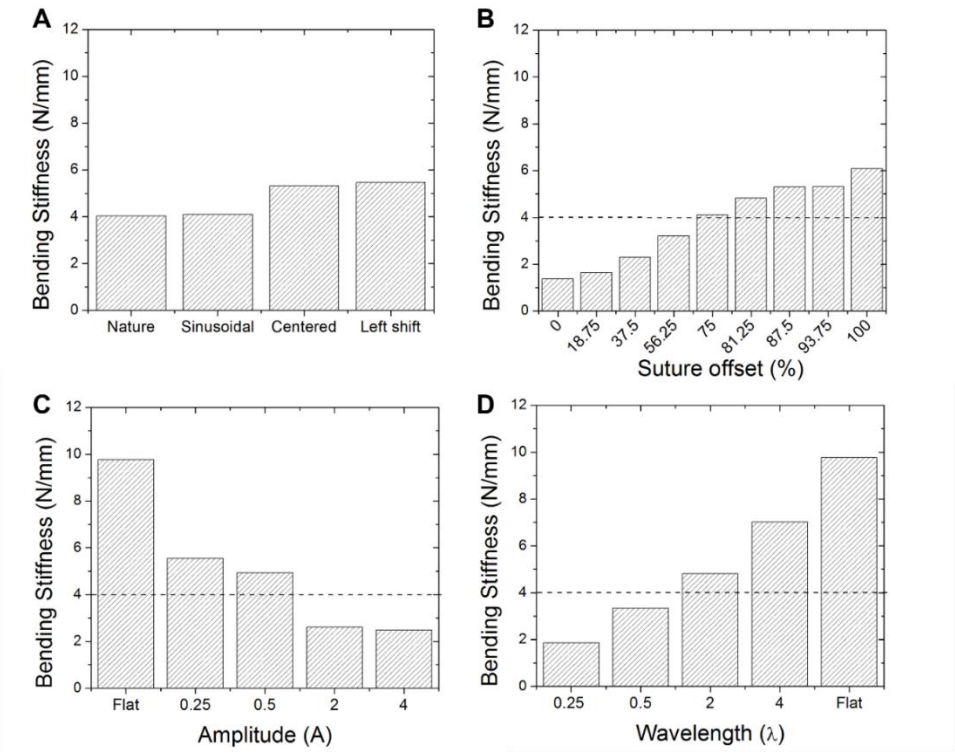

Figure 7.6. Effect of the parametric variations on the bending stiffness of the scale. A) Suture shift, B) suture offset, C) amplitude, and D) wavelength. The dotted line in B, C and D represents the stiffness of the natural scales as determined from experiments. ..

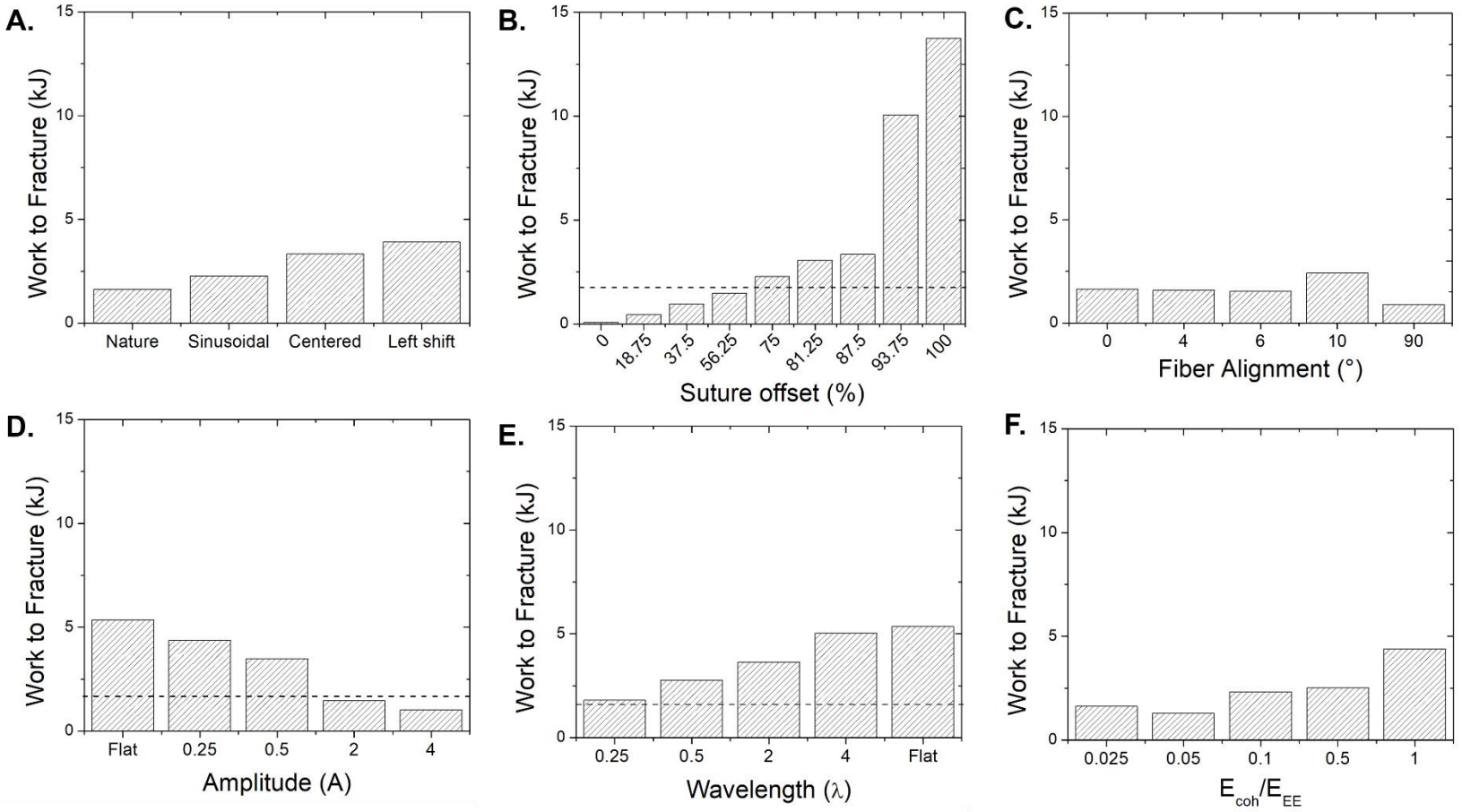

Figure 7.7. Effect of parametric variations of the limiting layer on the work to fracture. A) Suture shift, B) suture offset, C) fiber alignment in the cohesive interfaces, D) amplitude, E) wavelength and F) mineralization of the cohesive interfaces. The dotted line in B, D and E represents the response of the natural scales.

A parametric evaluation of the stress distribution at the LL/EE and EE/IE interfaces was also conducted. The influence of LL and suture geometry on the interfacial stresses acting on COHI and COHI are shown in **Figure 7.9**. The distributions in this figure represent the stresses along a representative window of evaluation. Although the tensile and shear stress were greater at the LL/EE interface for all the parametric conditions, they were at least an order of magnitude below the critical stress that would result in interfacial failure. For instance, when the carp scales are deformed to the smallest mandrel diameter (3 mm), the maximum tensile and shear stresses within the COHI were 2.7 and 4.7 MPa, respectively; the maximum values of stress in the COH II were 2.2 MPa and 1.4 MPa. The shearing stress was slightly greater than the opening-mode stress in all conditions. **Figure 7.9A** shows that the distribution of stress across the interfaces follow the geometry of the LL. The variations in geometry had a strong influence in the stress distribution across the scales. A simplification to a sinusoidal profile creates a distinct wave distribution of the stress, whereas a flat LL resulted in a mostly constant value of stress through the interfaces. Of note, the effect of the LL geometry and suture is most important to the LL/EE interface. Furthermore, single parameter geometric variations had multiple effects on the interfacial stress distribution. Changes in the stress distribution across the cohesive interfaces with variations in LL amplitude are shown in **Figure 7.9B**. Reducing the LL amplitude decreased the stress and caused only small differences in the wavelength. The effect of variations in the LL profile wavelength are presented in **Figure 7.9C**. Increasing the LL wavelength resulted in a larger amplitude and wavelength of the corresponding stress.

7.5 DISCUSSION

The microstructure of fish scales bestows them with an interesting combination of flexibility and toughness [18,20]. An understanding of contributions from the scale microstructure to achieve this unique multi-functional behavior is a prerequisite to realizing bioinspired flexible body armors and beyond. Based on their architecture, the structure of fish scales incorporates a large number of bi-material interfaces. These are utilized in other natural materials to endow toughness to systems that would otherwise exhibit brittle behavior [136]. This concept has potential for synthetic materials as well. For instance, suture-like features engraved in glass suppress brittle fracture and confer flexibility [12,75]. In this paper, the suture region of the limiting layer in elasmoid fish scales was evaluated for the first time, and its contribution to the structural behavior of elasmoid scales was characterized. Overall, this feature appears to play a key role on the structural behavior of the scales and is an important element of the topological design in achieving biomimetic materials with so-called protecto-flexibility [153], viz. the multi-functionality consisting of flexibility and toughness.

An ideal material for "wearable" armor applications would possess low bending stiffness and high toughness. Although important, an increase in strength is not necessarily of direct value to function. Interestingly, while parametric variations of the LL and suture line geometry had a substantial effect on the flexural stiffness (**Figure 7.6**) and the work to fracture (**Figure 7.7**), they did not influence the stress at failure of the LL (**Figure 7.8**). It is important to clarify that the work to fracture in **Figure 7.7** represents a measure of the work required to initiate failure of the limiting layer and not bulk fracture of the scale. In fact, the scales do not undergo fracture by flexure loading, even when folded on top of themselves. Here, the work to fracture was estimated from

the integration of area under the flexure load load-line displacement response that was obtained from the simulations. That measure of performance further exemplifies the incredible durability of these materials.

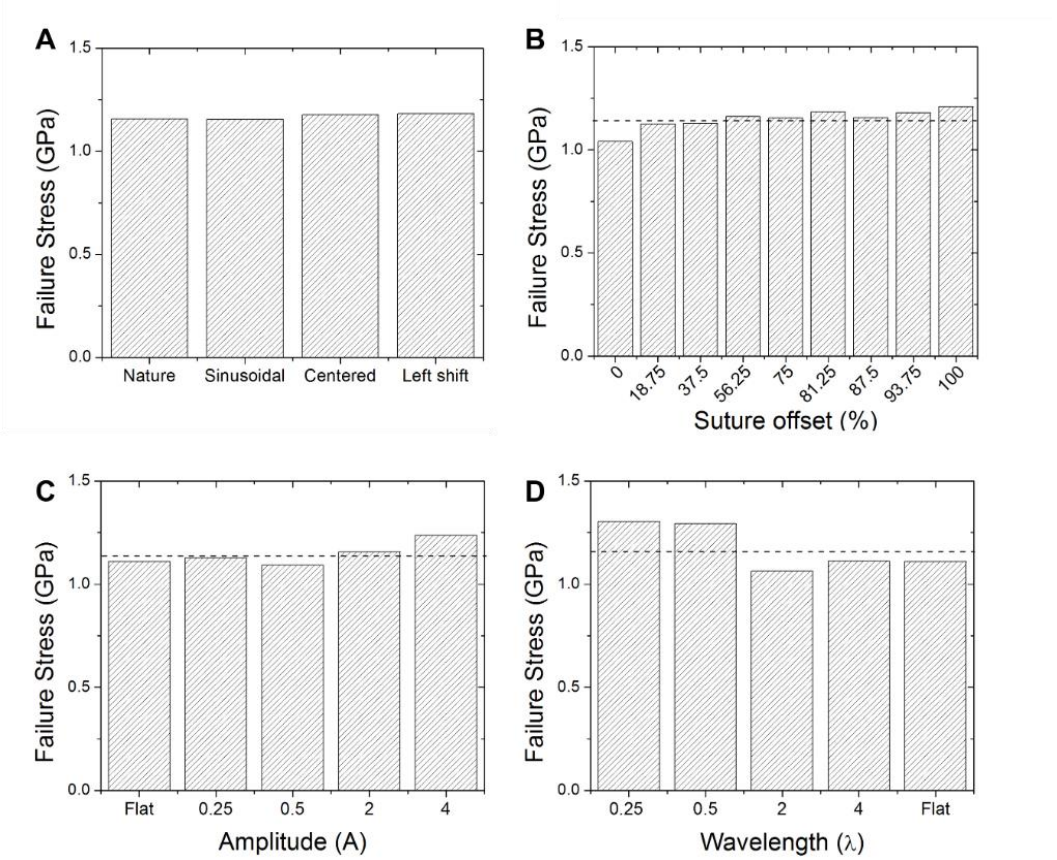

Figure 7.8. Effect of parametric variations of the suture geometry on the stress at failure. A) Suture shift, B) suture offset, C) amplitude and D) wavelength. In B, C and D the dotted line represents the stiffness of the natural scales.

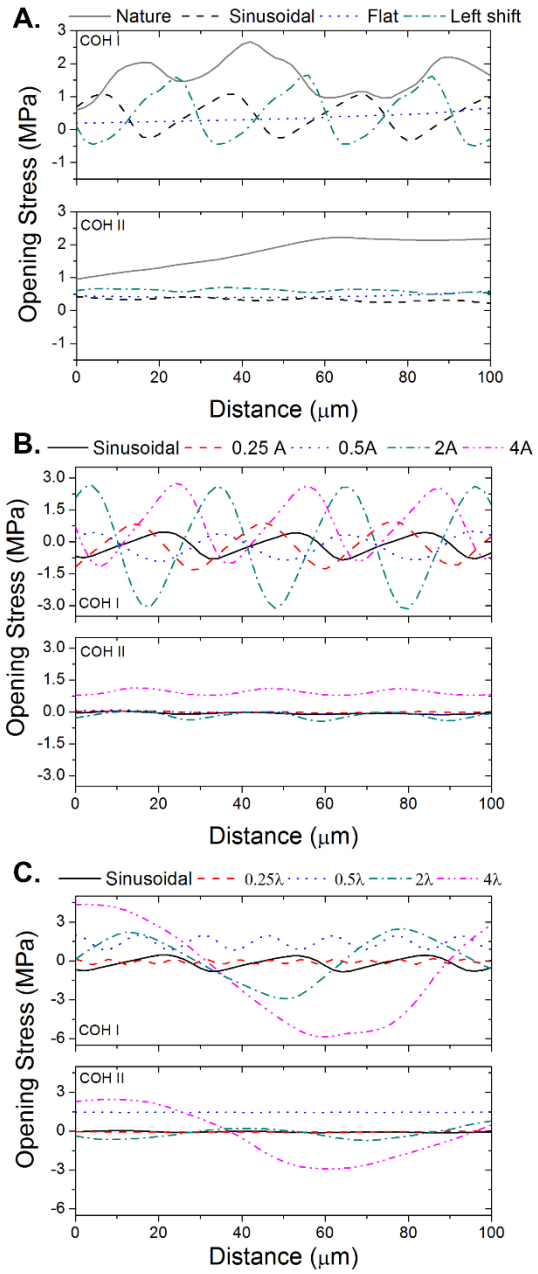

Figure 7.9. Distribution of the opening mode stress along the cohesive interfaces over a representative window of the total scale length. The stress distribution follows the wave pattern of the limiting layer. A) Influence of the general geometry and the suture shifted with parametric variations of the amplitude (B) and wavelength (C). In all of the parametric variations studied, the cohesive interface I had a higher opening stress than the cohesive interface II

An offset of the suture line relative to the surface of the scale has important contributions to the bending stiffness and work to fracture of the scales (**Figure 7.6B** and **Figure 7.7B**). As defined in the model, the degree of offset influences the relative thickness of the most highly mineralized layer of the LL. As such it contributes directly to the LL stiffness, as well as to the flexibility and work to fracture of the scale overall. As evident in **Figure 7.6B**, the flexibility decreases with an increase in offset, which results from the increased thickness of the highly-mineralized and consequently stiff portion, located farthest from the neutral axis. Variations in the amplitude and wavelength of the LL were also very important to the scale stiffness and work to fracture. These two parameters contribute to the relative thickness of the LL in relation to the elasmodine, including the suture region. They were also important to the degree of stress concentration posed by the circuli. Higher amplitudes of the LL profile displace the neutral axis of the scale closer to its nominal center, which increases the flexibility at the expense of resistance to failure due to the rise in stress concentrations at the root of the circuli. An increase in the wavelength, however, results in an increase of the bending stiffness and the work to fracture due to the reduced number of flexion points and the reduction in stress concentration associated with the circuli valleys.

In comparison to the LL and suture geometry, variations in the properties of the LL/EE and EE/IE interfaces were of limited importance to the structural behavior of the scales. Specifically, they had limited effect on the scale stiffness, and only moderate contributions to the work to fracture as evident from **Figure 7.7C** and **Figure 7.7F**; the largest contribution was observed in mineralization of the interface (**Figure 7.7F**). As such, the microstructure of these interfaces appears to have evolved to maintain cohesion under function, but not contribute to the macroscopic responses directly. Although cracking of the LL was observed during flexure loading, the scales did not

undergo delamination between the principle layers, even under flexure at the smallest radius of curvature. Indeed, the interfacial stresses in bending are small (**Figure 7.9**), which results from the distribution of the layers, and that the neutral axis position is very close to these interfaces (**Figure 7.4A**).

A comprehensive description of contributions from the LL geometry and suture parameters to the bending stiffness and work to fracture of the scales is presented in **Figure 7.10A** and **Figure 7.10B**, respectively. An optimized design for multi-functional behavior exhibiting the lowest stiffness (i.e. highest flexibility) and the highest work to fracture resides at the lower right corner of these plots. Although the natural carp scale design achieves the lowest stiffness of the biomimetic designs considered (**Figure 7.10A**), it is not optimal. Further improvement is achieved by removing the inclination of the circuli, which yields an increase in toughness with negligible change in the flexibility. As the LL profile geometry is dominated by the circuli distributed across the surface, the importance of valleys and crest in the topography have been considered in previous studies [149]. Circuli are interpreted as an evolutionary feature that increase the scale flexibility and facilitate anchoring them to the body. A flat surface profile of the carp LL would result in a 2.5 fold increase of the stiffness as indicated in Figure 10a, which is similar to a previous estimate for flat *Arapaima gigas* scales [32].

An interesting aspect of the scale microstructure is the potential for modifying the multifuntionality through changes in the interfaces of the layered system. **Figure 7.10B** suggests that the LL/EE and EE/IE interfaces should be mineralized and that up to nearly 3X improvement in the work to

fracture is achieved with mineralization of the cohesive interfaces, without a significant decrease of the scales flexibility. While changes in suture offset and suture wavelength caused coupled changes in stiffness and work to fracture, the interface design appears to influence the work to fracture only.

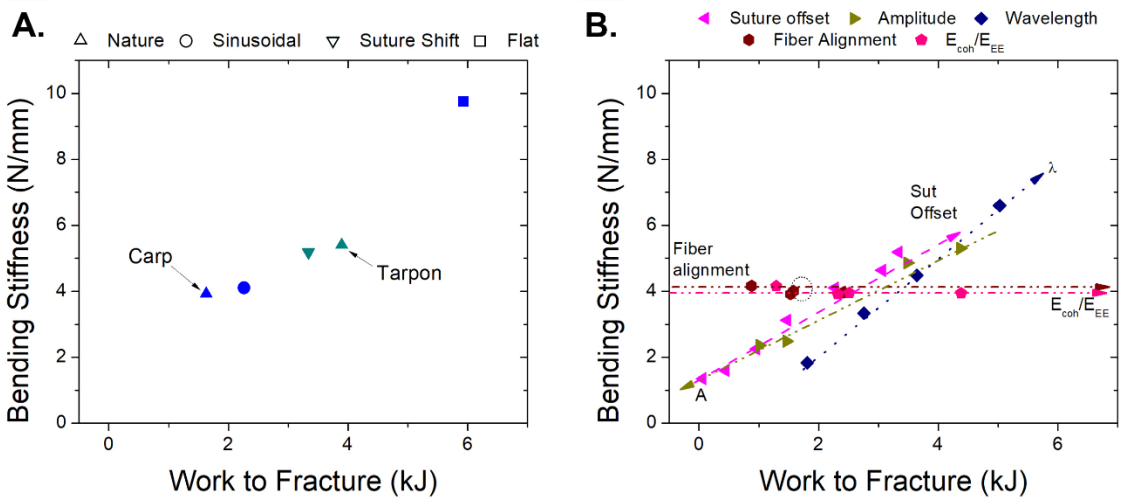

Figure 7.10. Relative performance of alternative suture and LL designs and the influence of the suture parameters on the bending stiffness and work to fracture. a) Effect of suture geometry and shift with respect to the natural designs of the carp and tarpon scales, as well as the influence of changes in LL geometry of the carp to flat profile. b) Modifying the suture offset, amplitude, wavelength and interface properties of the carp scales. In each case the dotted lines indicate the direction in which each parameter increases in value.

One of the most important findings of this study is that a desired performance of the scales can be achieved using multiple combinations of the LL and suture geometry. Considering the different environments and threats across multiple species, fish scales require different degrees of resistance to puncture, toughness and flexibility [29,131]. Previous studies have demonstrated that the LL is

the first barrier against puncture [24] and therefore a thicker LL is more desirable in fish with greater threat. For example, the arapaima has the piranha fish as one of its predators [32]. Perhaps as a consequence of the greater need for resistance to puncture, the arapaima scales have a significantly thicker LL in comparison to other teleost fish [87]. An increase in the highly mineralized layer of the scales decreases their flexibility. To modulate flexibility, the amplitude and wavelength of the circuli (**Figure 7.10B**) are adjusted accordingly. Based on previous work, the LL thickness of arapaima scales is up to 10 times greater than that of the carp [87]. Arapaima scales have LL amplitude and wavelength that are twice that of the carp and tarpon, which endow them flexibility without sacrificing protection against puncture [118].

The flexibility of the scales can be increased with suture and offset towards the LL/EE interface. This is a valuable lesson in biomimetic design as proper location of a suture region can increase the overall performance of the composite. An example is evident in comparing the layered structure of carp and tarpon scales. Both the LL thickness and EE ratio of the tarpon scales were higher than those of the carp scales. Tarpon fish can be found in different habitats and its predators range from birds, sharks and porpoises to crocodiles and alligators. In general, the larger LL thickness and depth of mineralization across the elasmodine serve to increase the puncture resistance of tarpon scales. Yet, the tarpon fish can reach speeds between 2 to 7 kph [154–156], which exceeds that of the carp and increases the importance of scale flexibility. The tarpon scales have of higher amplitude LL profile and a well-defined suture region, both yielding higher flexibility. Increasing the suture offset towards the LL/EE interface decreases flexibility and increases work to fracture of the scales. In the case of tarpon scales, it seems that nature assigned more weight to protection, than flexibility. Interestingly, previous studies have theorized scales

may serve as springs that store elastic energy during bending of fish to facilitate locomotion [52,157]. In such case, the offset of the suture line in tarpon would become of significant importance to the speeds they reach. Contrary to the carp and tarpon scales, the arapaima scales did not exhibit a visible suture region. As evident from **Figure 7.6** and **Figure 7.7**, the suture offset plays an important role on the scales structural behavior. A scale without suture results in nearly 70% increase of the bending stiffness but nearly 100% increase of the work to fracture. If puncture resistance is more important than flexibility, then the highest resistance to puncture can be achieved by the removal of the suture region.

It is important to put the results in perspective. Flexibility of the fish is a function of its exterior armor, and its oseo-muscular system [158]. In a recent study it was estimated that the smallest radius of curvature for the striped bass, which has similar body length and width to the carp [157], was 62 mm at the tail of the fish. This value is much higher than that evaluated in the present study. Clearly, gross failure of the scales is not expected to happen during simple locomotion of the fish! Scales have the potential to serve as a bioinspirational material beyond applications to body protection. The possibility of tailoring the response of composites by modifying its layered system and the geometry parameters of its profile opens the door to new exiting possibilities. Flexible substrates that are capable of withstanding small curvatures are highly desirable in modern technological developments. Flexible electronics exemplify an engineering application where materials with significantly different elastic moduli are bonded and are expected to withstand large deformations [159]. Clearly, scales have evolved to be resistant to puncture, however results of the layer architecture could be relevant to the design of materials systems for flexible displays, for

flexible circuits, or for biosensor that are required to conform to the natural curvature and movement of the human body.

Numerical modeling of complex systems usually begins with simplifications. In this study, a unit cell model was adopted to evaluate the structural behavior of the scales that involved the layered geometry and elastic-plastic definitions for the constitutive behavior. These aspects represent an advancement over prior efforts. Nevertheless, there are some additional aspects of the structural behavior noted in the experiments on scales that warrants discussion. While the model represented an idealized unit cell geometry, there were defects within the scale that influenced the flexure distribution and the contributing mechanisms. An optical evaluation of the scales under different degrees of flexure revealed that the scale radii serve as sites for the preferential initiation of cracks in the LL, as shown in **Figure 7.11A**. These are discontinuities in the LL and within these regions, crack propagation continued preferentially along the radii until reaching the EE/IE interface. Delamination occurred subsequently at the interface of plies of the IE, rather than at the EE/IE or LL/EE interfaces. With increasing levels of flexure, buckling of the elasmodine plies was noted (**Figure 7.11C**). The radii served as sites of concentrated strain that reduced the magnitude of strain elsewhere and its uniformity. Hence, the radii increase scale flexibility, as hypothesized previously [24,88], but also guide the growth of damage, and control the deformation response of the scale at the macro level. The next generation of numerical models for scales could include the radii of the limiting layer and individual plies of the elasmodine to better understand the functionality of these features and their contribution to localizing damage and as guides to delamination and fracture, which control failure of the scales.

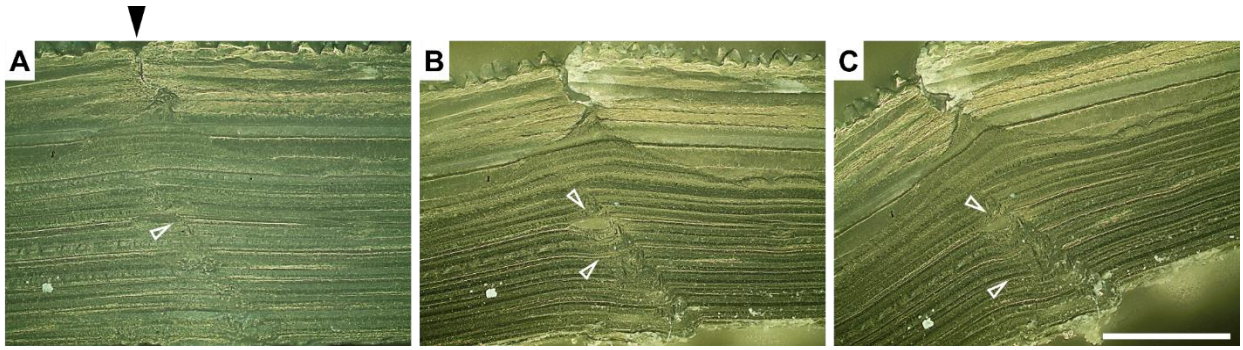

Figure 7.11. Dark field optical images of flexure of a tarpon scale with radii. From left to right deformation process evolved from: initial deformation until achieving a radius of curvature of 6 mm. A) Initial undeformed state, where a radii at the surface of the limiting layer is highlighted with black arrow. The radii extends within the elasmodine as indicated by the white arrow; B) scale at a radius of curvature of 26 mm and C) at a radius of curvature of 13 mm. In b and c the white arrows indicate delamination and buckling of the elasmodine plies. Scale bar = 200 μm

7.6 CONCLUSION

Contributions from the limiting layer (LL) and suture line geometry to the structural behavior of elasmoid fish scales was studied using complementary experimental and numerical evaluations. Experiments involved controlled flexural loading of the scales to understand the mechanisms of failure and numerical modeling enabled a quantification of effects from the LL and suture line geometry to the bending stiffness, stress at failure and work to fracture. Failure of the scales occurred by crack initiation at the valleys of the LL and propagation extended into the elasmodine with adequate driving forces. The bending stiffness and required work to fracture of the scales in flexure are reduced with increasing amplitude and decreasing wavelength of the LL profile. The circuli of the LL in natural carp scales decrease the bending stiffness up to 2.5X in comparison to a flat LL. Although the suture region did not contribute to the mechanisms of failure, the gradient in elastic modulus increases the scale flexibility substantially. As such, the scale flexibility can be tuned by appropriate suture line offset and increases in the flexibility achieved by placing the

suture line closer to the LL surface. In addition, the work to fracture can be increased by mineralizing the interfaces, without sacrificing flexibility. Overall, the results of this study establish the opportunity for tailoring the mechanical response of flexible composite laminates by adjusting the layer profiles and their interfaces. Application of the findings have tremendous potential in the bioinspired design of multifunctional laminated material systems.

Chapter 8. Conclusions, limitations and future work

8.1 CONCLUSIONS

A combination of experimental, analytical and numerical investigations were performed to understand the contributions of the architecture and composition of elasmoid fish scales to their structural behavior. This thesis describes these investigations in detail, the findings, and their importance in the field of structural materials. The long-term objective of this research is to develop a fundamental understanding of this natural dermal armor, and to obtain the essential knowledge that is necessary to support the development of a new class of flexible bioinspired composites materials.

In general, the elasmoid scales of teleost were found to be composed of type I collagen fibers with different degrees of mineralization that varied with anatomical location within species and also between species. Overall, the scales exhibited three different layers, including an external heavily mineralized layer called the limiting layer, followed by the elasmodine, which consists of a distribution of plies of unidirectional type I collagen fibrils with specific stacking sequence. The elasmodine is further divided into the external and internal layers according to the mineral content.

As a result of their composition and architecture, elasmodine fish scales are flexible and have the ability to undergo substantial inelastic deformation before failure, with strain to failure exceeding 15%. Based on these qualities, traditional methods for characterizing the fracture toughness are

rendered invalid and a new methodology for assessing the energy to fracture was adopted that follow a standardized method of tear testing. Using this approach it was shown that the fracture resistance of scales from the East Asian carp exceeded that of polycarbonate, a fracture resistant engineering polymer that is commonly used for safety devices. Through an evaluation that involved testing over a temperature range from 21 to 150 °C, it was observed that the energy to fracture of the scales decreased significantly at the lowest temperatures, which were below the transition temperature of collagen. The findings correct the statements of previous investigators suggesting that scales don't exhibit a decrease in toughness with decreasing temperature, even after the immersion in liquid nitrogen.

One of the most important findings of this investigation is that the microstructure of elasmoid scales is highly dependent on the anatomical region of the body from where the scales are located, and that the spatial distribution is unique for three particular species of fish evaluated. There were significant differences in scale thickness, number of plies in the elasmodine and the ratio of mineralized plies in the external elasmodine to that of the entire elasmodine. It was identified that many of the mechanical properties of scales are controlled by the external elasmodine ratio, and that the spatial variations in properties over the length of the fish appear to be highly correlated to this parameter. The results indicated that changes in the elasmodine ratio are responsible for the differences in fracture resistance along the body of a fish, which for carp was found to decrease from head to tail. The trend was not represented consistently in the three species of fish evaluated.

In addition to the external elasmodine ratio, results from the tear resistance measurements revealed the importance of the hierarchical structure of the scales, and the importance of molecular-level interactions on the structural behavior. This was especially true for the evaluations conducted over

the range in temperatures. Freezing of inter and intra molecular water reduces the ability of collagen to undergo inelastic deformation, and decreases its capacity for energy dissipation. The ice crystals serve as weak pins between the collagen molecules that have limited strength after initial failure. In contrast, the removal of water from the collagen matrix by chemical dehydration also caused a change in the collagen molecule interactions, but a completely different response structurally. The removal of the intra molecular water facilitated the formation of inter-peptide bonds, which increased the strength and elastic modulus up to 150% for scales of the tail. These bonds are also weak pins, but they have the ability to be broken and reform during sliding of the fibrils according to the proximity of appropriate polarity of the side groups. The presence of a larger percentage of mineral crystals at the intra-fibrilar spaces in the elasmodine of the head and middle regions impeded the formation of new inter-peptide bonds, and consequently interfered with the strengthening process. That observation has important ramifications to the effectiveness of mineral reinforcements in the development of bioinspired analogues.

As fish scales are a natural composite material, the lamination pattern, including the distribution of the three principal layers and the fiber orientation of the elasmodine plies, are expected to play pivotal roles on the structural behavior. Previous studies had reported anisotropic behavior of scales from particular species, yet no study in the literature had fully characterized the microstructure of the scales. This study was the first to fully characterize the lamination patterns of fish scales from different species, and to distinguish the stacking sequences. It was found that the LL thickness, the external elasmodine ratio and the stacking sequences of the elasmodine plies vary between species and appear to have evolved according to the unique multifunctional needs associated with locomotion and protection.

Scales of the *Arapaima gigas* possessed the highest degree of mineralization of the three species of fish evaluated, and also a thicker limiting layer and higher external elasmodine ratio. Plies of the elasmodine of the arapaima were arranged in a double twisted plywood structure with an average of approximately 90° between adjacent plies. In comparison, scales of modern fish that can achieve higher swim speeds, including both the carp and tarpon, have a twisted plywood structure with average rotation of 75° between adjacent plies. Furthermore, the preferred orientation of the collagen fibers was shown to have an offset angle from the primary longitudinal axis of the fish that is dependent on location and specie. Results from this study showed the distinct differences in microstructure of scales from the three fish species evaluated, and how the structure coincided with the different multi-functional demands of these three species with regards to their principal threats and habitats. The results also emphasized the importance of characterizing the microstructure of the scales in evaluations of structural behavior, especially in discussions of anisotropy.

Understanding the detailed architecture of scales will support future efforts aimed at the design and development of new composites. An understanding the contributions of each individual layer to the overall structural behavior is critical to this endeavor. In support of that, an analytical model was proposed that describes the elastic properties of scales by idealizing elasmoid scales as a system of parallel springs. Application of the model to interpret results of the experiments revealed that although the elastic modulus of mineralized plies of the EE can be orders of magnitude higher than that of the collagen matrix, misalignment of the plies due to rotations associated with the twisted plywood structure results in significant reductions in the in-plane elastic modulus of the complete scale. The LL plays the largest role on the elastic modulus, followed by the internal elasmodine (IE), which has a significant contribution that varies with anatomical location.

A detailed exploration of the limiting layer was also conducted, including a characterization of its composition, geometry and mechanical properties. Results showed that there is a decrease in the hardness and elastic modulus with increasing proximity to the LL/EE interface. This gradient in properties was found to be attributed to the spatial variation in the degree of mineralization, and which appears to result from the downward diffusion of mineralization from the surface of the scales. Despite a consistency in the LL of all the scales evaluated, the results also showed that there are significant differences in the LL between fish from different environments. The limiting layer of the tarpon scales was the hardest, followed by the carp and the arapaima. These results suggest that the growth environment can induce carbonate substitution for the phosphate of the apatite structure, leading to a change of the Ca/P ratio in the apatite crystal structure, and which can manifest as changes in the mechanical properties.

An experimental evaluation involving controlled deformation of the scales under flexure provided new knowledge regarding the initiation of failure under in-plane bending. The radii of the limiting layer were found to serve as initial sites for crack propagation through the mineral layers until the crack is arrested at the interface with the internal elasmodine. The deformation process evolved by delamination and buckling of plies of the internal elasmodine without gross failure of the limiting layer. It was shown that the scales are capable of large deformation and strains prior to failure of the limiting layer, indicating scales as an exciting option for the inspiration of substrates materials that require similar performance. In addition, a detailed examination of the limiting layer revealed the presence of a transition area of suture between the limiting layer and the external elasmodine in carp and tarpon scales. This region was found to follow the wavy geometry of the limiting layer as defined by the circuli that are formed by mineral protrusions on the surface of the scale.

Mechanical failure of the limiting layer initiated in the valleys of the LL via the initiation and propagation of cracks normal to the surface of the scales towards the LL/EE interface.

To understand contributions from the limiting layer and suture geometry to the structural behavior of the scales, a finite element analysis was conducted involving elastic-plastic models for the mechanical behavior. This numerical analysis represent the first detailed evaluation of the layered arrangement of fish scales and involving considerations of inelastic deformation of the elasmodine and the contributions of the LL and suture geometry. Furthermore, this is the first study to treat the elasmoid scales and their mechanical response as a material and not just a rigid plate on top of fish skin. Numerical simulations of controlled deformation process enabled an evaluation of both the bending stiffness, the work to failure of the scales and an increased understanding of the mechanisms of failure.

Using the numerical model it was found that the work to failure was maximized when the protrusions of the circuli were normal to the surface of the scales as found in the tarpon. However, the natural inclination of the circuli of carp scales decreases the work to failure. That reduced performance may be a result of evolutionary changes that have resulted from the domestication of these fish. One of the most important contributions of the numerical evaluation was the development of new knowledge concerning the influence of the limiting layer profile and suture geometry on the mechanical behavior of scales. An increase in the amplitude of the LL was found decrease the bending stiffness and the work to failure of the scales. In addition, the suture line location relative to the LL contributes to the scale performance. Specifically, the scale is rendered less flexible but possesses a larger work to fracture with translation of the suture closer to the LL/EE interface. Therefore, both the LL and the suture geometry can be tailored to control the

structural behavior of bioinspired composite laminates with layers that possess disparate elastic modulus geometry. These are important design parameters that would not have been appreciated without the numerical aspects of the investigation.

8.2 LIMITATIONS

With all studies there are potential limitations, and the present investigation is no exception. One of the most obvious limitations is related to the environment where the fish was raised, its growth and how that influenced the extracted scales. As all the fish used in this study were purchased without knowledge of the fish age or growth conditions. As a result, aging related deterioration of the collagen matrix could not be properly assessed. In comparing the results of mechanical properties between different fish, the environmental component could be a relevant concern. Even within the same species there may be different biological or environmental parameters that were not controlled. For example, the squamation process and ontogeny of the fish may be important to the microstructure of the scales and its variation across the body. Furthermore, differences in fish age may have been a contributing factor to some of the variation observed in the mechanical behavior, but was not considered.

Another limitation was the potential importance of scale shedding and regeneration to the properties of the scales. It is unknown whether the scales evaluated from any one fish were original or regenerated. Scale regeneration has been widely studied from a biological perspective [53-55], and it would be an exciting scientific pursuit to analyze if there are mechanical differences between old and regenerated scales. In addition, freezing of the fish during transportation and storage could

induce a thermal cycle within the scales that can result in loss of collagen integrity. There was no knowledge of the prior handling conditions or time of storage.

During locomotion, the highest bending moment is experienced along the lateral-line of the fish body. This lateral line is where the nerves or neuromats of the fish are located and they are heavily protected with an additional mineral layer [39]. These scales were excluded from the study since they presented prominent deviations in the tear and tensile response. So what was the limitation?? During the chemical dehydration of scales, ethanol was chosen since it is widely used for that purpose. Ethanol has similar Hansen solubility parameter for hydrogen bonding δ_h to that for collagen in air and it provided an effective basis for examining the importance of a fluid layer on the deformation mechanics of dehydrated and mineralized collagen. However, the degree of bound water removed from the collagen was not measured, which prevents the development of a complete mechanistic understanding concerning the mechanisms responsible for the changes in properties with dehydration.

In comparing the microstructure and mechanical properties of scales from different species of fish, the largest limitation was that scales from only a single fish were evaluated from each species. Although the investigation was designed to compare results of structure and lamination patterns between the three fish with elasmoid scales, it is not clear how consistent these qualities are among fish of the same species. There are variations in the mechanical behavior of scales from different fish of the same species [67], which appears to be a reflection of the variations in structure. Thus, it is important to consider that further work may be needed to assess the degree of variation in lamination patterns and the primary forms of variation.

Over the past decades there has been an increase in the number of studies being conducted regarding collagen and its interaction with apatite, in particular hydroxyapatite. In regards to fish scales, several questions remain unanswered regarding the geometry of the apatite crystals and for instance the aspect ratio, and their positions with respect the collagen fibers. In the present study, assumptions were made concerning the aspect ratio in the prediction of the elastic properties of scales. Further work may be needed regarding the reinforcement provided by the apatite crystals and its influence on the mechanical behavior of the scales.

8.3 FUTURE WORK

According to the findings and limitations of this study, the following topics are recommended for future work. Diffusion of substitutional atoms into the apatite structure of the scales is possible and could contribute to the mechanical properties of the mineral in the limiting layer. Further study involving environmental control of the fish growth would be desirable, which could be used to explore the mineralization process, including the chemistry of the environment and its effects on the LL chemistry. It would also be possible to control fish age and explore the effect of scale regeneration on the mineralization process, including the rate and depth of mineralization.

Explorations of the limiting layer of scales from the *Arapaima gigas* revealed wave-like patterns in the circuli that could be related to seasonal growth. In order to have a better understanding of this feature it would be necessary to perform a characterization of the limiting layer with high resolution elemental variations across the LL thickness. Ideally, an investigation of this type would be performed on fish that were monitored during the different stages of growth.

Furthermore, it was found that the removal of water by polar solvents had an important contribution to the mechanical behavior of the scales. The removal of water at the molecular level from the elasmodine using polar solvents with $\delta_h < 19$ $(J/cm^3)^{1/2}$ could provide additional understanding concerning the role of intermolecular water on the collagen and consequent mechanical properties of the scales. Additional techniques for measuring the bound water content in tissues could generate new knowledge concerning the locations where the water molecules reside in the chains of the tropocollagen molecules, as well as within the apatite mineral structure (regarded as "structural water"). The water located in these individual compartments requires different levels of energy for removal. Far less is known regarding the layers of bound water in fish scale collagen. Thus, the difficulty of displacing the water in fish scales using polar solvents and the amount of remaining bound water after ethanol treatment are unknown. Future studies aimed at understanding the contributions of the bound water layers to the mechanical behavior of fish scales may be fruitful.

Mechanical properties of the scales were found to depend on the mineral content and its distribution across the thickness of the scales. Of concern, collagen cross-linking has been shown to have a strong influence on the mechanical properties of collagen based materials. Therefore, an evaluation of collagen crosslinking in the scales and its effect on the strength, elastic modulus and toughness is recommended. Furthermore, in predicting the elastic modulus of the scales, it was necessary to assume some of the structural parameters in the model. Future work is warranted in determining the aspect ratio of the mineral crystals of the limiting layer. In addition, an evaluation of the elastic modulus of the limiting layer and external elasmodine in the hydrated condition would provide further insight into their contribution to the elastic behavior of scales.

The numerical model introduced some simplifications to describe the limiting layer and elasmodine. For instance, facture and delamination initiated at the radii, before gross failure of the scales. Yet, the radii were not included in the model. Future numerical models including the effect of the radii in the limiting layer and individual plies in the elasmodine is recommended. Furthermore, due to the stress concentration, the valleys of the LL were identified as sites where fractured initiated that caused failure of the scales. Definition of a path normal to the surface of the scale from these areas, would allow the prediction of the fracture toughness of the scales J_{IC} as damage of the LL is permitted.

Lastly, future work on applying the acquired knowledge in the design and development of new composites is strongly recommended. The majority of explorations of fish scales as an inspirational material has been focused on the design of body armors. However, the ability of scales to undergo large deformation without gross failure of the limiting layer suggests that scales could also serve as inspiration in the design of flexible laminated substrates for many other applications. These applications may involve laminates involving layers with widely disparate elastic moduli and that will experience large deformations, but cannot failing as part of their life cycle.

BIBLIOGRAPHY

.

[1] N.E. Walsh, W.S. Walsh, Rehabilitation of landmine victims: the ultimate challenge, Bulletin World Health Organization. 81 (2003) 665–670.

[2] T. Gibson, Power Suit, Mechanical Engineering.The Magazine ASME. 07 (2017) 38–41.

[3] H. Ehrlich, Biological materials of marine origin, Springer, 2010.

[4] E.B. Landreneau, Scales and Scale-like Structures, Texas A&M University, 2011.

[5] B. Laufer, Chinese clay figures, Field Museum of Natural History, 1914.

[6] I.H. Chen, W. Yang, M.A. Meyers, Alligator osteoderms: Mechanical behavior and hierarchical structure, Materials Science Engineering: C. 35 (2014) 441–448.

[7] I.H. Chen, W. Yang, M.A. Meyers, Leatherback sea turtle shell: A tough and flexible biological design, Acta Biomaterialia. 28 (2015) 2–12.

[8] Y. Lin, C. Wei, E. Olevsky, M.A. Meyers, Mechanical properties and the laminate structure of Arapaima gigas scales, Journal Mechanical Behavior Biomedical Materials. 4 (2011) 1145–1156.

[9] C. Ortiz, M.C. Boyce, Bioinspired structural materials, Science. 319 (2008) 1053–1054.

[10] W. Yang, I.H. Chen, B. Gludovatz, E.A. Zimmermann, R.O. Ritchie, M.A. Meyers, Natural flexible dermal armor, Advanced Materials. 25 (2013) 31–48.

[11] A. Browning, C. Ortiz, M.C. Boyce, Mechanics of composite elasmoid fish scale assemblies and their bioinspired analogues, Journal Mechanical Behavior Biomedical Materials. 19 (2013) 75–86.

[12] R.K. Chintapalli, M. Mirkhalaf, A.K. Dastjerdi, F. Barthelat, Fabrication, testing and modeling of a new flexible armor inspired from natural fish scales and osteoderms, Bioinspiration & Biomimetics. 9 (2014) 036005.

[13] K.V. Kardong, Vertebrates: Comparative Anatomy, Function, Evolution, 6th ed., McGraw-Hill, 2006.

[14] J.-Y. Sire, A. Huysseune, Formation of dermal skeletal and dental tissues in fish: a comparative and evolutionary approach, Biological Reviews. 78 (2003) 219–249.

[15] W. Raschi, C. Tabit, Functional aspects of placoid scales: a review and update, Marine Freshwater Research. 43 (1992) 123–147.

[16] P.G. Allison, M.Q. Chandler, R. Rodriguez, B. Williams, R. Moser, C. Weiss, A. Poda, B. Lafferty, A. Kennedy, J. Seiter, others, Mechanical properties and structure of the biological multilayered material system, Atractosteus spatula scales, Acta Biomaterialia. 9 (2013) 5289–5296.

[17] P.-Y. Chen, J. Schirer, A. Simpson, R. Nay, Y.-S. Lin, W. Yang, M.I. Lopez, J. Li, E.A. Olevsky, M.A. Meyers, Predation versus protection: fish teeth and scales evaluated by nanoindentation, Journal Materials Research. 27 (2012) 100–112.

[18] K.D. Jandt, Biological materials: Fishing for compliance, Nature materials. 7 (2008) 692–693.
[19] W. Yang, B. Gludovatz, E.A. Zimmermann, H.A. Bale, R.O. Ritchie, M.A. Meyers, Structure and fracture resistance of alligator gar (Atractosteus spatula) armored fish scales, Acta Biomaterialia. 9 (2013) 5876–5889.
[20] B.J. Bruet, J. Song, M.C. Boyce, C. Ortiz, Materials design principles of ancient fish armour, Nature Materials. 7 (2008) 748–756.
[21] L. Wang, J. Song, C. Ortiz, M.C. Boyce, Anisotropic design of a multilayered biological exoskeleton, Journal Materials Research. 24 (2009) 3477–3494.
[22] D. Arola, D. Bajaj, J. Ivancik, H. Majd, D. Zhang, Fatigue of biomaterials: hard tissues, International Journal Fatigue. 32 (2010) 1400–1412.
[23] A.M.C. Garrano, G. La Rosa, D. Zhang, L.-N. Niu, F. Tay, H. Majd, D. Arola, On the mechanical behavior of scales from Cyprinus carpio, Journal Mechanical Behavior Biomedical Materials. 7 (2012) 17–29.
[24] D. Zhu, C.F. Ortega, R. Motamedi, L. Szewciw, F. Vernerey, F. Barthelat, Structure and mechanical performance of a "modern' fish scale, Advanced Engineering Materials. 14 (2012) B185–B194.
[25] D.L. Zylberberg, G. Nicolas, Ultrastructure of scales in a teleost (Carassius auratus L.) after use of rapid freeze-fixation and freeze-substitution, Cell Tissue Research. 223 (1982) 349–367.
[26] A. Bigi, M. Burghammer, R. Falconi, M.H. Koch, S. Panzavolta, C. Riekel, Twisted plywood pattern of collagen fibrils in teleost scales: An X-ray diffraction investigation, Journal Structural Biology. 136 (2001) 137–143.
[27] A. Gautieri, S. Vesentini, A. Redaelli, M.J. Buehler, Hierarchical structure and nanomechanics of collagen microfibrils from the atomistic scale up, Nano letters. 11 (2011) 757–766.
[28] A.K. Dastjerdi, F. Barthelat, Teleost fish scales amongst the toughest collagenous materials, Journal Mechanical Behavior Biomedical Materials. 52 (2015) 95–107.
[29] D. Zhu, L. Szewciw, F. Vernerey, F. Barthelat, Puncture resistance of the scaled skin from striped bass: collective mechanisms and inspiration for new flexible armor designs, Journal Mechanical Behavior Biomedical Materials. 24 (2013) 30–40.
[30] T. Ikoma, H. Kobayashi, J. Tanaka, D. Walsh, S. Mann, Microstructure, mechanical, and biomimetic properties of fish scales from Pagrus major, Journal Structural Biology. 142 (2003) 327–333.
[31] S. Gil-Duran, D. Arola, E. Ossa, Effect of chemical composition and microstructure on the mechanical behavior of fish scales from Megalops Atlanticus, Journal Mechanical Behavior Biomedical Materials. 56 (2016) 134–145.
[32] M. Meyers, Y. Lin, E. Olevsky, P.-Y. Chen, Battle in the Amazon: Arapaima versus piranha, Advanced Engineering Materials. 14 (2012) B279–B288.
[33] F. Torres, E. Le Bourhis, O. Troncoso, J. Llamoza, Structure-property relationships in Arapaima Gigas scales revealed by nanoindentation tests, Polymers & Polymer Composites. 22 (2014) 369–374.
[34] F. Torres, M. Malásquez, O. Troncoso, Impact and fracture analysis of fish scales from Arapaima gigas, Materials Science Engineering: C. 51 (2015) 153–157.

[35] F. Torres, O. Troncoso, J. Nakamatsu, C. Grande, C. Gomez, Characterization of the nanocomposite laminate structure occurring in fish scales from Arapaima gigas, Materials Science Engineering: C. 28 (2008) 1276–1283.
[36] F.G. Torres, O.P. Troncoso, E. Amaya, The effect of water on the thermal transitions of fish scales from Arapaima Gigas, Materials Science Engineering C. 32 (2012) 2212–2214.
[37] W. Yang, V.R. Sherman, B. Gludovatz, M. Mackey, E.A. Zimmermann, E.H. Chang, E. Schaible, Z. Qin, M.J. Buehler, R.O. Ritchie, others, Protective role of Arapaima gigas fish scales: structure and mechanical behavior, Acta Biomaterialia. 10 (2014) 3599–3614.
[38] W. Yang, V.R. Sherman, B. Gludovatz, E. Schaible, P. Stewart, R.O. Ritchie, M.A. Meyers, On the tear resistance of skin, Nature Communications. 6 (2015) 6649.
[39] E.A. Zimmermann, B. Gludovatz, E. Schaible, N.K. Dave, W. Yang, M.A. Meyers, R.O. Ritchie, Mechanical adaptability of the Bouligand-type structure in natural dermal armour, Nature Communications. 4 (2013) 2634.
[40] S. Murcia, G. Li, M. Yahyazadehfar, M. Sasser, A. Ossa, D. Arola, Effects of polar solvents on the mechanical behavior of fish scales, Materials Science Engineering: C. 61 (2016) 23–31.
[41] J.D. Currey, The design of mineralised hard tissues for their mechanical functions, Journal Experimental Biology. 202 (1999) 3285–3294.
[42] R. Rivlin, A.G. Thomas, Rupture of rubber. I. Characteristic energy for tearing, in: Collected Papers RS Rivlin, Springer, 1997: pp. 2615–2642.
[43] A.A. Griffith, The phenomena of rupture and flow in solids, Philosophical Transactions Royal Society London. Series A, containing Papers mathematical Physical character. 221 (1921) 163–198.
[44] A. Ahagon, A. Gent, Threshold fracture energies for elastomers, Journal Polymer Science: Polymer Physics Edition. 13 (1975) 1903–1911.
[45] A. al Ahagon, A. Gent, H. Kim, Y. Kumagai, Fracture energy of elastomers in mode I (cleavage) and mode III (lateral shear), Rubber Chemistry Technology. 48 (1975) 896–901.
[46] L. Chen, Tear Energy of Natural Rubber Under Dynamic Loading, University of Akron, 2008.
[47] E. Gdoutos, I. Daniel, P. Schubel, Fracture mechanics of rubber, Facta universitatis Series Mechanics, Automatic Control Robotics. 3 (2003) 497–510.
[48] R. Zulkifli, C. Azhari, M.J.M. Nor, S. Oshkvor, The effect of plies and processing time on mode I and mode III fracture properties of woven silk fibre/polyester composites, in: Proceedings 4th WSEAS International Conference Applied Theoretical Mechanics, 2008.
[49] D-1938 Standard Test Method for Tear-Propagation Resistance (Trouser Tear) of Plastic Film and Thin Sheeting by a Single-Tear Method, ASTM, 2008.
[50] D. Mouzakis, M. Gahleitner, J. Karger-Kocsis, others, Toughness assessment of elastomeric polypropylene (ELPP) by the essential work of the fracture method, Journal Applied Polymer Science. 70 (1998) 873–881.
[51] G. Ramachandran, R. Chandrasekharan, Interchain hydrogen bonds via bound water molecules in the collagen triple helix, Biopolymers. 6 (1968) 1649–1658.
[52] F.J. Vernerey, F. Barthelat, On the mechanics of fishscale structures, International Journal Solids Structures. 47 (2010) 2268–2275.

[53] J.-Y. Sire, M.-A. Akimenko, Scale development in fish: A review, with description of sonic hedgehog (shh) expression in the zebrafish (Danio rerio), International Journal Developmental Biology. 48 (2004) 233–248.
[54] D. Le Guellec, G. Morvan-Dubois, J.-Y. Sire, Skin development in bony fish with particular emphasis on collagen deposition in the dermis of the zebrafish (Danio rerio), International Journal Developmental Biology. 48 (2004) 217–232.
[55] E.-H. Park, S.-H. Lee, Scale growth and squamation chronology for the laboratory-reared hermaphroditic fish Rivulus marmoratus (Cyprinodontidae)., Japanese Journal Ichthyology. 34 (1988) 476–482.
[56] Y. Tsukamoto, M. Okiyama, Metamorphosis of the Pacific tarpon, Megalops cyprinoides (Elopiformes, Megalopidae) with remarks on development patterns in the Elopomorpha, Bulletin marine science. 60 (1997) 23–36.
[57] F. Barthelat, Science and Engineering of Natural Materials: Merging Structure and Materials, Journal Mechanical Behavior Biomedical Materials. 19 (2013) 1–2.
[58] R.K. Nalla, J.H. Kinney, A.P. Tomsia, R.O. Ritchie, Role of alcohol in the fracture resistance of teeth, Journal Dental Research. 85 (2006) 1022–1026.
[59] E. Osorio, M. Toledano, F. Aguilera, F. Tay, R. Osorio, Ethanol wet-bonding technique sensitivity assessed by AFM, Journal Dental Research. 89 (2010) 1264–1269.
[60] J.S. Nyman, Q. Ni, D.P. Nicolella, X. Wang, Measurements of mobile and bound water by nuclear magnetic resonance correlate with mechanical properties of bone, Bone. 42 (2008) 193–199.
[61] D.H. Pashley, K.A. Agee, R.M. Carvalho, K.-W. Lee, F.R. Tay, T.E. Callison, Effects of water and water-free polar solvents on the tensile properties of demineralized dentin, Dental Materials. 19 (2003) 347–352.
[62] C.A. Grant, D.J. Brockwell, S.E. Radford, N.H. Thomson, Tuning the elastic modulus of hydrated collagen fibrils, Biophysical Journal. 97 (2009) 2985–2992.
[63] K. Maciel, R. Carvalho, R. Ringle, C. Preston, C. Russell, D.H. Pashley, The effects of acetone, ethanol, HEMA, and air on the stiffness of human decalcified dentin matrix, Journal Dental Research. 75 (1996) 1851–1858.
[64] J. Kim, L. Gu, L. Breschi, L. Tjäderhane, K.K. Choi, D.H. Pashley, F.R. Tay, Implication of ethanol wet-bonding in hybrid layer remineralization, Journal Dental Research. 89 (2010) 575–580.
[65] F. Barthelat, Biomimetics for next generation materials, Philosophical Transactions Royal Society London A Mathematical, Physical Engineering Sciences. 365 (2007) 2907–2919.
[66] M.A. Meyers, P.-Y. Chen, A.Y.-M. Lin, Y. Seki, Biological materials: Structure and mechanical properties, Progress Materials Science. 53 (2008) 1–206.
[67] S. Murcia, M. McConville, G. Li, A. Ossa, D. Arola, Temperature effects on the fracture resistance of scales from Cyprinus carpio, Acta Biomaterialia. 14 (2015) 154–163.
[68] M. Baudouin, M. Marengo, A. Pere, J.-M. Culioli, M.-C. Santoni, B. Marchand, E. Durieux, Comparison of otolith and scale readings for age and growth estimation of common dentex Dentex dentex, Journal Fish Biology. 88 (2015) 760–766.
[69] A.L. Ibáñez, P. O'Higgins, Identifying fish scales: The influence of allometry on scale shape and classification, Fisheries Research. 109 (2011) 54–60.

[70] B. Levin, A. Bolotovskiy, M. Levina, Body size determines the number of scales in cyprinid fishes as inferred from hormonal manipulation of developmental rate, Journal Applied Ichthyology. 28 (2012) 393–397.
[71] J. Metz, E. De Vrieze, E.-J. Lock, I. Schulten, G. Flik, Elasmoid scales of fishes as model in biomedical bone research, Journal Applied Ichthyology. 28 (2012) 382–387.
[72] R.M. Jones, Mechanics of Composite Materials, CRC press, 1998.
[73] P. Liu, D. Zhu, Y. Yao, J. Wang, T.Q. Bui, Numerical simulation of ballistic impact behavior of bio-inspired scale-like protection system, Materials & Design. 99 (2016) 201–210.
[74] N. Funk, M. Vera, L.J. Szewciw, F. Barthelat, M.P. Stoykovich, F.J. Vernerey, Bioinspired Fabrication and Characterization of a Synthetic Fish Skin for the Protection of Soft Materials, ACS Applied Materials & Interfaces. 7 (2015) 5972–5983.
[75] R. Martini, F. Barthelat, Stability of hard plates on soft substrates and application to the design of bioinspired segmented armor, Journal Mechanics Physics Solids. 92 (2016) 195–209.
[76] S. Rudykh, M.C. Boyce, Analysis of elasmoid fish imbricated layered scale-tissue systems and their bio-inspired analogues at finite strains and bending, IMA Journal Applied Mathematics. 79 (2014) 830–847.
[77] J. Bereiter-Hahn, L. Zylberberg, Regeneration of teleost fish scale, Comparative Biochemistry Physiology Part A: Physiology. 105 (1993) 625–641.
[78] E. de Vrieze, F. Sharif, J.R. Metz, G. Flik, M.K. Richardson, Matrix metalloproteinases in osteoclasts of ontogenetic and regenerating zebrafish scales, Bone. 48 (2011) 704–712.
[79] G. Helfman, B.B. Collette, D.E. Facey, B.W. Bowen, The diversity of fishes: biology, evolution, and ecology, John Wiley & Sons, 2009.
[80] P.J. Hart, J.D. Reynolds, Handbook of fish biology and fisheries, John Wiley & Sons, 2008.
[81] J.-Y. Sire, A. Quilhac, J. Bourguignon, F. Allizard, Evidence for participation of the epidermis in the deposition of superficial layer of scales in zebrafish (Danio rerio): a SEM and TEM study, Journal Morphology. 231 (1997) 161–174.
[82] F.J. Meunie, Spatial organization and mineralization of the basal plate of elasmoid scales in osteichthyans, American Zoologist. 24 (1984) 953–964.
[83] L. Zylerberg, Collagen and mineralization in the elasmoid scales, in: Biology Intervertebrate Lower Vertebrate Collagens, Springer, 1985: pp. 457–463.
[84] L. Zylberberg, J. Bereiter-Hahn, J.-Y. Sire, Cytoskeletal organization and collagen orientation in the fish scales, Cell Tissue Research. 253 (1988) 597–607.
[85] B. Hofer, Über den Bau und die Entwicklung der Cycloid-und Ctenoidschuppen, Sitzungsber. d. Ges. f. Morphol. u. Physiol., München. 90 (1889).
[86] B. Wang, W. Yang, V.R. Sherman, M.A. Meyers, Pangolin armor: overlapping, structure, and mechanical properties of the keratinous scales, Acta biomaterialia. 41 (2016) 60–74.
[87] S. Murcia, E. Lavoie, T. Linley, A. Devaraj, E.A. Ossa, D. Arola, The natural armors of fish: A comparison of the lamination pattern and structure of scales, Journal Mechanical Behavior Biomedical Materials. (2016).
[88] Y. Sire, J. Géraudie, F. Meunter, L. Zylberberg, On the origin of ganoine: Histological and ultrastructural data on the experimental regeneration of the scales of Calamolchthys calabaricus (osteichthyes, brachyopterygii, polypteridae), American Journal Anatomy. 180 (1987) 391–402.

[89] L.A. Jawad, Comparative morphology of scales of four teleost fishes from Sudan and Yemen, Journal Natural History. 39 (2005) 2643–2660.
[90] L.M. Gordon, L. Tran, D. Joester, Atom probe tomography of apatites and bone-type mineralized tissues, ACS nano. 6 (2012) 10667–10675.
[91] W.C. Oliver, G.M. Pharr, An improved technique for determining hardness and elastic modulus using load and displacement sensing indentation experiments, Journal Materials Research. 7 (1992) 1564–1583.
[92] W. Liu, Y. Zhang, G. Li, Y. Miao, X. Wu, Structure and composition of teleost scales from snakehead Channa argus (Cantor)(Perciformes: Channidae), Journal Fish Biology. 72 (2008) 1055–1067.
[93] B.G. Frushour, J.L. Koenig, Raman scattering of collagen, gelatin, and elastin, Biopolymers. 14 (1975) 379–391.
[94] V.A. Iconomidou, M.E. Georgaka, G.D. Chryssikos, V. Gionis, P. Megalofonou, S.J. Hamodrakas, Dogfish egg case structural studies by ATR FT-IR and FT-Raman spectroscopy, International journal biological macromolecules. 41 (2007) 102–108.
[95] T. Ikoma, H. Kobayashi, J. Tanaka, D. Walsh, S. Mann, Physical properties of type I collagen extracted from fish scales of Pagrus major and Oreochromis niloticas, International Journal Biological Macromolecules. 32 (2003) 199–204.
[96] A. Awonusi, M.D. Morris, M.M. Tecklenburg, Carbonate assignment and calibration in the Raman spectrum of apatite, Calcified tissue International. 81 (2007) 46–52.
[97] S. Gamsjaeger, K. Klaushofer, E.P. Paschalis, Raman analysis of proteoglycans simultaneously in bone and cartilage, Journal Raman Spectroscopy. 45 (2014) 794–800.
[98] M. Gkasior-Glogowska, M. Komorowska, J. Hanuza, M. Mkaczka, A. Zajkac, M. Ptak, R. Bkedziski, M. Kobielarz, K. Maksymowicz, P. Kuropka, others, FT-Raman spectroscopic study of human skin subjected to uniaxial stress, Journal mechanical behavior Biomedical materials. 18 (2013) 240–252.
[99] M. Kazanci, H. Wagner, N. Manjubala, H. Gupta, E. Paschalis, P. Roschger, P. Fratzl, Raman imaging of two orthogonal planes within cortical bone, Bone. 41 (2007) 456–461.
[100] S. Koutsopoulos, Synthesis and characterization of hydroxyapatite crystals: a review study on the analytical methods, Journal biomedical materials research. 62 (2002) 600–612.
[101] G. Penel, G. Leroy, C. Rey, E. Bres, MicroRaman spectral study of the PO4 and CO3 vibrational modes in synthetic and biological apatites, Calcified Tissue International. 63 (1998) 475–481.
[102] M. Seeley, N. Miller, B. Walther, High resolution profiles of elements in Atlantic tarpon (Megalops atlanticus) scales obtained via cross-sectioning and laser ablation ICP-MS: a literature survey and novel approach for scale analyses, Environmental Biology Fishes. 98 (2015) 2223–2238.
[103] M. Spinner, M. Kortmann, C. Traini, S.N. Gorb, Key role of scale morphology in flatfishes (Pleuronectiformes) in the ability to keep sand, Scientific reports. 6 (2016).
[104] D.K. Wainwright, G.V. Lauder, Three-dimensional analysis of scale morphology in bluegill sunfish, Lepomis macrochirus, Zoology. 119 (2016) 182–195.
[105] E.J. Anderson, W.R. Mcgillis, M.A. Grosenbaugh, The boundary layer of swimming fish, Journal Experimental Biology. 204 (2001) 81–102.
[106] R.C. Hibbeler, others, Mechanics of Materials-Prentice Hall, Inc., New Jersey. (2000).

[107] C.N. Trueman, A. Moore, Use of the stable isotope composition of fish scales for monitoring aquatic ecosystems, Terrestrial Ecology. 1 (2007) 145–161.
[108] E.A. McNally, H.P. Schwarcz, G.A. Botton, A.L. Arsenault, A model for the ultrastructure of bone based on electron microscopy of ion-milled sections, Plos ONE. 7(1) (2012) e29258.
[109] H.P. Schwarcz, E.A. McNally, G.A. Botton, Dark-field transmission electron microscopy of cortical bone reveals details of extrafibrillar crystals, Journal Structural Biology. 188 (2014) 240–248.
[110] A. Schönbörner, G. Boivin, C. Baud, The mineralization processes in teleost fish scales, Cell Tissue Research. 202 (1979) 203–212.
[111] L. Zylerberg, Collagen and mineralization in the elasmoid scales, in: Biology Intervertebrate Lower Vertebrate Collagens, Springer, 1985: pp. 457–463.
[112] B. Wopenka, J.D. Pasteris, A mineralogical perspective on the apatite in bone, Materials Science Engineering: C. 25 (2005) 131–143.
[113] L.M. Gordon, M.J. Cohen, K.W. MacRenaris, J.D. Pasteris, T. Seda, D. Joester, Amorphous intergranular phases control the properties of rodent tooth enamel, Science. 347 (2015) 746–750.
[114] A. La Fontaine, A. Zavgorodniy, H. Liu, R. Zheng, M. Swain, J. Cairney, Atomic-scale compositional mapping reveals Mg-rich amorphous calcium phosphate in human dental enamel, Science Advances. 2 (2016) e1601145.
[115] W. Suchanek, M. Yoshimura, Processing and properties of hydroxyapatite-based biomaterials for use as hard tissue replacement implants, Journal Materials Research. 13 (1998) 94–117.
[116] C. Tang, P. Uskokovic, C. Tsui, D. Veljovic, R. Petrovic, D. Janackovic, Influence of microstructure and phase composition on the nanoindentation characterization of bioceramic materials based on hydroxyapatite, Ceramics International. 35 (2009) 2171–2178.
[117] D. Zhang, A. Nazari, M. Soappman, D. Bajaj, D. Arola, Methods for examining the fatigue and fracture behavior of hard tissues, Experimental Mechanics. 47 (2007) 325–336.
[118] S. Murcia, M. Stossel, R. Pahuja, T. Linley, A. Devaraj, M. Ramulu, E.. Ossa, J. Wang, D. Arola, The Limiting Layer of fish scales: structure and properties, Acta Biomaterialia. (submitted) (2017).
[119] J.D. Currey, The relationship between the stiffness and the mineral content of bone, Journal Biomechanics. 2 (1969) 477–480.
[120] K.-N. An, Y.-L. Sun, Z.-P. Luo, Flexibility of type I collagen and mechanical property of connective tissue, Biorheology. 41 (2004) 239–246.
[121] Y.P. Kato, D.L. Christiansen, R.A. Hahn, S.-J. Shieh, J.D. Goldstein, F.H. Silver, Mechanical properties of collagen fibres: a comparison of reconstituted and rat tail tendon fibres, Biomaterials. 10 (1989) 38–42.
[122] G.D. Pins, F.H. Silver, A self-assembled collagen scaffold suitable for use in soft and hard tissue replacement, Materials Science Engineering: C. 3 (1995) 101–107.
[123] L.L. Hench, J. Wilson, An Introduction to Bioceramics, World scientific, 1993.
[124] N. Bouslama, Y. Chevalier, J. Bouaziz, F.B. Ayed, Influence of the sintering temperature on Young's modulus and the shear modulus of tricalcium phosphate–fluorapatite

composites evaluated by ultrasound techniques, Materials Chemistry Physics. 141 (2013) 289–297.
[125] L. Yang, K.O. Van der Werf, C.F. Fitié, M.L. Bennink, P.J. Dijkstra, J. Feijen, Mechanical properties of native and cross-linked type I collagen fibrils, Biophysical Journal. 94 (2008) 2204–2211.
[126] A.K. Nair, A. Gautieri, S.-W. Chang, M.J. Buehler, Molecular mechanics of mineralized collagen fibrils in bone, Nature Communications. 4 (2013) 1724.
[127] L. Nielsen, P. Chen, Young's modulus of composites filled with randomly oriented fibers, Journal Materials. (1968).
[128] L.E. Nielson, Mechanical Properties of Polymer and Composites, Marcel Dekker, 1974.
[129] Y. Lu, Mechanical Properties of Random Discontinuous Fiber Composites Manufactured from Wetlay Process, Virginia Polytechnic Institute and State University, 2002.
[130] B. Depalle, Z. Qin, S.J. Shefelbine, M.J. Buehler, Influence of cross-link structure, density and mechanical properties in the mesoscale deformation mechanisms of collagen fibrils, Journal Mechanical Behavior Biomedical Materials. 52 (2015) 1–13.
[131] P. Liu, D. Zhu, J. Wang, T.Q. Bui, Structure, Mechanical Behavior and Puncture Resistance of Grass Carp Scales, Journal Bionic Engineering. 14 (2017) 356–368.
[132] M. Yahyazadehfar, D. Bajaj, D.D. Arola, Hidden contributions of the enamel rods on the fracture resistance of human teeth, Acta biomaterialia. 9 (2013) 4806–4814.
[133] M. Yahyazadehfar, J. Ivancik, H. Majd, B. An, D. Zhang, D. Arola, On the mechanics of fatigue and fracture in teeth, Applied mechanics Reviews. 66 (2014) 030803.
[134] Y. Li, C. Ortiz, M.C. Boyce, Stiffness and strength of suture joints in nature, Physical Review E. 84 (2011) 062904.
[135] F. Barthelat, Architectured materials in engineering and biology: fabrication, structure, mechanics and performance, International Materials Reviews. 60 (2015) 413–430.
[136] F. Barthelat, Z. Yin, M.J. Buehler, Structure and mechanics of interfaces in biological materials, Nature Reviews Materials. 1 (2016) 16007.
[137] A.K. Dastjerdi, R. Rabiei, F. Barthelat, The weak interfaces within tough natural composites: experiments on three types of nacre, Journal Mechanical Behavior Biomedical Materials. 19 (2013) 50–60.
[138] I. Malik, M. Mirkhalaf, F. Barthelat, Bio-inspired "jigsaw?-like interlocking sutures: Modeling, optimization, 3D printing and testing, Journal Mechanics Physics Solids. 102 (2017) 224–238.
[139] F.A. Cordisco, P.D. Zavattieri, L.G. Hector, B.E. Carlson, Mode I fracture along adhesively bonded sinusoidal interfaces, International Journal Solids Structures. 83 (2016) 45–64.
[140] P.D. Zavattieri, L.G. Hector, A.F. Bower, Cohesive zone simulations of crack growth along a rough interface between two elastic–plastic solids, Engineering Fracture Mechanics. 75 (2008) 4309–4332.
[141] E. Lin, Y. Li, J.C. Weaver, C. Ortiz, M.C. Boyce, Tunability and enhancement of mechanical behavior with additively manufactured bio-inspired hierarchical suture interfaces, Journal Materials Research. 29 (2014) 1867–1875.
[142] V. Imbeni, J. Kruzic, G. Marshall, S. Marshall, R. Ritchie, The dentin–enamel junction and the fracture of human teeth, Nature materials. 4 (2005) 229–232.

[143] R. Ghosh, H. Ebrahimi, A. Vaziri, Non-ideal Effects in Bending Response of Soft Substrates Covered with Biomimetic Scales, Journal Mechanical Behavior Biomedical Materials. (2017).
[144] J. Song, C. Ortiz, M.C. Boyce, Threat-protection mechanics of an armored fish, Journal Mechanical Behavior Biomedical Materials. 4 (2011) 699–712.
[145] M.Q. Chandler, P.G. Allison, R.I. Rodriguez, R.D. Moser, A.J. Kennedy, Finite element modeling of multilayered structures of fish scales, Journal Mechanical Behavior Biomedical Materials. 40 (2014) 375–389.
[146] D. Zhang, M. Luo, D.D. Arola, Displacement/strain measurements using an optical microscope and digital image correlation, Optical Engineering. 45 (2006) 33605–33605.
[147] H. Ryou, L.-N. Niu, L. Dai, C. Pucci, D. Arola, D.H. Pashley, F. Tay, Effect of biomimetic remineralization on the dynamic nanomechanical properties of dentin hybrid layers, Journal dental research. 90 (2011) 1122–1128.
[148] J. Blaber, B. Adair, A. Antoniou, Ncorr: open-source 2D digital image correlation matlab software, Experimental Mechanics. 55 (2015) 1105–1122.
[149] S. Murcia, M. Stossel, R. Pahuja, T. Linley, A. Devaraj, M. Ramulu, E.. Ossa, J. Wang, D. Arola, The Limiting Layer of fish scales: structure and properties, Acta Biomaterialia. (submitted) (2017).
[150] P. Miguez, P. Pereira, P. Atsawasuwan, M. Yamauchi, Collagen cross-linking and ultimate tensile strength in dentin, Journal dental research. 83 (2004) 807–810.
[151] Z.L. Shen, M.R. Dodge, H. Kahn, R. Ballarini, S.J. Eppell, Stress-strain experiments on individual collagen fibrils, Biophysical Journal. 95 (2008) 3956–3963.
[152] R. Nalla, J. Kinney, R. Ritchie, On the fracture of human dentin: Is it stress-or strain-controlled?, Journal Biomedical Materials Research Part A. 67 (2003) 484–495.
[153] S. Rudykh, C. Ortiz, M.C. Boyce, Flexibility and protection by design: imbricated hybrid microstructures of bio-inspired armor, Soft Matter. 11 (2015) 2547–2554.
[154] N. Hammerschlag, J. Luo, D.J. Irschick, J.S. Ault, A comparison of spatial and movement patterns between sympatric predators: bull sharks (Carcharhinus leucas) and Atlantic tarpon (Megalops atlanticus), PLoS One. 7 (2012) e45958.
[155] J.M. Shenker, E. Cowie-Mojica, R.E. Crabtree, H.M. Patterson, C. Stevens, K. Yakubik, Recruitment of tarpon (Megalops atlanticus) leptocephali into the Indian River Lagoon, Florida, Contrib Mar Sci. 35 (2002) 55–69.
[156] H.Q. Tran, R.S. Mehta, P.C. Wainwright, Effects of ram speed on prey capture kinematics of juvenile Indo-Pacific tarpon, Megalops cyprinoides, Zoology. 113 (2010) 75–84.
[157] L. Szewciw, D. Zhu, F. Barthelat, The nonlinear flexural response of a whole teleost fish: contribution of scales and skin, Journal Mechanical Behavior Biomedical Materials. (2017).
[158] L. Szewciw, F. Barthelat, Mechanical properties of striped bass fish skin: Evidence of an exotendon function of the stratum compactum, Journal mechanical behavior Biomedical materials. (2016).
[159] J.A. Rogers, T. Someya, Y. Huang, Materials and mechanics for stretchable electronics, Science. 327 (2010) 1603–1607.
[160] M.N. Subramanian, Polymer Blends and Composites: Chemistry and Technology, John Wiley & Sons, 2017.
[161] ABAQUS Documentation, Dassault Systèmes, Providence, RI, USA, 2016.

APPENDIX A: Numerical and analytical validation of the DIC measurements

Validation of the strain field measured with Ncorr was performed on thin sheet polycarbonate with a thickness of 0.16 mm. Dog bone tensile specimens were sectioned and loaded according to the specifications of the ASTM D638 – 10 standard. Loading was performed using a universal testing machine (Instron ElectroPuls E1000). The instrument's load cell has a full-scale range of 250 N and precision of 0.01%. To measure the axial strains the surface of the specimens were prepared by generating a speckle pattern that was monitored by a high resolution digital camera (16 megapixels). Sequential images were acquired incrementally during each tensile test at a frequency of 0.2 Hz, which were synchronized with the load and displacement during post-processing for the results. The stress vs strain curve was calculated for each specimen and the strain was compared to the DIC strain field. **Figure A.1** shows a representative specimen where it can be seen that strains are comparable. A more detailed examination showed that in average, Ncorr was capable of calculating the strain field of the tensile specimens within a 1.65% error when compared with the tensile test results.

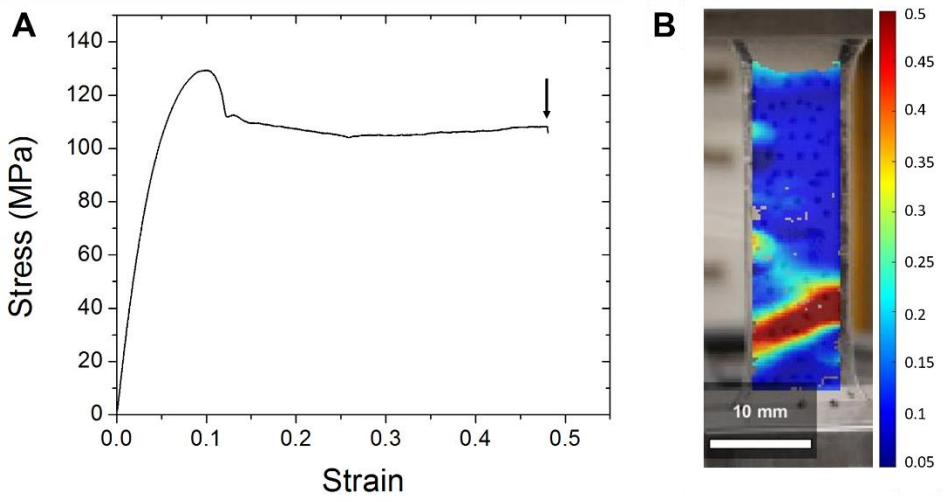

Figure A.1. Validation of strain field of a polycarbonate sheet under tensile stress. A) Stress vs strain curve. The strain field in the specimen at the point indicated by the arrow was processed with Ncorr and is shown in B).

In order to validate strain fields captured by optical microscopy, polycarbonate specimens were cut to 10x50 mm rectangles and their sides were polished following the procedures outlined for the scales to generate a similar surface. Specimens were conformed to the mandrels to have a radii of curvature of 51, 27, 16 and 12 mm and the strain field was obtained as is shown in Figure **Figure A.2**. The strain obtained at the tensile surface was compared to analytical and numerical calculations. Mechanics of materials define the maximum flexural stress of a beam as

$$\sigma_{\max} = \frac{M * c_{\max}}{I} \qquad \text{(A1. 18)}$$

where M is the flexural moment, c is the distance from the neutral axis to the point of evaluation and I is the moment of inertia. The flexural moment is related to the radii of curvature of the beam as:

$$\frac{1}{\rho} = \frac{M}{EI} \tag{A1. 19}$$

where ρ the radii of curvature and E is is the elastic modulus. Therefore if the geometry of the beam and its elastic modulus is known, the maximum flexural stress with its correspondent strain can be calculated analytically. Additionally, the numerical model of the in-plane bending and transverse tension of scales was used with the polycarbonate specimens. For both numerical and analytical calculations an elastic modulus of 2.8 GPa and a poisons ratio 0.38 of were used [160]. A summary of the analytical, numerical an experimental can be found in Table A1.6. On average, the results of the DIC and numerical model had an error of 11% and 5% with the analytical calculations, respectively.

Table A1.6. Flexural response of a polycarbonate thin sheet subjected to flexure.

	Analytical		***Numerical***		***Experimental***
Mandrel diameter (mm)	**σ max (MPa)**	**Strain (%)**	**σ max (MPa)**	**Strain (%)**	**Strain (%)**
12	8.33	0.32	9.73	0.34	0.30
16	7.54	0.29	7.29	0.26	0.25
27	4.18	0.16	4.31	0.15	0.18
51	2.28	0.08	2.26	0.08	0.08

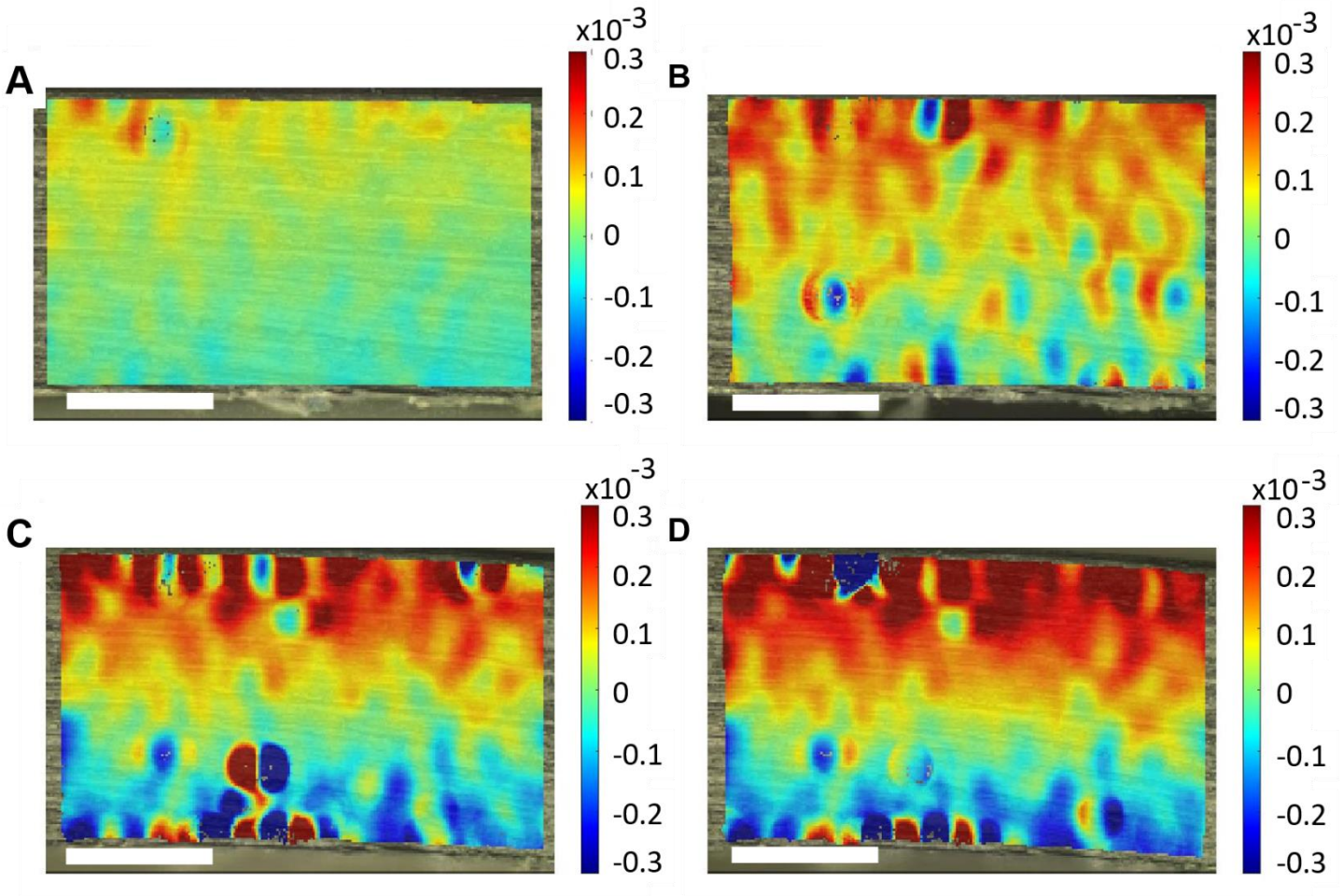

Figure A.2. Strain field evolution of a polycarbonate sheet subjected to flexure to conform to a mandrel of A) 51 mm, B) 27 mm, C) 16 mm and D) 12 mm of diameter. Sale bar 100 μm

APPENDIX B: COHESIVE ELEMENTS MODEL

Cohesive elements can be used to model interfacial debonding using a cohesive zone in which an infinitesimally thin layer of adhesive material is defined in terms of the traction versus the relative motion across the interface. Defining the cohesive behavior in terms of a traction-separation law assumes a linear elastic traction-separation law prior to damage followed by progressive degradation of the material stiffness, which is driven by a damage process.

The elastic behavior is written in terms of an elastic constitutive matrix that relates the nominal stresses to the nominal strains across the interface. In the case of a 2D simulation, the nominal traction stress vector, **t** , consists of two components, t_n and t_s , which represent the normal and shear traction, respectively. The corresponding separations are denoted by δ_n and δ_s. Therefore the nominal strains can be defined as

$$\varepsilon_n = \frac{\delta_n}{T_o}; \varepsilon_s = \frac{\delta_s}{T_o} \qquad \text{(A2. 20)}$$

The default value of the original constitutive thickness is T_o =1.0 which ensures that the nominal strain is equal to the separation (i.e., relative displacements of the top and bottom faces). The nominal stresses are the force components divided by the original area at each integration point. In the present model, a maximum nominal stress was defined as a damage initiation criterion. The

definition of peak values of the nominal stress when the deformation is either purely normal to the interface (t_n^o) or purely in the shear direction (t_s^o) allows the determination of the nominal strains. From equation 3 it becomes evident that with an if T_o =1, the nominal strain components, ε_n^o and ε_s^o, are equal to the respective components of the relative displacement δ_n and $\delta_s$between the top and bottom of the cohesive layer. Once a damage initiation criterion is met, material damage can occur according to a linear damage evolution based on effective displacement [161].

Propagation of the damage through the interface is sensitive to the element size and therefore mesh size. Furthermore, the critical element size is also dependent of the fracture process zone (FPZ) that defines the characteristic length l_{cz}. Therefore, simulations of mode I fracture propagation of a collagen bonded external/internal elasmodine were preformed where the element size was varied from 120 μm to 1 μm. Results starting to converge at a l_{cz} ~ 78 μm for an element size bellow 20 μm, which can be seen in **Figure B.1**. Nonetheless, convergence for the stress value across the interface was found with an element size bellow 5 μm.

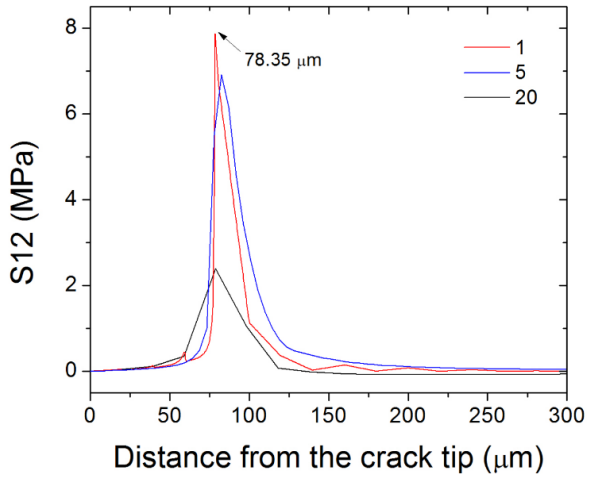

Figure B.1. . Mesh sensitivity analysis. Representative results of a mesh element size of 20, 5 and 1 μm are shown. Element sizes below 20 μm resulted in a characteristic length of 78 μm.

VITA

Name: Sandra Carolina Murcia.

Degree and date to be conferred: Ph.D., summer 2017

Collegiate institutions attended:

University of Washington, Seattle WA

Doctor of Philosophy 2014 to 2017
Major: Materials Science and Engineering

Master of Science, 2014 to 2015
Major: Materials Science and Engineering

University of Maryland Baltimore County, Baltimore MD

Doctor of Philosophy 2013 to 2014
Transferred in December 2013
Major: Mechanical Engineering

EAFIT University, Medellin, Colombia

Master of Science, 2010 to 2012
Major: Materials Design and Computational Mechanics

Specialist in Materials Design, 2010 to 2011

Bachelor of Engineering, 2006 to 2010
Major: Production Engineering

Professional Publications:

Murcia, S., Lavoie, E., Li, G., Ossa, A., Linley, T, Devaraj, A & Arola, D. (**2016**). A comparison of the microstructure of teleost fish scales. Journal of the Mechanical Behavior of Biomedical Materials,73,17-27

Murcia, S., Li, G., Yahyazadehfar, M., McConville, M., Ossa, A., & Arola, D. (**2016**). Effects of polar solvents on the mechanical behavior of fish scales. Materials Science and Engineering C, 61, 23-31.

Murcia, S., McConville, M., Li, G., Ossa, A., & Arola, D. (**2015**). Temperature effects on the fracture resistance of scales from Cyprinus carpio. Acta Biomaterialia, 14, 154-163.

Murcia, S. C., Ossa, E. A., & Celentano, D. J. (**2014**). Nodule evolution of ductile cast iron during solidification. Metallurgical and Materials Transactions B, 45(2), 707-718.

Murcia, S. C., Paniagua, M. A., & Ossa, E. A. (**2013**). Development of as-cast dual matrix structure (DMS) ductile iron. Materials Science and Engineering: A, 566, 8-15.

Ossa, A, **Murcia, S**, & Paniagua, M (**2011**). Effect of Ni Addition on the Production of As-Cast Bainitic Ductile Iron. Minerals, Metals and Materials Society/AIME, 420 Commonwealth Dr., P. O. Box 430 Warrendale PA 15086 United States.

Murcia, S., Stossel, M., Pahuja, R. Linely, T., Devaraj, A., Ramulu, M., Ossa, A., Wang, J. & Arola, D. (**2017**) The Limiting Layer of fish scales: structure and properties. (Submitted to Acta Biomaterialia)

Murcia, S., Miyamoto, Y., Varma, M., Ossa, A. & Arola, D. (**2017**) Prediction of the elastic modulus and strength of fish scales. (Submitted to Materials Science and Engineering C)

Murcia, S., Ossa, A. & Arola, D. (**2017**) Flexural behavior of laminated natural composites: Mineral gradient and profile design. (Submitted to Advanced Materials)